Università Campus Bio-Medico di Roma

Corso di Dottorato di Ricerca in
Scienze e Ingegneria per l'Uomo e l'Ambiente/Science and Engineering for Humans and the Environment
XXXIII ciclo a.a. 2017-2018

Design and Development of Wearable Devices and Methods to Study Three Aspects of Motor Redundancy: Wrist Posture, Wrist Impedance and Supernumerary Limbs

Luigi Raiano

Coordinator
Prof. Giulio Iannello

Tutors
Prof. Domenico Formica
Prof. Giovanni Di Pino

09/04/2021

Abstract

The Motor Redundancy of the Neuromuscular system is by far one of the most investigated aspects in Neurosciences and its effective and proper management, implemented by the Central Nervous System (*CNS*), is probably the key aspect that allows humans to safely, stably and gracefully move and physically interact with the environment.

In this context, the present work aims at investigating three aspects related to the motor redundancy: i) managing the wrist redundancy during unconstrained kinematically-redundant tasks, ii) studying the wrist mechanical impedance during the physical interaction with the environment and iii) interfacing with redundant effectors, *i.e.* supernumerary robotic limbs (*SRL*s) by extending the concept of redundancy related to the human motor control, for augmenting human capabilities.

Concerning the first scenario, we studied the control of the wrist and the management of the redundancy during the pointing with the wrist. It requires two degrees of freedom (*DOF*s) and previous studies have showed that the redundant *DOF* is bonded with the other twos on the basis of an empirical law, called *Donders' Law*. It is subject specific, path dependent and volatile (*i.e.* violations to this law have been reported in literature) and, geometrically, the *Donders' Law* represents a quadratic surface (also called *Donders' Surface*). In this work we further investigated this topic to study i) the stability over time of the *Donders' Law* and whether it remains during the motor adaptation to a visuomotor disturbance provided in the task space. Concerning the first scientific question, we carried out an experiment in which the enrolled subjects were asked to perform a pointing task in four different days and we found that the *Donders' Law* did not change over days within subjects, in terms of shape of the *Donders' Surface*. On the other hand, to study the effect of the adaptation to a visuomotor disturbance on the *Donders' Law*, the enrolled subjects were asked to perform a pointing task with and without the presence of a visuomotor disturbance provided in the task space. The main result that we obtained is the following: despite the subjects adapted to the disturbance, the specific implementation of

the redundancy management (expressed in terms of shape of the *Donders' Surface*) did not change.

Regarding the second scenario, in this thesis we presented the design and the validation of a portable wrist exoskeleton, conceived to be used in unstructured environments, to measure wrist stiffness/impedance and Parkinson's Disease related rigidity. The device consists in five revolute joints, of which four are passive and one is active; it allows providing mechanical perturbation to the wrist around Flexion-Extension. In a first experiment, we used the device to estimate the wrist stiffness both in healthy and in PD subjects. The device successfully allowed discriminating between i) healthy subjects and PD subjects and ii) PD subjects before and after the L-DOPA based treatment. In addition, we carried out a second experiment in which we validated the device in estimating the wrist impedance around Flexion-Extension, obtaining results congruent to the values reported in the literature.

Lastly, concerning the third scenario, we presented a wearable device for providing vibrotactile feedback of a *SRL*. In a first experiment, we compared two feedback approaches considering unconstrained planar movements of the *SRL*: a kinematic feedback (*i.e.* the subjects received the end-effector position of the robot) and a dynamic feedback (*i.e.* the subjects received the torque of the two robot joints enabled). As result, we found the kinematic to be more reliable with respect the dynamic one, since it allowed subjects to correctly estimate the movements performed by robot. In a second experiment, we investigated the feasibility of a real-time estimation of the *SRL*'s movement. To this aim, by providing the end-effector position of the robot, the enrolled subjects were able to correctly estimate the movement of the robot in real-time (while receiving the feedback).

Acknowledgments

I wish to thank all wonderful people I met during my Ph.D. path. First of all, I wish to thank Profs. Domenico Formica and Giovanni Di Pino, who did not limit to be just two normal supervisors, rather they showed me the way for the real science and engineering. They believed in my capabilities and I must thank them if I did something good during my path. In addition, I wish to thank Prof. Emiliano Schena and Dr. Carlo Massaroni for their support and insights. I am also very grateful to all people from NeXT Lab (@ UCBM) and MTMBi Lab (@ UCBM) (too many people to mention singularly, but thank you all guys for everything!). Moreover, I wish to thank the Universitá Campus Bio-Medico di Roma for its support in all my activities and the Reviewers for their feedback and insights that helped improving the quality of my work.

Last but not least, a special and warm acknowledgement goes to my family, my father and my mother, and Angela, for their patience, support, encouragement and love.

Thank you all!

To my Mother and my Father.
To Angela.

Contents

Chapter 1

Introduction

1.1 Motivation and Objective

The astonishing capability of the *Central Nervous System* (*CNS*) to effectively and efficiently control the human body while moving and interacting with the external environment has led to a tremendous growth of the Neurosciences over the last few decades to further investigate the human motor control [1]. Such a capability becomes even more relevant, and appealing from a researcher point of view, if we consider that the *Sensorymotor System* is highly redundant. Indeed, most of the motor tasks that we perform during the everyday life can be generally implemented in different alternative ways [2, 3]. For example, there is an infinite number of joint configurations that can be used to grab and manipulate the smartphone to send a text message. However, if from one side the motor redundancy allows the *CNS* to flexibly and robustly control the *Sensorymotor System*, on the other hand it poses the following challenging problem: "How to (properly) select a specific combination of elemental units of the *Neuromuscular System* to perform the specific task" [3].

To this aim, several studies have postulated that the *CNS* may implement "simplifying approaches". Specifically, it may use *dynamic primitives* consisting in a set of elemental units, whose proper combination allows the *CNS* to control the human body and accomplish the specific task [3, 4, 5]. Therefore, instead of defining a specific command for each single movement, the brain needs only to combine a reduced set of "instructions", which has been already experienced in the past, leading to a dramatic reduction of the number of degrees of freedom (*DOF*s) to be controlled [3, 4, 6, 7, 8, 9].

An example of using a simplifying approach implemented by the *CNS* during unconstrained (no interaction with the environment) is the pointing task

with the wrist. Concisely, when pointing to a target in the space, only two *DOF*s are needed. Therefore, controlling the wrist (characterized by three *DOF*s) requires to manage one degree of redundancy. It has been suggested that the *CNS* adopts a simplifying approach which consists in controlling actively two *DOF*s and constraints the residual one using a bidimensional surface. Such a simplifying approach has been named *Donders' Law* (also known as Donders' Surface) [10, 11].

The above-mentioned example is related to unconstrained movements. Nonetheless, the use of simplification approaches is still valid when the *CNS* has to control the the physical interaction with the environment. To this aim, the strategy adopted by the brain is to select the appropriate mechanical impedance, which is the dynamic relationship existing between force/torque and movement [12]. Different theories on human motor control are based on this aspect, *e.g.* the Equilibrium Point Hypothesis [13, 14] or its "reviewed" version proposed by Hogan and Sternad [4]. By selecting a mechanical impedance of the joints (through a specific muscle co-activation) involved in the task, the *CNS* assures the controlled system (e.g. the arm) to robustly move along a desired equilibrium trajectory, allowing for a reliable compensation of possible external forces [13, 4].

So far, the focus has been pointed to the redundancy as essential characteristic of the *Sensorymotor System*. However, in the scientific area of the augmentation of human physiological capabilities, this idea could be even extended. Indeed, as the redundancy allows the *Sensorymotor System* to be flexible, robust and efficient, the use of redundant artificial arms might allow healthy subjects to perform everyday or job-related tasks differently, *i.e.* with increased manipulation and dexterity capabilities [15, 16, 17]. Although this topic appears to be as a part of a science fiction, supernumerary robotic limbs (*SRLs*) have started to gain momentum over the few past years. To date, few attempts have been proposed, all of them related to use a wearable *SRL* for helping workers during their job-related activities [18, 19]. Nonetheless, to facilitate the integration of the *SRL* within the human body schema, *i.e.* to help the embodiment of the *SRL*, the user should perceive the device from different sensory sources. In other words, the embodiment of *SRL* could be enhanced if the brain implemented a sensory integration [20, 21, 22], through a supplementary sensory feedback conveyed to the user.

The aim of the present thesis is to study different aspect of the redundancy in human motor control, and in particular under three perspectives: i) controlling the movements of the wrist during kinematically redundant task, ii) studying the wrist impedance in healthy subjects and in patients with Parkinson's Disease and iii) interfacing with *SRL*.

Concerning the first scenario, we show that the subject-specific strategies

implemented to solve wrist redundancy (*i.e. Donders' law*) does not change over time and during the adaptation to visuomotor perturbations. Regarding the second scenario, we present the design and the validation of a wearable robot designed to measure wrist stiffness/impedance and its experimental validation [23, 24, 25]. Lastly, for what concerns the third scenario, we present a wearable device designed to provide proprioceptive feedback of a *SRL* in order to boost its embodiment for augmenting able-bodied human capabilities [26].

1.2 Thesis Outline and Contribution

Chapter 2 describes the background behind the problem of the redundancy, by focussing on the simplifications implemented by the human brain to control the posture and the movement. Moreover, by extending the idea of motor redundancy to supernumerary limbs, in Chapter 2 it is also provided a review of the current works related to this topic with a specific interest to feedback technologies that may enhance the embodiment of supernumerary systems.

Chapter 3 demonstrates that the simplifying control synergies adopted by the *CNS* to manage the redundancy of the wrist during pointing tasks (kinematically redundant task for the wrist joint) are stable over time and remain unchanged even during the visuomotor adaptation.

Chapter 4 describes the design and the experimental validations of the proposed wearable exoskeleton to estimate both the wrist stiffness and the wrist impedance, with the final goal of providing experimental evidences to study the wrist impedance during interactive tasks. This chapter demonstrates that using our device, the wrist stiffness and the wrist impedance can be properly estimated in healthy subjects. Moreover, we provide experimental evidences regarding the reliability of the device in discriminating (i) Parkinson's Disease (PD) subjects with respect healthy subjects and (ii) PD subjects before and after the pharmacological treatment.

Chapter 5 moves toward supernumerary limbs and here we present a novel approach to convey feedback to the user, in order to boost embodiment and controllability aiming at augmenting human capabilities during interactive tasks.

Chapter 6 briefly resumes the main findings of this thesis, underlining main Author's contributions, and provides an outlook on future works.

1.3 Author's Publications

1.3.1 Published Papers

Journal Papers

1. Di Tocco, J., **Raiano, L.**, Sabbadini, R., S., Massaroni, C., Formica, D. & Schena, E., (2021). A Smart Garment Embedding Conductive Textile and IMU for Unobtrusive Cardio-Respiratory Monitoring. Submitted to MDPI Sensors (under review).

2. Di Tocco, J., Sabbadini, R., **Raiano, L.**, Fani, F., Ripani, S., Schena, E., Formica, D. & Massaroni, C. (2021). Breath-Jockey: Development and Feasibility Assessment of a Wearable System for Respiratory Rate and Kinematic Parameter Estimation for Gallop Athletes. Sensors, 21(1), 152.

3. **Raiano, L.**, Di Tocco, J., Massaroni, C., Schena, E., & Formica, D. (2020). A PCA-based method to select the number and the body location of piezoresistive sensors in a wearable system for respiratory monitoring. IEEE Sensors Journal, 21(5), 6847-6855.

4. Pinardi, M., Ferrari, F., D'Alonzo, M., Clemente, F., **Raiano, L.**, Cipriani, C., & Di Pino, G. (2020). Doublecheck: a sensory confirmation is required to own a robotic hand, sending a command to feel in charge of it. Cognitive Neuroscience, 11(4), 216-228.

5. **Raiano, L.**, Di Pino, G., Di Biase, L., Tombini, M., Tagliamonte, N. L., & Formica, D. (2020). PDMeter: A Wrist Wearable Device for an at-home Assessment of the Parkinson's Disease Rigidity. IEEE Transactions on Neural Systems and Rehabilitation Engineering, 28(6), 1325-1333.

Conference Papers

1. **Raiano, L.**, Di Tocco, J., Massaroni, C., Di Pino, G., Schena, E., & Formica, D., "Respiratory Rate Estimation During Walking/Running Activities Using Principal Components Estimated from Signals Recorded by a Smart Garment Embedding Piezoresistive Sensors". Submitted to 2021 IEEE INTERNATIONAL WORKSHOP ON Metrology for Industry 4.0 and IoT.

2. Pinardi, M., **Raiano, L.**, Noccaro, A., Formica, D., & Di Pino, G., "Cartesian space feedback for real time tracking of a supernumerary

robotic limb: a pilot study," accepted for 2021 10th International IEEE EMBS Conference on Neural Engineering (NER).

3. **Raiano, L.**, Di Pino, G., & Formica, D., "Flexion-extension wrist impedance estimation using a novel portable wrist exoskeleton: a pilot study," in 2020 8th IEEE RAS/EMBS International Conference for Biomedical Robotics and Biomechatronics (BioRob), pp. 440-445, IEEE.

4. Noccaro, A., **Raiano, L.**, Pinardi, M., Formica, D., & Di Pino, G., "A novel proprioceptive feedback system for supernumerary robotic limb," in 2020 8th IEEE RAS/EMBS International Conference for Biomedical Robotics and Biomechatronics (BioRob), pp. 1024-1029, IEEE.

5. Pinardi, M., **Raiano, L.**, Formica, D., & Di Pino, G. (2020, July). Altered Proprioceptive Feedback Influences Movement Kinematics in a Lifting Task. In 2020 42nd Annual International Conference of the IEEE Engineering in Medicine & Biology Society (EMBC) (pp. 3232-3235). IEEE.

6. Le Jeune, F., D'Alonzo, M., Noccaro, A., **Raiano, L.**, Formica, D., & Di Pino, G. (2020, July). Manipulating The Body Representation: Assessment Of A Novel Platform. In 2020 42nd Annual International Conference of the IEEE Engineering in Medicine & Biology Society (EMBC) (pp. 3248-3251). IEEE.

7. **Raiano, L.**, Di Tocco, J., Massaroni, C., Di Pino, G., Schena, E., & Formica, D. (2020, June). Clean-Breathing: a Novel Sensor Fusion Algorithm Based on ICA to Remove Motion Artifacts from Breathing Signal. In 2020 IEEE International Workshop on Metrology for Industry 4.0 & IoT (pp. 734-739). IEEE.

8. Di Tocco, J., Massaroni, C., **Raiano, L.**, Formica, D., & Schena, E. (2020, June). A wearable system for respiratory and pace monitoring in running activities: a feasibility study. In 2020 IEEE International Workshop on Metrology for Industry 4.0 & IoT (pp. 44-48). IEEE.

9. Massaroni, C., Di Tocco, J., Sabbadini, R., Carnevale, A., Presti, D. L., Schena, E., **Raiano, L.,** ... & Sterzi, S. (2020, May). Influence of torso movements on a multi-sensor garment for respiratory monitoring during walking and running activities. In 2020 IEEE International Instrumentation and Measurement Technology Conference (I2MTC) (pp. 1-6). IEEE.

10. Schena, E., Massaroni, C., Iacoponi, S., Berté, A., Leone, A., Musicco, S., Formica, D., **Raiano, L.**, ... & De Filippis, A. (2019, June). Force monitoring during Peripheral Nerve Blocks: design and feasibility assessment of a new noninvasive system. In 2019 II Workshop on Metrology for Industry 4.0 and IoT (MetroInd4. 0&IoT) (pp. 154-157). IEEE.

11. Noccaro, A., **Raiano, L.**, Di Pino, G., & Formica, D. (2018, August). Evaluation of hand-eye and robot-world calibration algorithms for TMS application. In 2018 7th IEEE International Conference on Biomedical Robotics and Biomechatronics (Biorob) (pp. 1115-1119). IEEE.

12. **Raiano, L.**, Di Pino, G., Noccaro, A., Accoto, D., & Formica, D. (2018, August). Design of a Wearable Mechatronic Device to Measure the Wrist Rigidity in Parkinson's Disease Patients. In 2018 7th IEEE International Conference on Biomedical Robotics and Biomechatronics (Biorob) (pp. 497-502). IEEE.

13. Cordella, F., Taffoni, F., **Raiano, L.**, Carpino, G., Pantoni, M., Zollo, L., ... & Formica, D. (2016, August). Design and development of a sensorized cylindrical object for grasping assessment. In 2016 38th Annual International Conference of the IEEE Engineering in Medicine and Biology Society (EMBC) (pp. 3366-3369). IEEE.

1.3.2 Other Works

1. Raiano L., et al. Do bionic hand prostheses need wrist flexion/extension? A wearable device to evaluate the employment of wrist flexion/extension in ADLs. In: 2ndInternational Symposium on Innovations Amputation Surgery and Prosthetic Technologies (IASPT 2018).

2. Raiano L., et al. Design of a wearable mechatronic device to measure the wrist rigidity in Parkinson's Disease patients. In: Sixth National Congress of Bioengineering (GNB2018).

Chapter 2

Background: Posture, Impedance Modulation and Supernumerary Limbs

2.1 Introduction

This chapter will provide the background of the main scientific problem that this thesis aims at studying, *i.e.* the motor redundancy declined into three specific aspects: i) control of the wrist during unconstrained and redundant tasks, ii) modulation of the mechanical impedance, with a specific focus to the wrist and iii) enhancing the embodiment of *SRL*s through supplementary feedback conveyed to the users. Although the three topics are all related to the motor redundancy, the latter one will be kept separated from the formers when presenting its background. Indeed, while topic (i) and (ii) refer to the most common branch of the motor redundancy, topic (iii) mainly refers to techniques for conveying haptic feedback, applied in this work to *SRL*s, which are redundant systems used to augment able-bodied human capabilities.

2.2 The Degrees-of-Freedom Problem in Motor Control

Interacting with the environment and controlling the posture requires the *Central Nervous System* (*CNS*) to adequately control many degrees-of-freedom (*DOF*s) [3]. This is known as the *Degrees-of-Freedom Problem* and it was firstly introduced by Bernstein [27]. Over the years, scientists have postulated that the brain adopts simplifying approaches to successfully manage

such a demanding and complex task [3]. Specifically, the *CNS* may combine some fundamental and stereotyped *motor commands* that are called *motor primitives* or *dynamic primitives* [4, 6, 9]. Similarly to the letters of the alphabet which are the fundamental components for generating the language, the *dynamic primitives* are considered as the *motor bricks* for the human behaviours. In this context, generating movements and maintaining the posture is achieved by using task specific and stereotyped patterns of muscle activation combined together to achieve a given task. Furthermore, in this context the motor learning can be thought as how the *CNS* learns to combine such fundamental motor bricks [4, 3].

Among the body segments controlled by the brain, the human wrist can be considered by far one of the most used joint, being involved in all manipulation tasks. It is a high compact anatomical structure (see Fig. 2.1), which corresponds to the carpal bones that connect the metacarpal bones of the palm with the forearm bones [28]. According to Fig. 2.1, the relative motion between such bones make the wrist as characterized by two DOFs:

- *flexion-extension* (*FE*): the palm of the hand rotates upward (*extension*) or downward (*flexion)*);
- *radial-ulnar Deviation* (*RUD*): the hand rotates toward the radius (*radial deviation*) or toward the ulna (*ulnar deviation*).

However, the wrist is typically assumed to be characterized by three DOFs. Indeed, although the *prono-supination* (*PS*) is confined within the forearm, it can be functionally attributed to the wrist [28].

If from one side, the three DOFs allow the hand to assume any configuration in the free space, they make the wrist a complex biomechanical structure involving a large number of muscles to be controlled (nine group of muscles [28]). Therefore, studying how the *CNS* controls the wrist movement is appealing under the point of view of the redundancy management both considering movements in the free space and the physical interaction with the environment.

2.2.1 Controlling the Wrist During Redundant Tasks: the Donders' Law

To control the hand for performing a pointing task, the *CNS* has to coordinate the wrist muscles to cope with a redundant task. Indeed, pointing a target in the space requires only two DOFs, while, as mentioned earlier, the wrist is (functionally) a 3-DOF kinematic chain. Thus, the pointing task is

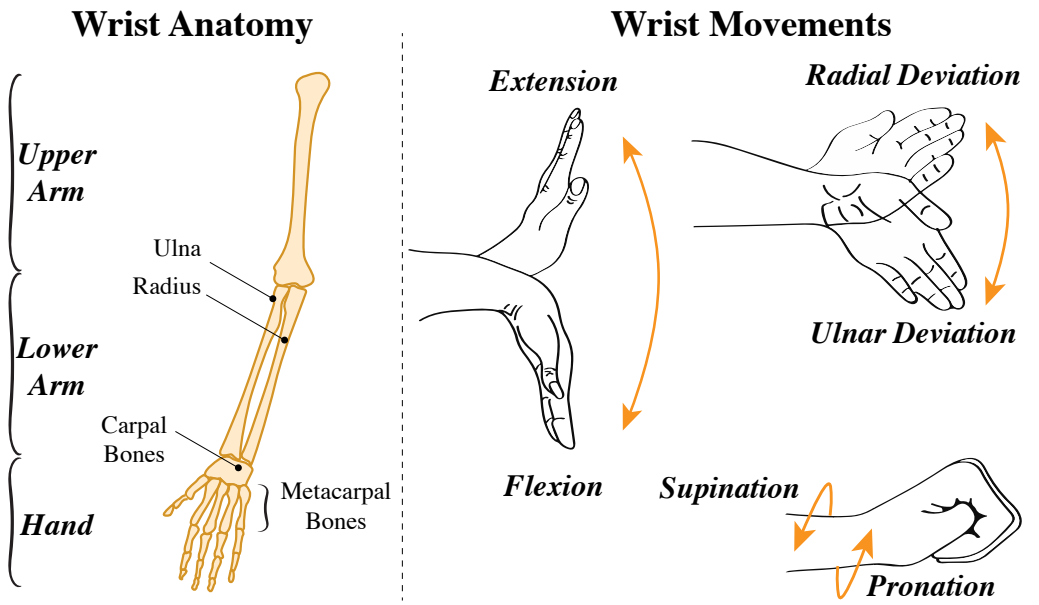

Figure 2.1: Description of the main anatomical components of the human wrist joint (left) and DOFs of the wrist and the forearm.

defined as a kinematically redundant task for the wrist [10]. Despite the infinite configurations that the wrist could assume to point a target in the space, the brain adopts a stereotypical coordination of the redundant DOF, leading to a unique posture for a given pointed target. In other words, the brain may to constrain the redundant DOF to belong to a subject-specific configuration depending on the the other two DOFs, called *Donders' Law*[10, 29]. Experimentally, the *Donders' Law* is estimated by performing a numerical fitting of the recorded data. Subjects are asked to point targets in space with the wrist and forearm unconstrained. The performed wrist movements are supposed to be pure rotations around a reference frame placed within the wrist and the hand is supposed to be a rigid body (see Fig. 2.2). The wrist rotations are recorded using motion sensors, *e.g* magneto-inertial measurement units (M-IMU), and they are typically expressed as rotation vectors ($\boldsymbol{r}(t) = [r_x(t), r_y(t), r_z(t)]^T$). Therefore, the *Donders' Law* poses that the redundant DOF (according to Fig. 2.2, the rotation around the x-axis) can be well approximated by the following quadratic relationship:

$$\tilde{r}_x(t) = C_1 + C_2 r_y(t) + C_3 r_z(t) + C_4 r_y^2(t) + 2C_5 r_y(t) r_z(t) + C_6 r_z^2(t). \quad (2.1)$$

In (2.1), $\tilde{r}_x(t)$ denotes the fitted $r_x(t)$. Moreover, the coefficients $C_i, (i = 1 \div 6)$ determine the shape and configuration of the *Donders' surface* [10, 11]; specifically:

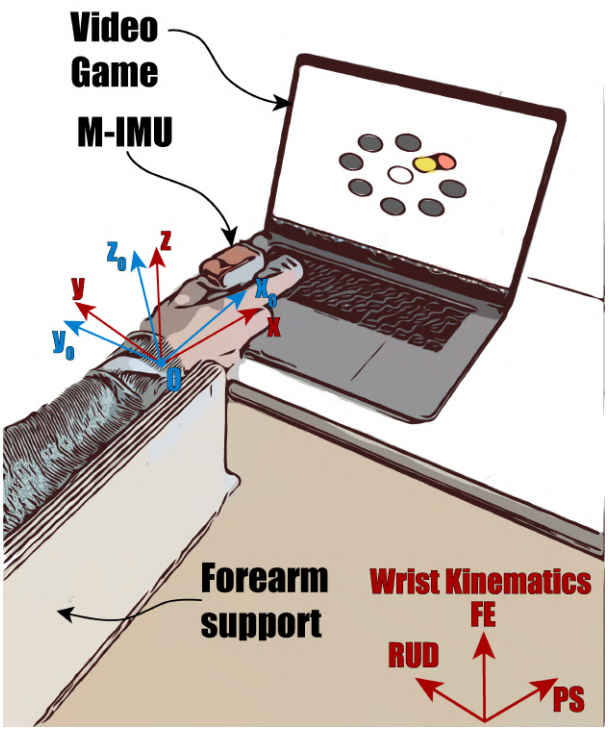

Figure 2.2: Typical Setup for assessing *Donders' Law*: a video-game is used to present to the subjects the target to be pointed (red circle) while recording hand movements using a motion sensors (the yellow circle indicates the actual pointed position on the screen), *e.g.* an M-IMU. The blue frame (O_0) is the reference one; the red frame is the moving one, whose orientation is recorded by the motion sensor during the experiment.

- C_1 indicates the offset value;
- C_2 and C_3 represent the linear relationship, *i.e.* the surface orientation;
- C_4 and C_6 represent the amount curvature of the edge of the surface;
- C_5 determines the amount and direction of surface twisting.

A graphical representation of (2.1) is depicted in Fig. 2.3.

To resume, when pointing a target in the space the wrist has a configuration dependent to the specific target pointed, since the *CNS* controls the redundant DOF dependently on the other two DOFs involved in the task. Such a redundancy management has been defined as a *soft constraint* since it can be either imposed by the brain to cope with redundant tasks or violated by voluntary control [30, 29]. Moreover, previous studies have also showed that the *Donders' Law* is subject specific. This means that, even though the

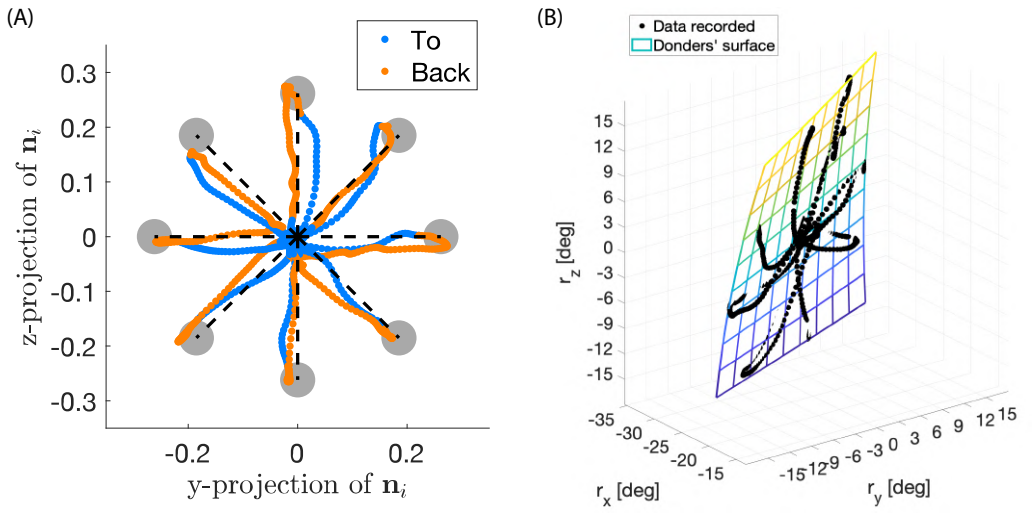

Figure 2.3: (A) Pointing trajectories recorded during an experimental session. Orange points represent real-time projections of the pointing vector ($\boldsymbol{n}_i$) from the starting point (central cross) toward the targets. Blue points represent real-time projections of $\boldsymbol{n}_i$ from the reached target toward the starting point. Red circles represent the targets. (B) Donders surface estimated using recorded data (overimposed black points).

configuration of the wrist is unique and depends on the pointed direction, the shape and the orientation depend strictly on the subjects' biomechanics. Nonetheless, it is still unclear whether this redundancy management is robust over time for each subject. In this thesis we studied this aspect by performing a within-subject assessment of the Donders' Law, demonstrating that the Donders' Law is a time stable redundancy management solution implemented by the brain. See Chapter 3.2 for further details.

Another aspect of the *Donders' Law* that is still unclear is whether and how it changes during all those tasks in which the *CNS*s has to adapt to an external visuomotor disturbance. In other words, how does the brain manage the redundancy while contemporarily pointing a target in the space and adapting to an unknown external disturbance? In this regard, a previous study aimed at providing first evidences and within this work we further investigated this topic. We showed that, despite the presence of an external and unknown visuomotor disturbance, the subject-specific redundancy management implemented does not change with respect a normal condition. This study is presented in Chapter 3.3.

2.2.2 Modulating the Mechanical Impedance to Control the Physical Interaction with the Environment

Besides controlling the hand during free movements, the *CNS* has to control the physical interaction with the external environment, in terms of forces exchanged. Regarding the wrist, this aspect becomes crucial, since it is involved in all manipulation tasks, which are pivotal in almost all activities of daily living [4, 31]. Despite a comprehensive knowledge of strategies implemented by the brain for achieving interactive tasks still lacks [31], a valuable group of theories poses that the *CNS* adopts a simplifying approach, consisting in the modulation of the mechanical impedance of the joints that allow the target body segments to move, leading to a desired behaviour at the end-effector (*e.g* the hand) in terms of human-environment interaction [3, 4, 9, 14, 32, 33, 34, 35]. This solution allows the brain to reduce the parameters to be controlled, while assuring smooth, graceful and stable movements, even in presence of external unstable force fields [4, 5, 32, 36].

The joint-space mechanical impedance ($\boldsymbol{Z}$) is the dynamic relationship between torque and movement in the joint space [12]. Mathematically, $\boldsymbol{Z}$ is a dynamic operator that maps joint angular movements ($\boldsymbol{\theta}(t)$) onto the joint torques ($\boldsymbol{\tau}(t)$) [4]:

$$\boldsymbol{Z} = \boldsymbol{\theta}(t) \rightarrow \boldsymbol{\tau}(t). \tag{2.2}$$

If the mechanical system considered is linear and time-invariant, $\boldsymbol{Z}$ can be computed considering the following mechanical model:

$$\boldsymbol{\tau} = \boldsymbol{K}\boldsymbol{\theta}(t) + \boldsymbol{b}\dot{\boldsymbol{\theta}}(t) + \boldsymbol{J}\ddot{\boldsymbol{\theta}}(t). \tag{2.3}$$

In (2.3), $\boldsymbol{\theta}(t)$, $\dot{\boldsymbol{\theta}}(t)$ and $\ddot{\boldsymbol{\theta}}(t)$ denote the angular rotation, velocity and acceleration respectively, while $\boldsymbol{K}$, $\boldsymbol{b}$ and $\boldsymbol{J}$ denote the stiffness, damping and inertia matrices respectively. Therefore, according to (2.2) and it simplified version expressed in (2.3), the modulation of the impedance influences the torque exerted by the joint to produce a given angular movement, leading to a net interaction at the end-effector. This approach allows the brain to stabilize the interaction between the controlled system and the environment, the former conceived as a "*multi-joint system*", even while interacting with novel and unstable tasks. In this perspective, the modulation of the mechanical impedance is crucial also to learn novel interactive tasks [4, 37, 38, 39].

To resume, through the modulation of the mechanical impedance the *CNS* aims at achieving a two-fold purpose:

- to control the interaction force between end-effector, *e.g.* the hand, and the environment;

- to stabilize the system when performing novel/unstable tasks.

Under a physiological perspective, the *CNS* can modulate $\boldsymbol{Z}$ by controlling the co-contraction pattern of the muscles involved in actuating the target joints [4, 40, 37, 31]. It is worth considering that in addition to the voluntary contraction of the muscles, their activity can be also modulated by means of *low level* controllers, which mainly occur within the spinal cord. Such controllers are called *spinal reflexes* and they mainly involve a specific type of proprioceptors, named *muscle spindles*. If an external force field determines an undesired muscle contraction, the *muscle spindles* change the activity of the *alpha motor neurons*, in order to adjust the muscle contraction according the desired one [41].

A schematic representation of a generic movement that requires an interaction with the environment can be represented as in Fig. 2.4. A *multi-body system* has to be controlled to reach a given target in the task space and the mechanical impedance needs to be properly set up to assure an adequate interaction.

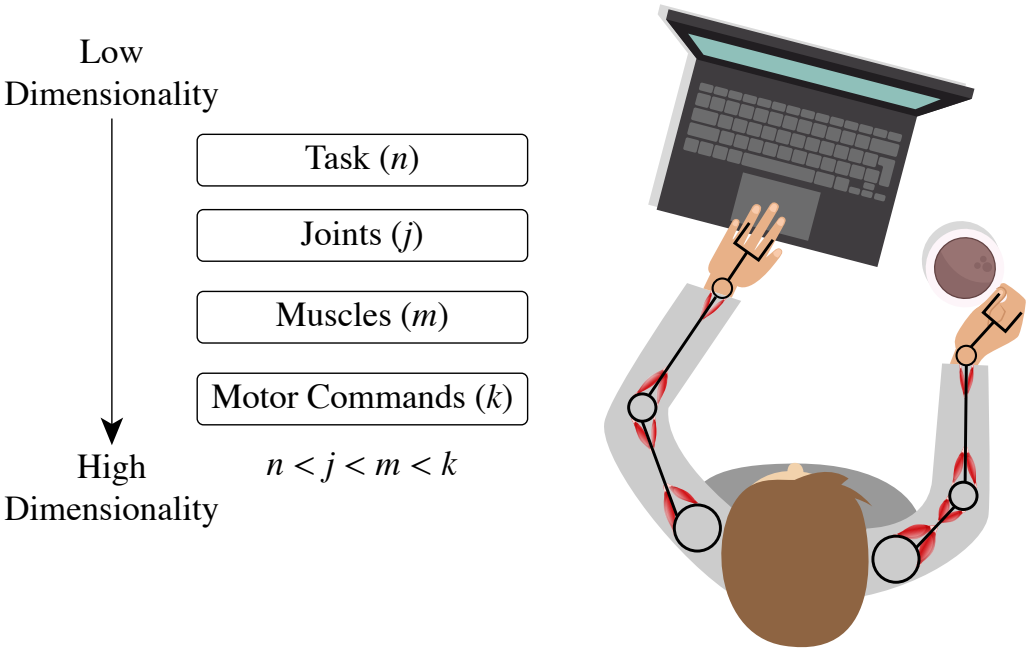

Figure 2.4: To perform a movement, a one to many hierarchical sequence of transformations should be implemented by the brain. The movement and the impedance of the end-effector is determined by the movements and the impedance in the joint space. Once the joint space planning has been implemented, motor commands can be provided to the muscles in order to define their proper activation for achieving the given task. Adapted from [3, 42]

Measurements of Wrist Mechanical Impedance

According to 2.2, the mechanical impedance is the dynamic relationship between torques and movements at the wrist joint [43] and it is used by the *CNS* to control the human-environment interactions during manipulation tasks [4, 29]. Considering the wrist as a linear time-invariant mechanical multi-joint system, its dynamics can be generally expressed as second-order 3-DOF mechanical model [44]:

$$\boldsymbol{\tau} = \boldsymbol{I}\ddot{\boldsymbol{\theta}} + \boldsymbol{B}\dot{\boldsymbol{\theta}} + \boldsymbol{K}\boldsymbol{\theta} + \boldsymbol{g}(\boldsymbol{\theta}), \tag{2.4}$$

denoting $\boldsymbol{I}$ the inertia matrix, $\boldsymbol{B}$ the damping matrix and $\boldsymbol{K}$ the stiffness matrix. Moreover, in (2.4) $\ddot{\boldsymbol{\theta}}$, $\dot{\boldsymbol{\theta}}$ and $\boldsymbol{\theta}$ represent the wrist angular accelerations, angular velocities and rotations respectively; $\boldsymbol{g}$ denotes the gravitational torques and $\boldsymbol{\tau}$ denotes the vector containing the active torques due to muscle contraction required to move the hand [44]. Under this hypothesis, estimating the wrist impedance means generally estimating $\boldsymbol{I}$, $\boldsymbol{B}$ and $\boldsymbol{K}$.

The experimental measurement of the wrist impedance requires an actuated system for providing a known mechanical perturbation. In other words, it requires to gently perturb the wrist and record its induced movements. An example of wrist impedance estimation is reported in Fig. 2.5, where the numerical estimation has been performed by regressing the recorded data related to the torque applied around flexion-extension and the angular velocities and rotations (angular accelerations are neglected due to the slowness of the applied movements).

In the Author's knowledge, in all attempts reported in literature, researchers have mainly focussed on measuring the impedance of the wrist [45, 46, 33] or its statical component (*i.e.* the stiffness) [31, 47, 48, 49, 50, 51] within structured environments, due to the instrumentation available. Indeed, to this aim general purpose robotic devices have been employed. Such systems are typically conceived for rehabilitation purposes and thus characterized by high-torque actuators [51]. This aspect strongly hinders their use in unstructured environments. An example of device used is reported in Fig. 2.5. On other hand, a continuous monitoring of the wrist impedance in unstructured environments would enable to deepen the current knowledge on human motor control during interactive tasks, *e.g.* activities of daily living, which is in fact the scenario where the *CNS* currently has to modulate the joint impedance for achieving the every-day life tasks [4].

The Parkinson's Disease and the Assessment of the Rigidity

The estimation of the mechanical impedance/stiffness is crucial also for assessing neurological disorders that involve movement disorders, such as the

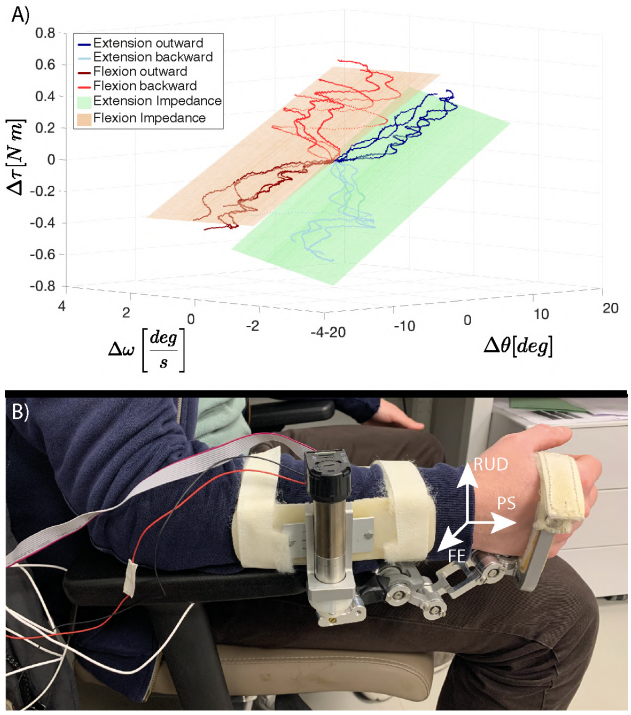

Figure 2.5: A) Example of numerical passive wrist impedance estimation. The estimation has been performed by considering a simplified version of (2.4) in which only the movements around flexion-extension have been considered; moreover, since the mechanical perturbation applied to the wrist have been slowly applied, the estimation takes into account only the effect of damping and stiffness. In addition, the gravitational effects have been neglected since the flexion-extension axis was parallel to the gravity. According to such hypotheses, the estimated impedance is represented by a plane whose orientation is determined by stiffness and damping coefficients. B) Experimental apparatus used to estimate the stiffness depicted in A). Adapted from [25].

Parkinson's Disease (PD). The PD consists on a progressive deterioration of the *Substantia Nigra Pars Compacta*, which causes a lack of dopamine in the Central Nervous System (CNS) and leads to an over-inhibition of the efferent neural pathway.

According to Fig. 2.7, the PD is characterized by several symptoms and its three cardinal ones are [53]:

- *bradykinesia*: slowness of movement;
- *resting tremor*: involuntary and periodic oscillations of the body extremities, mostly the hands;
- *rigidity*: increased resistance in response to the passive motion of joints.

Despite the disease can be symptomatically treated using drugs acting on the dopamine pathway, such as L-DOPA [55], dopaminoagonists [56], con-

Figure 2.6: Typical setup used for estimating the wrist stiffness, consisting of a robot mainly conceived to be used in rehabilitation tasks, thus characterized by a cumbersome structure and bulky actuators [48, 52]. Picture adapted from [48]

tinuous biochemical infusion of L-DOPA [57], or Deep Brain Stimulation [58], patients still suffer of wide fluctuations of the symptoms, reflecting the fluctuations of dopamine level into the brain. Therefore, a continuous daily motor monitoring may help in patients' management [59].

The clinical assessment of PD is performed on the basis of rating scales and the most used is the MDS-UPDRS, which mainly focuses on the wrist and the elbow joints for what concerns the clinical rigidity assessment of the upper limb [54] Anyhow, these scales may suffer from objectiveness lacking, because they are dependent on the expertise of the clinicians; in addition, their administration is time consuming [60].

While tiny and portable wearable motion sensors, *e.g.* M-IMU, have been successfully employed to quantitatively assess *bradykinesia* [61, 62] and *resting tremor* [63, 64], the quantitative assessment of the *wrist rigidity* requires more complex systems, capable to provide mechanical perturbations and record induced movements. Indeed, *wrist rigidity* is well described by the wrist stiffness, or more generally by the wrist impedance [65].

In order to boost clinical assessments and optimize the therapeutical approaches of the PD, a continuous assessment of the motor symptoms needs to be implemented, including the rigidity [59] Therefore a device capable to implement a comprehensive assessment in unstructured environments, *e.g.*

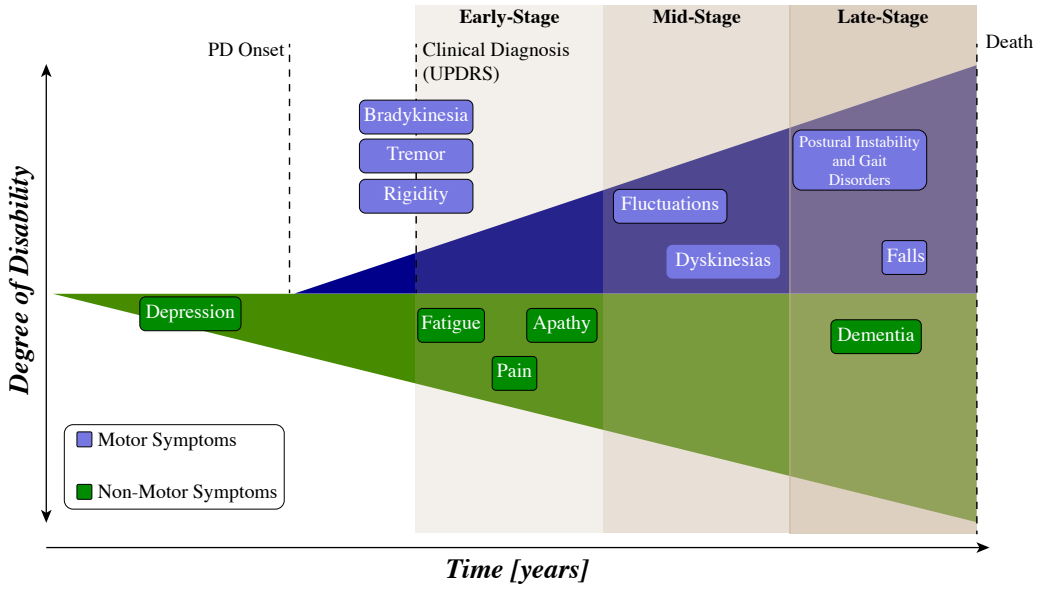

Figure 2.7: Parkinson's disease is characterized by several motor and non-motor symptoms. However, according to MDS-UPDRS [54], the PD is diagnosed when bradykinesia and one among rigidity and tremor are clinically evident [53]. Adapted from [53].

an at-home monitoring, may be pivotal, also for reducing both the costs for the national healthcare system and the personnel time [59, 60].

Design of a wearable device for estimating wrist impedance in unstructured environments

As mentioned earlier, manipulation tasks represent an essential aspect of our everyday life and the *CNS* mainly controls the physical interactions between human hand and environment by modulating the wrist impedance. In addition, any pathological condition that causes abnormalities in modulating the joint impedance may lead to an ineffective human-environment interaction, such as the Parkinson's Disease in which this aspect has a huge impact in properly performing activities of daily living [66]. In this scenario, in order to deepen the knowledge of how the brain modulates the impedance during interactive tasks [67, 51] and improve clinical approaches for treating the Parkinson's Disease [59], a continuous monitor in unstructured environments of the wrist impedance is thus needed. To this aim, in this thesis work we present the design and the validation a novel wearable device conceived to be portable, low weight and low size in order to allow a long-term monitoring of the wrist stiffness and impedance. In Chapter 4.2 we will present the design steps of the device. In Chapter 4.5 we will present the validation of the de-

vice in measuring stiffness and PD-related rigidity considering both healthy subjects and PD patients. In Chapter 4.6 we will present the validation of the device in estimating the wrist impedance in healthy subjects.

2.3 Supernumerary Robotic Limbs to Augment Human Motor Capabilities

Motor redundancy is the key aspect of the human capability both to produce graceful and efficient movements and to interact with the environment in a safe, stable and dexterous way [3]. However, Humans have always tried to augment their physical and cognitive capabilities by using artificial external devices [15, 68]. In this scenario, supernumerary robotic limbs (SRLs) have gained momentum since they may enhance the capabilities of able-bodied individuals [69, 18, 70].

Despite augmenting able-bodied capabilities through SRLs might be considered as appealing for a wide range of applications, *e.g.* from dangerous conditions to health care applications or even to improve multitasking capabilities, currently SRLs are mainly designed to support workers during their job-related activities, in order to minimize risks and their physical effort [69, 18].

However, it has been demonstrated that the embodiment of artificial external devices, *i.e.* the representation within the *CNS* of the one's own body part, promotes an intuitive control of the object itself, facilitates the learning and increases user's satisfaction [71, 72]. Therefore, favouring the embodiment of SRLs may pave the way for using such technologies to perform tasks that are impossible only with natural limbs alone [15, 72]. In fact, *SRL*s can be conveniently used in different scenarios such as job-related tasks, dangerous situations and biomedical applications, to improve manipulation and dexterity capabilities and even the safety of the users [17]. To this aim, establishing a bi-directional communication (see Fig. 2.8) between user and SRL, through a non-invasive supplementary sensory feedback of the artificial tool, is quintessential [15, 73, 74]. Although in this specific application the end user is supposed to be an able-bodied individual, therefore able to use the eyesight, a supplementary feedback regarding the SRL may boost its embodiment because it allows the user's brain to integrate different sources of information of the same object, similarly to what usually happen with our own body limbs [75]. Furthermore, providing a source of information different to the one perceived by the visione, may allow the user to have an alternative feedback related to the controlled system, *e.g.* during all those

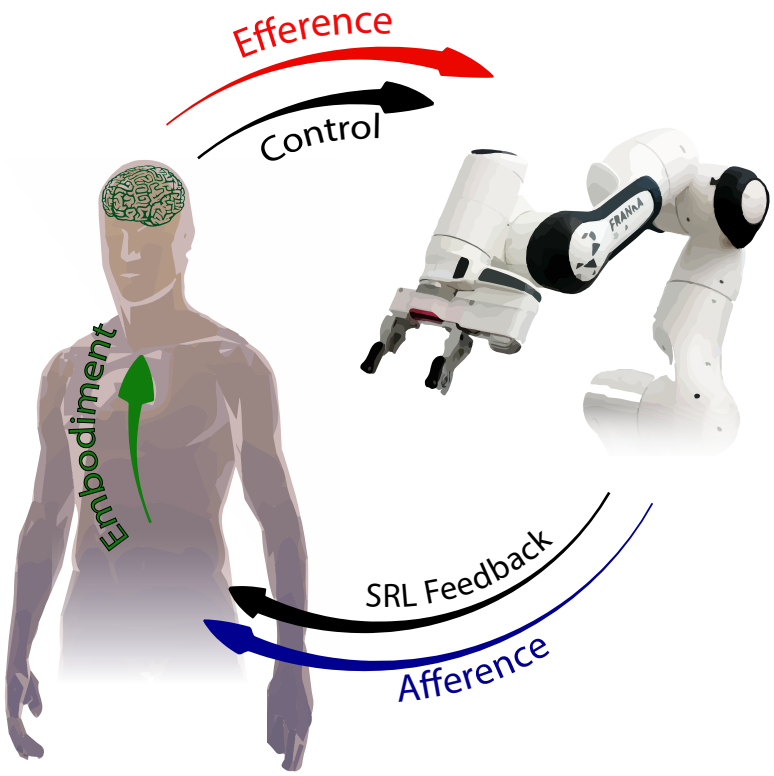

Figure 2.8: Concept of the bi-directional loop between SRL and user: controlling robot represents the efferent part, while the provided feedback represents the afferent part that is essential for enhancing the embodiment of the SRL.

tasks in which the vision is highly loaded, thus promoting multitasking [76].

2.3.1 Non-Invasive Feedback Techniques

To date, several studies have demonstrated that providing a sensory feedback enhances the user performance in controlling external tools [77, 78, 79, 80]. In this scenario, different approaches can be employed [81, 82]:

- vibrotactile feedback [78, 83, 84, 85];
- electrotactile feedback [79, 80, 86, 87];
- mechanotactile feedback [88, 89, 90];
- temperature feedback [91].

In the rest of this section the above-mentioned feedback techniques will be discussed.

Vibrotactile Feedback

The information is conveyed through vibrator DC motors applied to the skin surface of the subjects (see Fig. 2.9). These are commercially available eccentric DC motors whose vibration activates the *Pacinian* corpuscle mechanoreceptors [82]. Vibrator Motors ara characterized by low size and weight of the stimulators and can be easily integrated in wearable systems. Due to rotating parts, they are characterized by medium vibrating bandwidth (up to 300 Hz). Anyway, the vibration provided do not induce pain. However, due to their size, they cannot selectively elicit mechanoceptrs and the vibrational sensitivity threshold is subject-dependent. Concerning power supply, vibration motors absorb up to ~ 0.2 A and they are compatible with supply voltage used in wearable integrated systems (~ 3.3 V) [92]. Being eccentric DC motors, it is not possible to separate amplitude and frequency of the vibration provided since they are inherently coupled (*i.e.* an increase of the vibration frequency corresponds to an increase of the vibration amplitude).

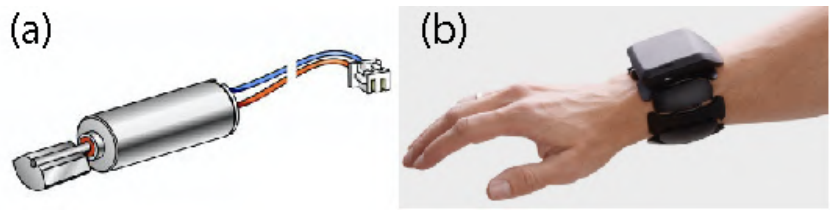

Figure 2.9: Vibrotactile feedback. (a) eccentric motor used to provide vibrotactile feedback [93]; (b) concept of a wearable bracelet integrating six vibrator motors [94]

Electrotactile Feedback

The stimulation is implemented by providing low-intensity current pulses (from ~ 0.1 mA to ~ 1 mA provided for few milliseconds or less) through tiny electrodes (few millimeter). No moving parts are required, leading to high bandwidth (up to kilohertz) and low power consumption. Due to the small size of the electrodes, they can be easily integrated in array stimulators as well as wearable systems (see Fig. 2.10) Similarly to vibrotactile feedback, the threshold of sensitivity is subject-dependent and this approach allows modulating independently the amplitude and the frequency of the stimuli provided. However, the electrical stimuli provided may be perceived as painful.

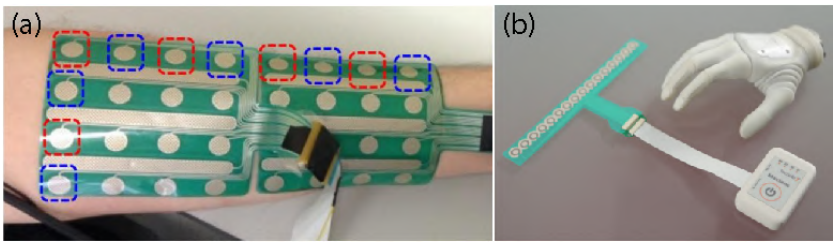

Figure 2.10: Electrotactile feedback. (a) an example of array stimulator [80]; (b) example of a commercially available electrotactile stimulator [95]

Mechanotactile Feedback

With this approach skin stretch or force/pressure is conveyed to the subject using "robotic" structures, which allow modulating independently frequency and amplitude of the stimuli provided. However, the bandwidth of the system is lower than the stimulators used for providing vibrotactile feedback. Due to DC motors embedded they are characterized to a power consumption similar to the vibrotactile approach. Nonetheless, the higher size of the stimulators does not allow their integration in wearable systems (each stimulator is a wearable robot itself), as reported in Fig. 2.11. Anyhow, if compared to other tactile stimulators (vibrotactile and electrotactile) the sensation of touch conveyed is more natural.

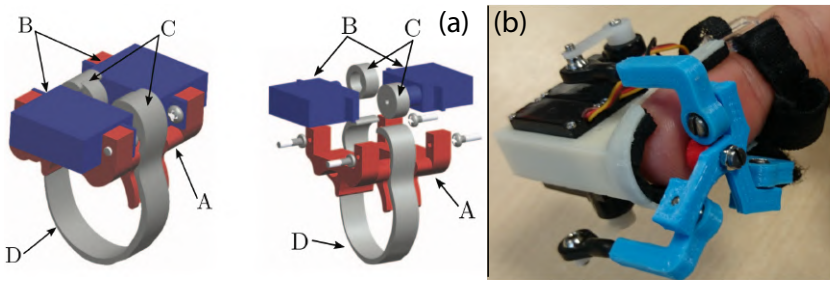

Figure 2.11: Mechanotactile feedback. (a) bel-based device for providing 2D skin stretch [96] (b) device for providing skin stretch using a 3-DOF parallel mechanism [97]

Temperature Feedback

The information is conveyed to the skin through Peltier elements, which are typically characterized by a large size (see Fig. 2.12). This approach does not allow providing high-bandwidth information. Anyhow, because providing temperature feedback does not involve mechanoreceptors, it is typically associated either with vibrotactile or electrotactile feedback.

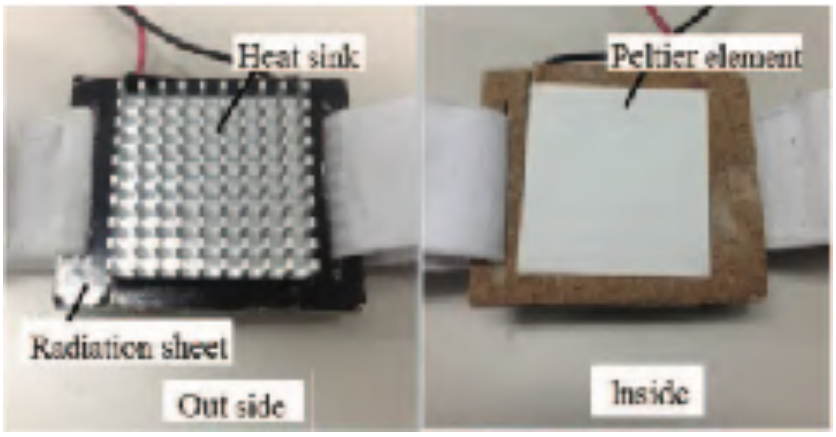

Figure 2.12: Temperature feedback. Peltier based device for conveying thermal feedback [91]

2.3.2 Vibrotactile Feedback of a Supernumerary Robotic Limb

Almost the entire range of SRLs developed so far are automatic systems, thus not conceived to be controlled in real-timed by the user, and none of them is characterized by a sensory feedback system [18, 98, 99, 100]. The only trace of returned feedback is the reaction force of the worn device [19]. However, although this conveys the interaction force between the wearable SRL and the environment, it could not be considered as an active supplementary feedback to be modulated accordingly to a given information that should be conveyed.

In the Author's knowledge, just one attempt has been done to provide an active feedback of a SRL [101, 102]. Specifically, the Authors demonstrated that providing the grasping force of an artificial hand connected to a SRL increased the embodiment of the system. Nonetheless, any source of information regarding the either the kinematics or the dynamics of the SRL is provided to the user.

To this aim, in Chapter 5 two pilot studies are reported. The first one compares the effectiveness of a kinematic feedback (*i.e.* related to the SRL movements) with respect a dynamic feedback (*i.e.* related to the SRL dynamics in terms joint torques) to let subjects understand the robot posture. The second study, based on the results obtained in the first one, aims at investigating whether subjects are able to perceive in real-time the posture of the SRL. In both studies vibrotactile stimulation to convey proprioceptive feedback was employed, being non-invasive, highly informative and versatile [103].

Chapter 3

Donders' Law: Assessing the Stability Over Time and the Adaptation to a Visuomotor Disturbance

The pointing task is kinematically redundant if wrist and forearm rotations are considered, thus generally speaking the *CNS* could control the wrist with an infinite set of configurations (among all those allowed by wrist biomechanics). However, according to the background reviewed in the previous chapter, it has been showed that the wrist assumes a unique path-dependent configuration. Such a behaviour is well modelled by the Donders' Law, an empirical model that represents a subject-specific simplifying solution implemented by the *CNS* to reduce the complexity of the wrist controlling during pointing tasks.

Within this chapter, this topic will be further investigated. The first scientific question addressed is whether the Donders' Law can be considered robust in terms of stability over time within subjects. The second one is whether the Donders' Law is violated or not during the adaptation to a visuomotor disturbance provided in the task space.

3.1 Introduction

During the everyday tasks the Central Nervous System (*CNS*) has to deal with motor redundancy while controlling voluntary movements [104, 105, 106, 3]. When it comes to control wrist and forearm rotations for pointing tasks, the CNS faces with the redundancy since the task requires 2 degrees

of freedom (DOFs) while controlling 3 ones (wrist flexion/extension and radial/ulnar deviation and forearm pronation/supination). Previous studies showed that the brain manages the redundancy during the pointing with the wrist by implementing a neural constraint named *Donders' Law*. In other words, the *Donders' Law* poses that the additional DOF is not left uncontrolled, yet it is constrained to lie on a two-dimensional surface, called *Donders' surface*, which was found to be *subject specific* and *volatile* [8, 10, 11, 42]. The adjective *volatile* refers to the contingency that *Donders' Law* can be violated and therefore considered as a "soft" constraint imposed by the brain, rather a physical constraint due to specific biomechanical characteristics. Indeed, violations to *Donders' Law* have been reported when subjects were asked to perform pointing tasks attached to a 3D mechanism, which caused the Donders' Surfaces to disappear [8]. Moreover, violations of *Donders' Law* have been reported also for unconstrained movement of the human arm [107, 108, 109] or for the eye when subjects were instructed to move as fast as possible [110].

However, it is not clear so far whether this law is stable over time [11]. To this aim, in Section 3.2 we studied this aspect. Specifically, we analyzed three indices related to three different aspects of the task: i) motor performance during the task in terms of deviation between an ideal straight line connecting the staring position and the target, ii) reliability of the Donders' Law and iii) specific implementation of the Donders' Law during the tasks. Specifically, the analysis will focus on the temporal assessment of the above-mentioned movement characteristics, testing whether they change within subjects over four different days.

Another aspect that has been poorly investigated so far is whether and how a visuomotor disturbance presented in the task space influences the management of the redundancy during pointing with the wrist. A preliminary study has been conducted in [11], in which the Authors showed that the specific implementation of the Donders' Law does not change if a visuomotor disturbance is provided to subjects. However, this study is limited in terms of structure of the protocol, number of subjects enrolled, and analysis, and no further studies about this topic have been carried out. In Section 3.3 we analyzed the three above-mentioned parameters with and without the presence of a visuomotor disturbance presented to the subjects during the pointing tasks and we tested whether they change over sessions within subjects.

3.2 Assessment of the Danders' Law Stability over Time

3.2.1 Materials and Methods

Subjects

Twelve right-handed healthy subjects (4 male and 8 female, aged between 21 and 34 years old) with neither history of neuromuscular disorders nor previous wrist injuries, were asked to complete a series of pointing tasks with their right wrist in four different days, at least one week apart. Right handedness for all subjects was verified by means of a standard test of laterality (Oldfield test), which has been administered to the subjects before starting the experiments. The research was carried out in accordance with the Declaration of Helsinki and following amendments. All subjects gave written informed consent.

Setup

Subjects were seated and then strapped to an arm-support by appropriate belts to minimize torso, shoulder and elbow movements, so that only wrist rotations were left unconstrained. Wrist rotations were measured by means of a Magneto-Inertial Measurement Unit (M-IMU, MTx-28A33G25 device by XSens Inc.; static orientation accuracy: < 1 deg; bandwidth: 40 Hz), mounted on top of an ergonomic hand-held device, in terms of rotation matrices. The M-IMU, wirelessly connected to a laptop in charge of recording the data, was configured to continuously record the sequence of rotation matrices ($\boldsymbol{R}_i$ related to the i-th samples) with a sampling rate equal to 100 Hz. Before starting the trial, the wrist was oriented in its neutral configuration hereafter denoted as *zero position* [111], which was used as fixed frame for evaluating relative rotations while performing the pointing task [11], [112]. The complete setup is reported in Fig. 3.1.

Pointing tasks were implemented through an interactive MATLAB™ based video-game, in which subjects could see the pointed target in real-time, according to the protocol defined in 3.2.1. For a generic orientation of the hand expressed by $\boldsymbol{R}_i$, the *pointing vector* ($\boldsymbol{n}$) che be evaluated as the first column of the $\boldsymbol{R}_i$:

$$\boldsymbol{n}_i = \boldsymbol{R}_i[1, 0, 0]^T \tag{3.1}$$

During the task, the i-th pointing position projected onto the screen plane was evaluated in real-time and provided to the user as visual feedback.

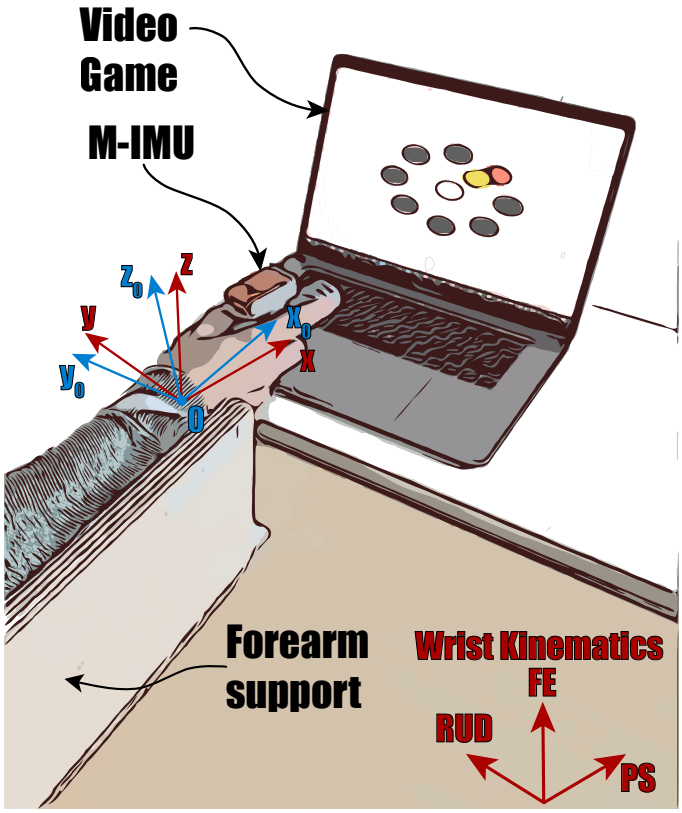

Figure 3.1: Overview of the experimental setup. The wrist kinematics refers to [10]. The blue reference frame refers to the neutral position of the wrist, while the red one is moving, *i.e.* the one recorded by the M-IMU.

Protocol

Subjects were asked to complete the same task four times, in four different days, at least one week apart. They were instructed to move the cursor on the screen towards eight randomly highlighted peripheral targets. The position of the targets has been designed such that subjects are required to rotate the wrist of 15 deg around FE and RUD to hit them, while PS can rotate without constraints. Moreover, all subjects were placed to the same distance between the screen and the center of rotation of the wrist (point 0), according to Fig. 3.1. Once a randomly highlighted target have been reached, the next target was highlighted. A single trial is completed once the subjects reached all eight peripheral targets. In each session day, all subjects performed 30 trials in total and the first 10 trials were used to let subjects experience with the

system and were not included in the statistical analysis. An example of the pointing trajectories for a representative subject are presented in Fig. 3.2.

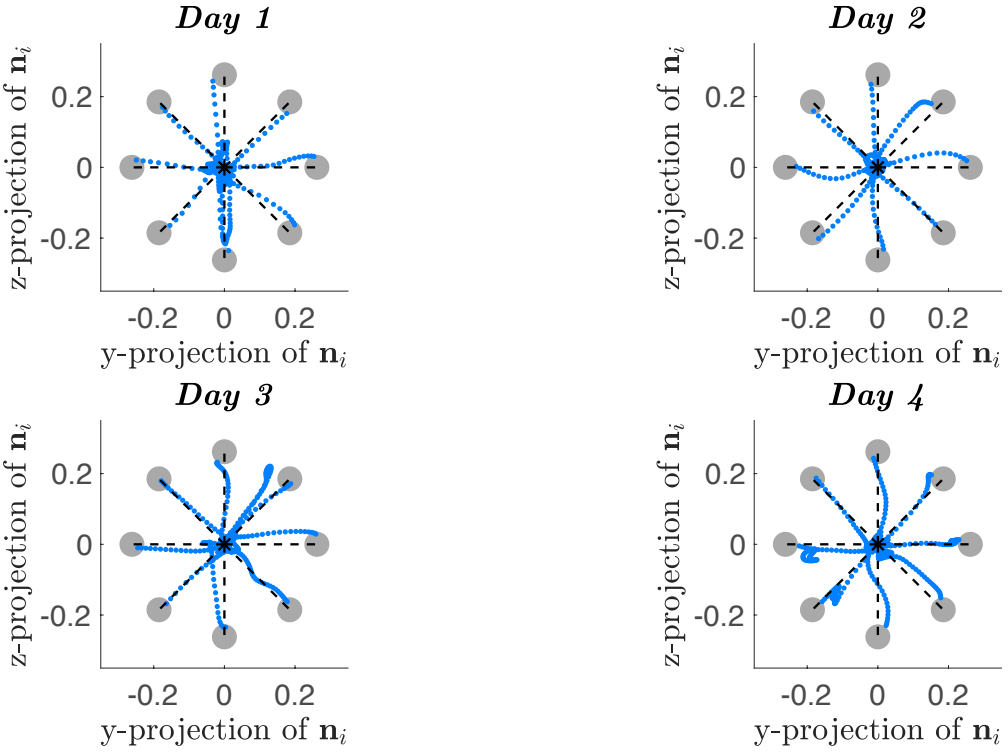

Figure 3.2: Recorded pointing trajectories for a representative subject over days. Blue points represent movements from central position to peripheral targets, while grey circles represents the targets to be reached.

Data Analysis

Given the sequence of wrist rotations $\boldsymbol{R}_i$ relative to each trial, the sequence of rotation vectors $\boldsymbol{r}_i$ is derived as follows:

$$\boldsymbol{r}_i = \frac{1}{1 + R_{i1,1} + R_{i2,2} + R_{i3,3}} \begin{bmatrix} R_{i3,2} - R_{i2,3} \\ R_{i1,3} - R_{i3,1} \\ R_{i2,1} - R_{i1,2} \end{bmatrix} \tag{3.2}$$

According to the specific experimental setup, second and third components of $\boldsymbol{n}_i$ were used to provide real-time visual feedback to subjects.

Despite pointing is a 2-dimensional task, the rotation vector belongs to 3-dimensional space. Indeed, the pointing is a redundant task for the wrist and previous studies demonstrated that r_{ix} depends on r_{iy} and r_{iz} through a

2-dimensional surface, called *Donders' Law* [42], [11], [112]. It is evaluated by means of a least-square fitting, based on the following model:

$$\tilde{r}_{ix} = C_1 + C_2 r_{iy} + C_3 r_{iz} + C_4 r_{iy}^2 + 2C_5 r_{iy} r_{iz} + C_6 r_{iz}^2, \tag{3.3}$$

denoting C_1-C_6 the coefficients computed by the fitting procedure. An example of estimated surfaces for a representative subject are reported in Fig. 3.3.

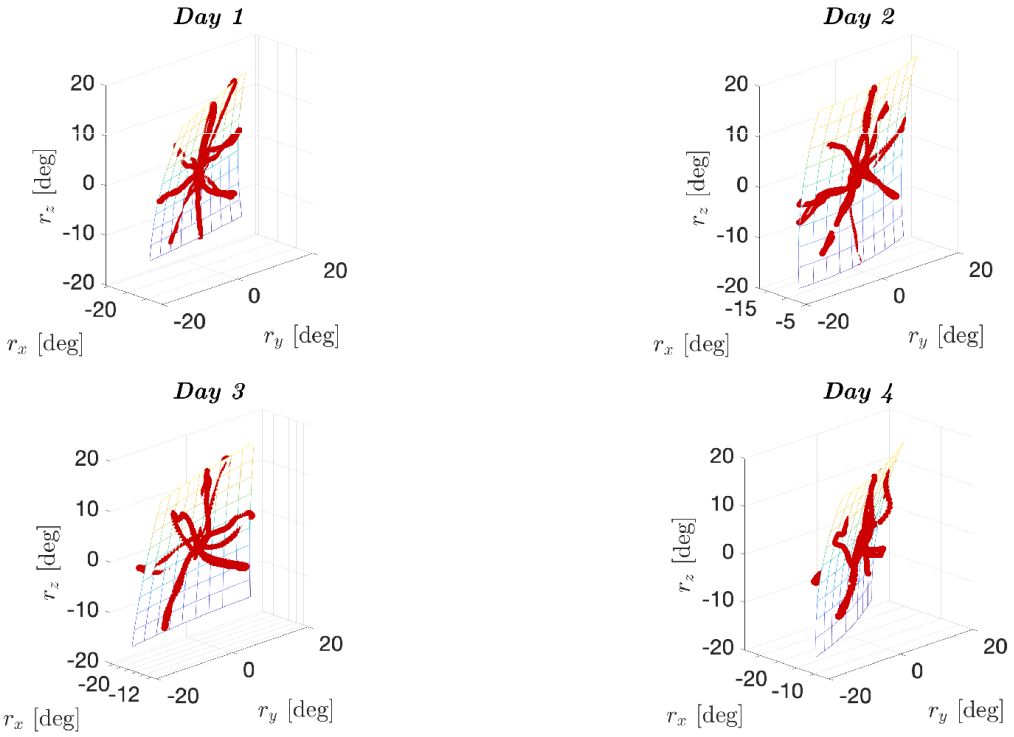

Figure 3.3: Estimated Donders' surfaces for representative subject over days. Red points represents the recorded data with the M-IMU.

In order to assess the stability over time of the Donders' Law, we identified three independent parameters to analyse: i) A_{sum}, ii) *Thickness* and iii) *Shape Index*.

A_{sum} measures the path total deviation from a straight line connecting the starting position to a peripheral target, and vice-versa, for each movement [11, 113]. It provides information about the accuracy in performing the task.

In order to assess the reliability of the Donders' Law we considered the standard deviation of the error between $\tilde{r}_{ix}$ (*i.e.* the fitted rotation around x-axis, according to (3.3) and r_{ix} (first component of the measured rotation

vector, according to (3.2)), named *Thickness*. The lower the thickness, the better Donders' Law predicts the recorded data. Therefore, the *Thickness* denotes how well the subjects implement the Donders' Law.

In addition, in order to discard badly fitted trials, we considered as outliers those trials in which the *Thickness* is above the mean (along all trials of a single day) plus 2 standard deviations. Outliers were defined for all subjects in each day and these trials were not considered in the statistical analysis. The number of trial outliers discarded for each day are reported in table 3.1.

Table 3.1: Outliers discarded on the basis of the computed *Thickness*. The values reported takes into account all subjects for each day.

	Day 1	**Day 2**	**Day 3**	**Day 4**
N. of Trial Outliers	17	16	15	16
Percentage of Trial Outliers	7.08%	6.67%	6.25%	6.67%

To assess whether the implementation of the kinematic control policy changes over days, we considered the shape of the Donders' Surface. To this aim, we considered the *Shape Index*, defined as follows:

$$Shape\ Index = \frac{2}{\pi} atan2(H, \sqrt{H^2 - K}) \tag{3.4}$$

denoting H and K the *Mean Curvature* and the *Gaussian Curvature* of the Donders' surface respectively [114], [10]. Further details can be found in [10]. Being the *Donders' Law* geometrically represented by a 3D surface, *Shape Index* denotes the specific implementation of the Donders' Law, *i.e.* the implemented policy.

Finally, in all cases, we considered only signals from center to target (labelled as "*to*" in Fig. 3.2) in order to computes the above-mentioned parameters.

Statistical Analysis

We firstly checked for the normality of the data by means of the Shapiro-Wilk test [115]. According to the results of the normality test, we run either 1-Way Repeated Measures Analysis Of Variance (RM-ANOVA) or 1-Way Friedman Test in order to assess whether the above-mentioned parameters vary over days. Specifically, we run the analysis considering the 'Days' as the 4-level within subjects independent variable. We used the software JASP [116] to

perform all statistical tests and we selected the significance threshold equal to 0.05 in all cases.

3.2.2 Results

All the above-mentioned indices have been evaluated in each subject for each trial, and then averaged along the 20 trials, thus neglecting the familiarization part.

Subjects improved their performance in terms of accuracy, indeed A_{sum} statistically differs over days ($p = 0.04$, $F = 4.49$; Greenhouse-Geisser sphericity correction method was used), as reported in Fig. 3.4. However, according

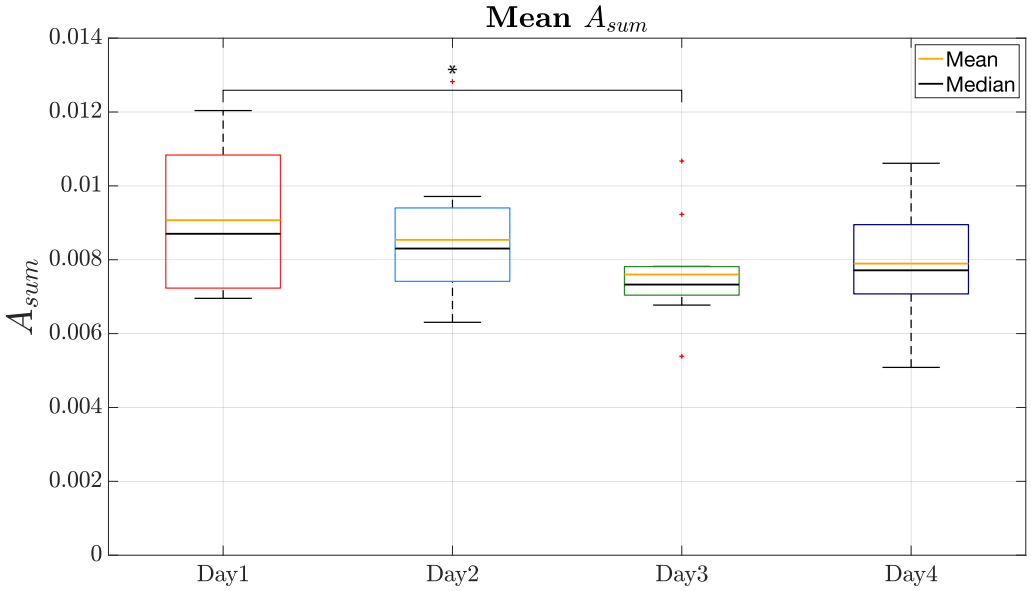

Figure 3.4: Box-plot plot of the A_{sum} averaged along trials.

to the post-hoc analysis implemented, only *Day 1 vs Day 3* showed a significant difference ($p = 0.01$, $t = 3.4$).

Concerning the *Thickness*, firstly it is worth noting that all values computed are below 3 deg, congruently with previous studies on this topic [10]. Concerning the effect of factor *Days*, a similar trend to A_{sum} is reported in Fig.3.5 and confirmed by the implemented RM-ANOVA ($p = 0.03$, $F = 3.24$). Post-hoc analysis revealed that, similarly to A_{sum}, only the difference between *Day 1 vs Day 3* was found to be significant ($p = 0.03$, $t = 3.07$), suggesting that A_{sum} and *Thickness* may be somehow related to each other. To this aim, we run a correlation (by using Spearman's method) between

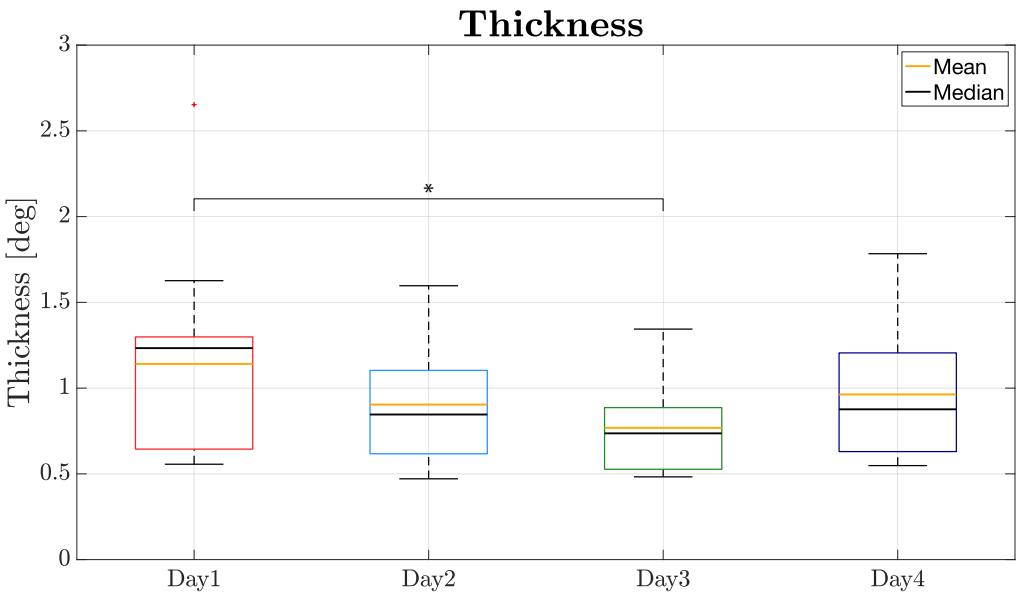

Figure 3.5: Box-plot plot of the *Thickness* averaged across trials, neglecting outliers.

such parameters, whose outcome is presented in Fig. 3.6 ($\rho = 0.62$, $p = 3.82 \cdot 10^{-6}$). We implemented the correlation considering all trials (except for the outliers).

As regards the *Shape Index*, by means of a 1-way ANOVA (considering subjects as independent factor), we confirmed that the peculiar shape of the Donders' surface is subject-specific (see Fig. 3.7), according to previous studies on this topic [8, 10, 11]. Indeed, a significant difference was found along subjects ($p = 1.15 \cdot 10^{-54}$, $K = 281.68$), suggesting that Donders' Law is a subject specific implementation of the redundancy management policy. On the other hand, the RM-ANOVA revealed that *Shape Index* did not change within subjects over the days ($p = 0.74$, $F = 0.28$, Greenhouse-Geisser sphericity correction method was used), as reported in Fig. 3.8. This result suggests that Donders' Law can be reliably used to model subjects specific redundancy management policy.

3.2.3 Discussion

Firstly, subjects presented a learning effect, since A_{sum} significantly reduced over the days (see Fig. 3.4), despite the tasks involve the management of the wrist redundancy. However, a significant reduction has been found also concerning the *Thickness* (see Fig. 3.5), suggesting a possible correlation

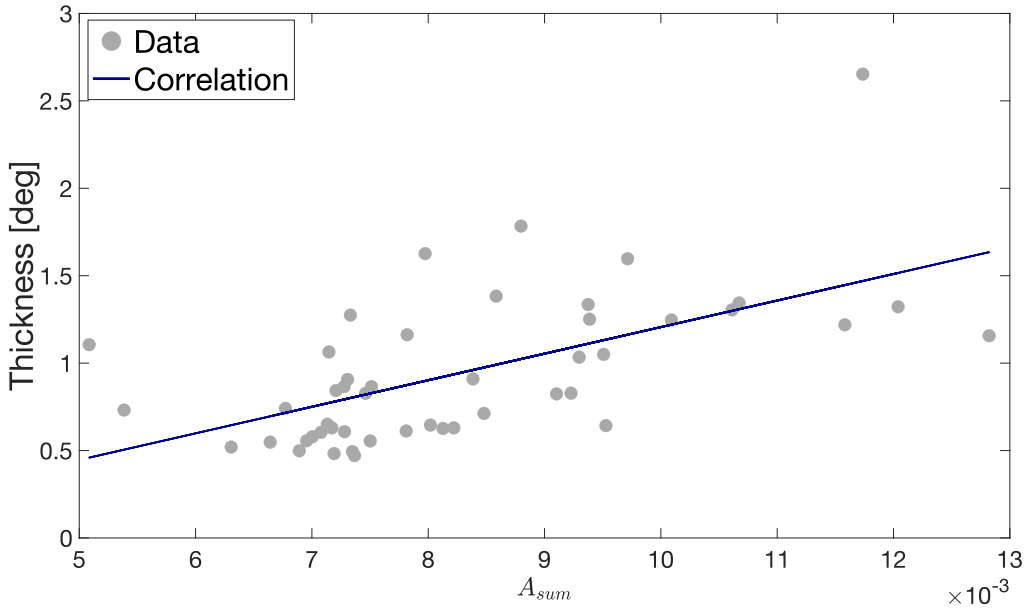

Figure 3.6: Correlation between *Thickness* and A_{sum}. Pearson's $R = 0.62$ with a $p = 3.8 \cdot 10^{-6}$.

between the two parameters. In order to deepen this aspect, we run a correlation between A_{sum} and *Thickness* and we found a significant correlation between the two parameters with a correlation coefficient equal to 0.62 (Spearman's correlation coefficient), suggesting that the more the subjects learn the task, the better they implement the Donders' Law. In other words, the two aspects may be thus coupled. Indeed, reducing the error in the task space and improving the management of the redundancy (in terms of accuracy) may compete in an iterative and concurrent way in the wrist coordination: the more a subject learns to control the redundancy, the lower the errors result. In this way, the brain can develop an internal model focussing step-by-step to a specific part of the whole model to be developed. Such evidences are in line with the most popular theories of human motor control, in which the motor output is the result of a cooperative and iterative process for optimizing all factors involved, *i.e.* the accuracy in performing the task and the management of redundancy (for optimizing the energy spent in performing the task itself) [117, 118, 119].

Concerning the policy implemented, *i.e.* the peculiar choice of the Donders' Law coefficients which reflects the shape of the Donders' surface, we verified that it is subject specific and, above all, it is stable over time, since any statistical difference has been found over days. Therefore, we confirmed that Donders' Law, expressed through the *Shape Index*, may be considered as

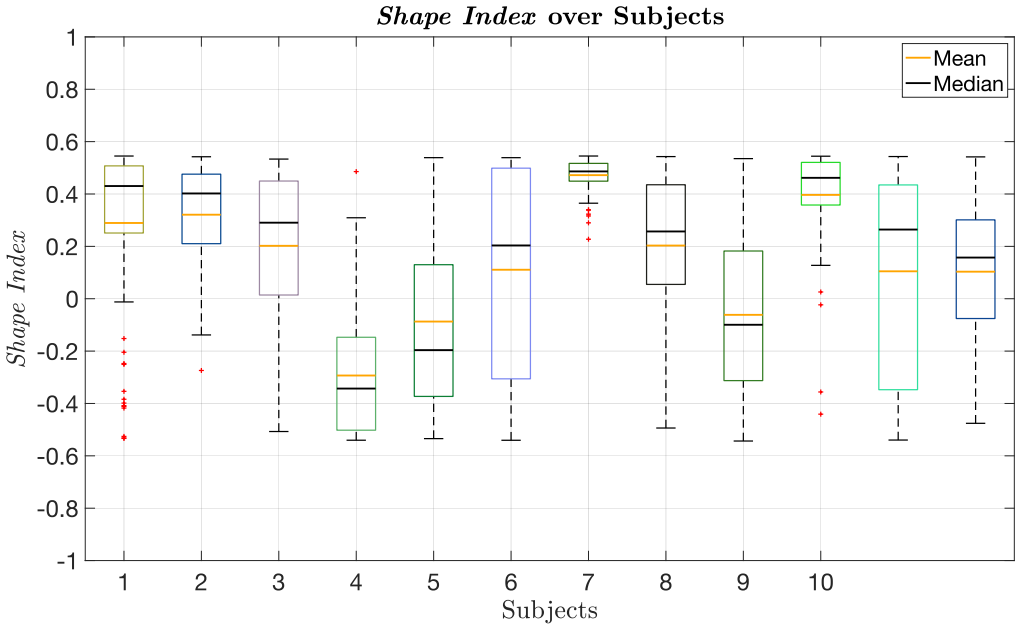

Figure 3.7: Box-plot of *Shape Index* for each subject, considering the trials recorded in all days.

a *personal motor sign*. This aspect may underlie in the subject biomechanical individuality. Indeed, although the redundancy control can be considered as a *soft constraint*, *i.e.* it is not due to any physical constraint since it can be violated in some conditions [8, 42], it could be strictly correlated to the subject specific muscle-skeletal conformation and thus to subject specifici biomechanics [120]. Certainly, this may be affected also from muscle-skeletal injuries or even movement disorders, such as the Parkinson's Disease. Therefore, future works deserve to be implemented in order to investigate this aspect. This finding is in agreement to what has been already demonstrated in previous works, even though different parameters were used [112, 11]. Therefore, we can also conclude that the *Shape Index* may be denoted as a suitable tool for assessing how the redundant control policy is implemented in each subject. On the other hand, we demonstrated that *Shape Index* beside being personal, it is stable over days if task conditions do not change. In other words, due to subject specific biomechanics, the observed behaviour (*i.e.* the *Donders' Law*) might be attributed to a side effect of a control strategy applied to FE and RUD [120].

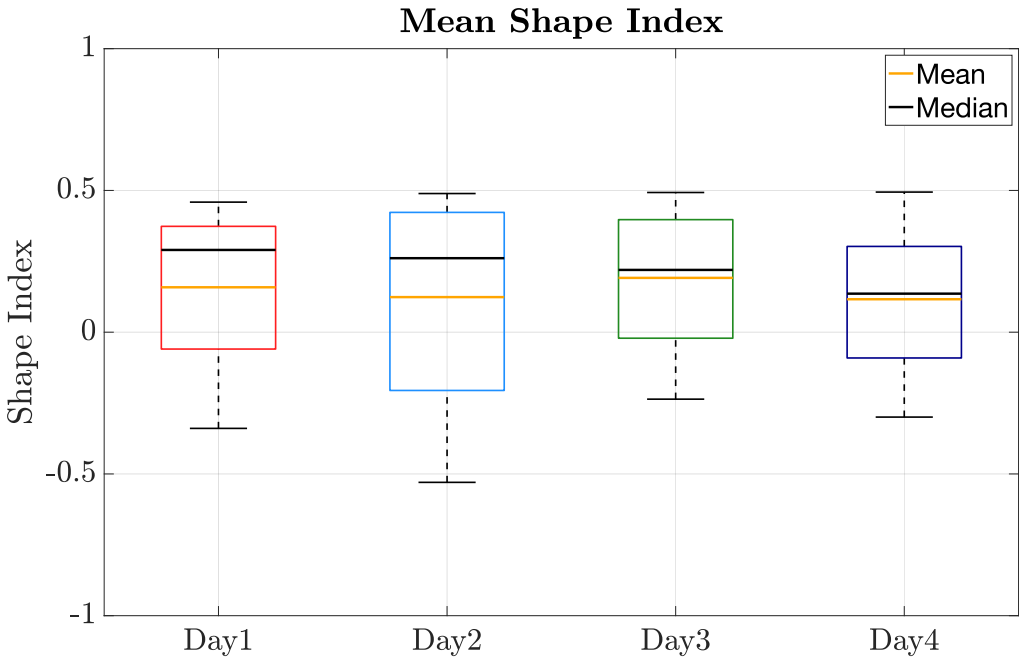

Figure 3.8: Box-plot plot of the *Shape Index* averaged along trials. We discarded thickness trial outliers.

3.3 Assessment of the Danders' Law During Motor Adaptation

3.3.1 Materials and Methods

Subjects

Ten right-handed subjects (4 male and 6 female, aged between 19 and 30 years old) with neither history of neuromuscular disorders nor previous wrist injuries, were asked to complete a series of pointing tasks with their right wrist. Right handedness for all subjects was verified by means of a standard test of laterality (Oldfield test), which has been administered to the subjects before starting the experiments. The study was carried out along the principles laid down in the Helsinki Declaration.

Setup

The setup used for the experiments is the same as the one described in Section 3.2.1 and Fig. 3.1. To briefly resume, the subjects were asked to stay sit with their forearm strapped on a forearm-support, so that only the PS movements were unconstrained. The rotations of the wrist were recorded using an M-IMU (MTx-28A33G25 device by XSens Inc.; static orientation accuracy: < 1 deg; bandwidth: 40 Hz) mounted on ergonomic hand-held device and grasped by the subjects during the whole experiment. The M-IMU was connected to a PC which in real time acquired the rotations of the wrist (expressed as rotation matrices $\boldsymbol{R}_i$, denoting i the i-th acquired sample) which allowed the MATLAB based application to display the current pointed position onto the screen.

Protocol

Subjects were asked to perform a pointing task implemented by means an interactive MATLAB-based video game (see Fig. 3.1 and Fig. 2.3 (A)). Specifically, each trial consists in pointing the eight targets that randomly appeared (one by one) on the screen and then back to the central position. The eight targets are equally distributed in a circle whose radius is defined so that the wrist has to be rotated around either FE or RUD of 15 deg with respect the neutral position [111]. Moreover, the subjects received in real-time the visual feedback of their pointed position via the video-game.

Each subject underwent to the following four sessions:

1. *Familiarization*: 5 trials used to let the subjects fimiliarize with the proposed setup; these trials are not considered in data analysis;
2. *Baseline*: 20 trials, considered as basis values for each subject;
3. *Adaptation*: 40 trials, in which a 30 deg counter clockwise (CCW) visual rotation is fed-back to the subject (*i.e.* the position pointed by the subjects is presented as rotated of 30 deg with respect the real one);
4. *Washout*: 40 trials, in which the visuomotor disturbance is removed.

Between two consecutive trials a 2 s pause is set. Moreover, each task has a time limit, such that if a single target is not reached within 2 s, the next target is highlighted.

3.3.2 Data Analysis

The implemented data analysis recalls the one presented in Section 3.2.1. Specifically, we considered the following parameters:

- *Thickness*: parameter that measures the reliability of the Donders' Law (3.3), *i.e.* the subject accuracy in implementing the Donders' Law;
- *Shape Index*: parameter that summarize the shape of the Donders' Surface, thus denoting how the Donders' Law (*i.e.* the redundancy control policy) is implemented; it is computed according to (3.4);
- Task space related accuracy parameters [113]:
  - A_{sum}: measurement of the total path deviation from a straight line connecting starting and ending point of each movement; in other word it represents the amount of error committed by the subject during the pointing;
  - A_{net}: measurement of the preferential path deviation from a straight line, *i.e.* the side more spanned by the subject during each movement; in other words, it allows providing a deeper estimate of the motor learning, since adaptation and washout are both supposed to induce error, however in different directions [11].
- Adaptation time (τ_{sum}): estimate of time needed for the subjects to adapt to the disturbance (or its removal) both in *Adaptation* and in *Washout* sessions; τ_{sum} has been computed by fitting A_{sum} using a

single-exponential curve, corresponding to a single state learning process over trials of the same session [121], as follows:

$$A_{sum}[t] = A^0_{sum} e^{-t/\tau_{sum}} + A^\infty_{sum}, \tag{3.5}$$

denoting A^0_{sum} the zero value, A^∞_{sum} the value of the error at steady state and τ the time constant; such parameters have been estimated by the MATLAB^{TM} embedded function *fit*, which implements a least square error minimization.

The aim of the statistical analysis is to test whether the above-mentioned parameters differ over sessions, *i.e. baseline*, *adaptation* and *washout*. We firstly checked for the normality of the data by using the Shapiro-Wilk test [115]. Subsequently, according to the results of the normality test, we run either a parametric (Repeated Measure ANOVA) or non-parametric (Friedman Test) 1-Way Repeated Measures Analysis in order to test the difference between sessions in A_{sum}, A_{net}, *Thickness* and *Shape Index*. Moreover, we checked for the difference between *adaptation* and *washout* in τ_{sum} using a paired sample test. Similarly to the first part (Section 3.2), only signals from center to targets were considered (labelled as "*to*"). We used JASP software [116] to perform all statistical tests and we selected the significance threshold equal to 0.05 in all cases.

3.3.3 Results

We computed all the above-mentioned parameters in each trial, for each subject. In order to provide a clearer view of the task performed, the pointing trajectories over sessions for a representative subjects are presented in Fig. 3.9, while the Donders' surfaces estimated for a representative subjects over sessions are reported in Fig. 3.10.

Moreover, all parameters were found to be normally distributed, thus we used RM-ANOVA and t-test (for implementing post-hoc analysis) in all cases except for τ_{sum}, for which we employed Wilcoxon Signed-Rank test. Corrections in post-hoc tests were implemented through the Bonferroni's method.

Motor Learning Assessment

The results related to A_{sum} and A_{net} averaged for all subjects over trials are reported in Fig. 3.11. Both in adaptation and washout sessions, A_{sum} exhibits a sudden increase with respect the end of the previous session. However, it decreases with training, thus showing that motor learning has occurred [122, 11]. Concerning A_{net}, it exhibits a similar behaviour to A_{sum},

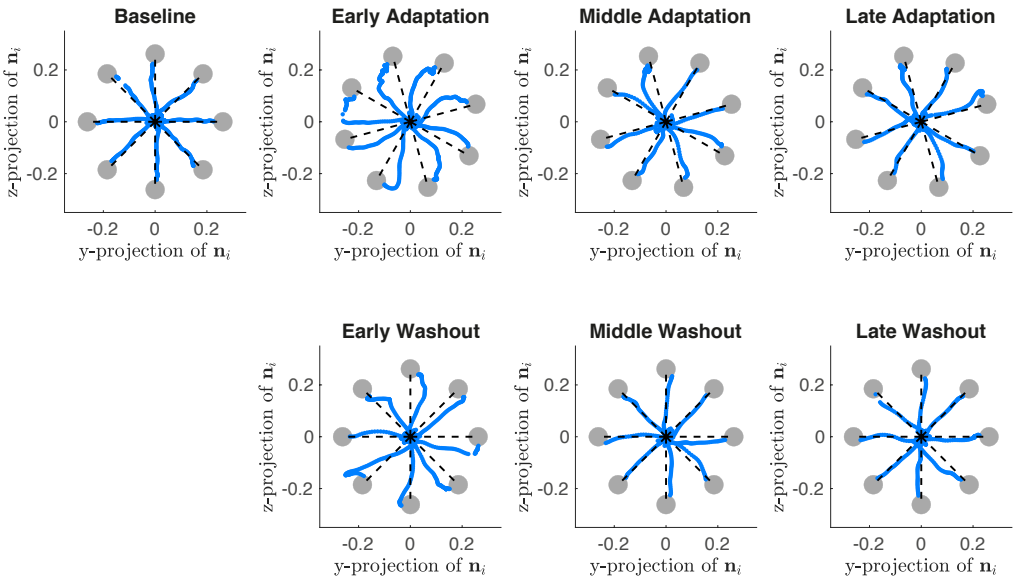

Figure 3.9: Pointing trajectories for a representative subject, presented for *baseline*, *adaptation* (divided into early - trials 1÷10 -, middle - trials 11÷25 - and late - trials 26÷40 - stages) and washout (divided into early, middle and late stages). Blue points represent movements from center to peripheral targets, while grey circles represent the targets that the subjects are asked to point. Moreover, the grey circles in the Adaptation phases are rotated according to the provided visuomotor disturbance (*i.e.* 30 deg CCW rotation).

except for the opposite sign assumed at the beginning of the washout session. This aspect clearly shows the different internal model learnt during *adaptation* and the aftereffect during *washout*.

According to Fig. 3.12, both A_{sum} and A_{net} statistically differ over sessions (A_{sum}: p = $1.89{\cdot}10^{-7}$, F = 41.27; A_{net}: p = $9.17{\cdot}10^{-13}$, F = 186.78, Greenhouse-Geisser sphericity correction was implemented).

Concerning A_{sum}, post-hoc tests revealed a significant difference in all cases: *baseline vs adaptation* (p = $1.18{\cdot}10^{-7}$, t = -9.06), in *baseline vs washout* (p = $7.93{\cdot}10^{-4}$, t = -4.02) and in *adaptation vs washout* (p = $1.70{\cdot}10^{-4}$, t = 5.04). Similar results were found concerning A_{net}. Indeed, a significant difference was found in all cases: *baseline vs adaptation* (p = $2.49{\cdot}10^{-8}$, t = -10.05), *baseline vs washout* (p = $8.42{\cdot}10^{-8}$, t = 9.27) and *adaptation vs washout* (p = $5.23{\cdot}10^{-13}$, t = 19.32).

Finally, τ_{sum} during adaptation statistically differs from washout (p = $5.86{\cdot}10^{-3}$, W = 53), confirming that while performing the same task with a visuomotor disturbance applied, the adaptation time takes longer then adapting to a previously experienced condition. The box-plot of τ_{sum} for all subjects is reported in Fig. 3.13. For the sake of the completeness,

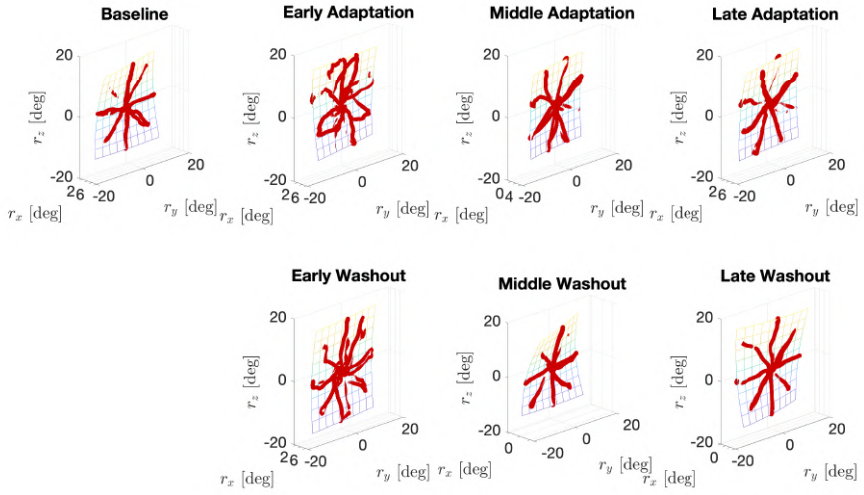

Figure 3.10: Donders' surfaces for a representative subject, presented for *baseline*, *adaptation* (divided into early - trials 1÷10 -, middle - trials 11÷25 - and late - trials 26÷40 - stages) and washout (divided into early, middle and late stages). Red points represent recorded wrist rotations.

the exponential fitting of the average A_{sum} is also reported in Fig. 3.11, superimposed to recorded data.

Wrist Redundancy Management Assessment

According to Fig. 3.14, *Thickness* is always below to 1.27 deg in *Baseline*, 2.31 deg in *Adaptation* and 2.13 deg in *Washout*, congruently with previous studies on this topic [112, 11, 42] and results obtained in Section 3.2.1. Moreover, *Thickness* significantly differs over sessions within subjects ($p = 5.35 \cdot 10^{-5}$, $F = 7.09$) and post-hoc tests revealed a significant increase with respect the *Baseline* both in *Adaptation* ($p = 0.01$, $t = -3.20$) and in *Washout* ($p = 0.01$, $t = -3.32$). Conversely, any statistically significant difference was found concerning *Adaptation vs Washout*.

Because *Thickness* describes how well subjects implement the Donders' Law, it may be considered as a parameter that lies in between the motor learning and the motor redundancy management. Indeed, according to Fig. 3.12 and Fig. 3.14, an increase of A_{sum} corresponds to an increase of the *Thickness*. Similarly to the data analysis presented in Section 3.2, we investigated this aspect by implementing a correlation between A_{sum} and *Thickness*. To this aim, we considered the values averaged along trials of each session, we grouped all data from all subjects and we run the correlation by using the Spearman's technique. According to Fig. 3.15, the correlation

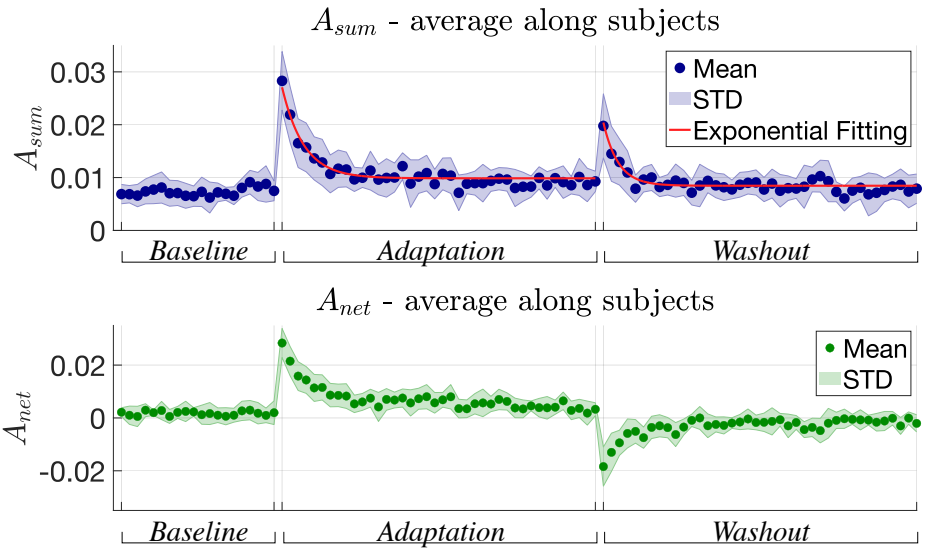

Figure 3.11: Behaviour of A_{sum} and A_{net} over trial. Moreover, according to (3.5), the fitting curve is superimposed on A_{sum} data.

resulted to be statistically significant (p = 0.03) and characterized by a ρ = 0.4.

The presented results did not contain outliers. Similarly to Section 3.2.1, we considered as outliers those trials (for each subject and each session) characterized by a *Thickness* that is above the mean (along all trials of the same session) plus 2 standard deviations. In addition, since *Shape Index* can be estimated only assuming the Donders' Law as verified, we discarded such outliers also for estimating *Shape Index*. The number of trial outliers discarded in all subjects for each session are reported in table 3.2.

Table 3.2: Thickness trial outliers discarded. For each trial thickness and in each subject, the threshold was set to the sum of the mean and two times the SD evaluated for all subjects in a single session day. It is worth underlying that the discarded outliers refer to all subjects (10).

	Baseline	***Adaptation***	***Washout***
N. of Trial Outliers	14/200	26/400	22/400
Percentage Trial Outliers	7%	6.5%	5.5%

Regarding *Shape Index* and according to Fig. 3.16, despite a decreasing trend in *Baseline vs Adaptation* and *Baseline vs Washout*, no statistical difference has been found over sessions (p = 0.12, F = 2.75, Greenhouse-

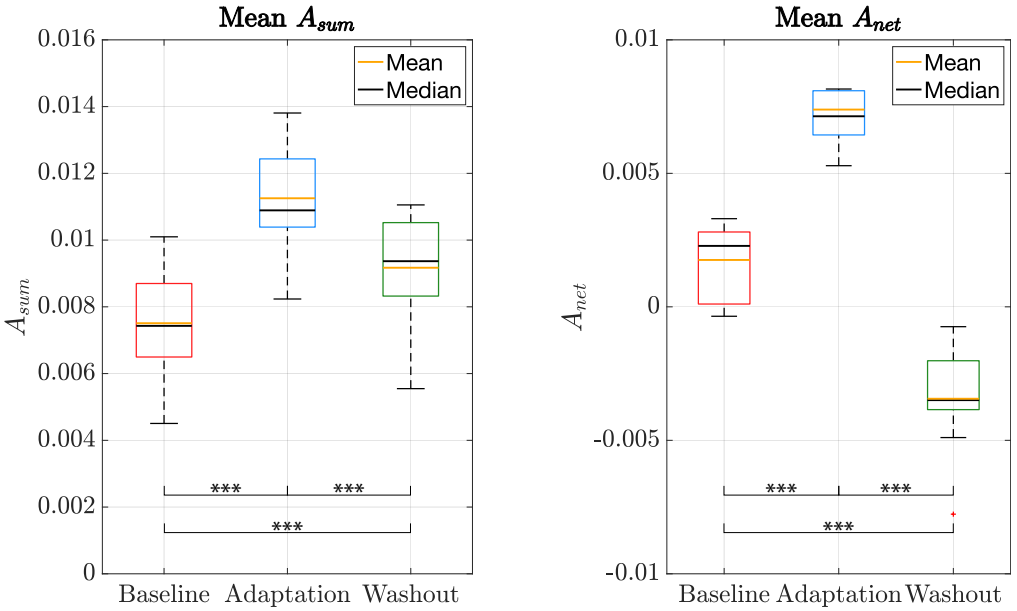

Figure 3.12: Boxplots related to A_{sum} and A_{net} averaged along trials of the same session.

Geisser sphericity correction method was applied). However, *Shape Index* resulted to be subject specific, which means that every subject has a specific way to implement the Donders' Law, as if it is a peculiar *motor sign* [8, 10, 11, 42]. Indeed, *Shape Index* was found to be significantly different over subjects (p ¡ 0.0001, Z = 565.12) by using a Kruskal-Wallis test (considering all trials). The distribution of the Shape Index over subjects is reported in Fig. 3.17.

3.3.4 Discussion

The analysis carried out on the task space errors (*i.e.* A_{sum} and A_{net}), revealed that despite the task involved the management of the wrist redundancy, motor learning did occur. Indeed, according to Fig. 3.11 and Fig. 3.12, when the visuomotor disturbance is provided (and when removed) in the very first trials subjects show suddenly decrease of their performance (in terms of error committed). However, training allow subjects to learn the new internal model, leading to an improvement of their performance. Moreover, another finding is that, according to other studies on motor learning, subjects take longer to learn a new internal model, *i.e.* pointing with a visuomotor disturbance, then learning again an already experienced task condition. In-

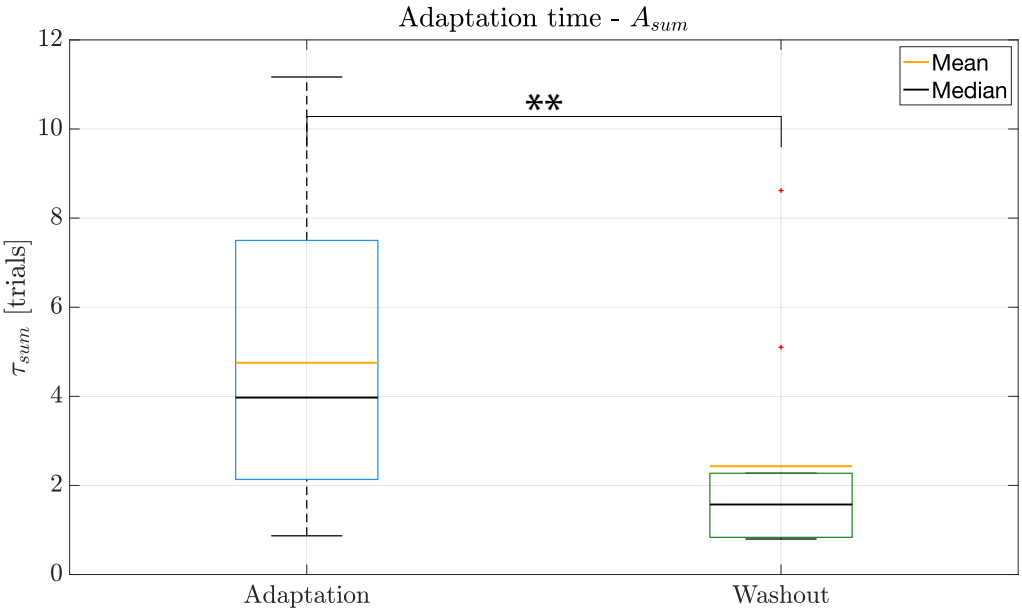

Figure 3.13: Boxplot of τ_{sum} of all subjects estimated by applying (3.5) on A_{sum} recorded.

deed, the estimated time constant, by using a single state learning model (see equation 3.5), related to the *Adaptation* is significantly higher then the one related to the washout (see Fig. 3.13). These two aspects confirm that despite the redundancy of the task, motor learning occurs similarly to classical and widely studied problems of adapting to a constant disturbance [122, 123, 124]. Moreover they confirm the preliminary findings presented in [11].

Concerning the wrist redundancy management, the first finding to be noticed is that the use of Donders' Law to manage redundancy is preserved during the adaptation to a visuomotor disturbance, since, in all cases, the thickness obtained is below 3 deg, congruently with previous studies on this topic [112, 11] and the results presented in 3.2.2. However, during both *Adaptation* and *Washout*, *Thickness* is higher then *Baseline* (see Fig. 3.14, suggesting that the presence of the disturbance could influence how well subjects implement the Donders' Law, in terms of accuracy. A possible explanation to this aspect may underlie in the hierarchical processes that occur during motor learning [121, 125]. Learning how to adapt to a disturbance in the task space, may have a higher priority than managing the redundancy. Specifically, when subjects face with a task to which they have to adapt, the brain might be more focussed in reducing task space error than optimally controlling the redundancy. Likely, if the subjects could train for longer,

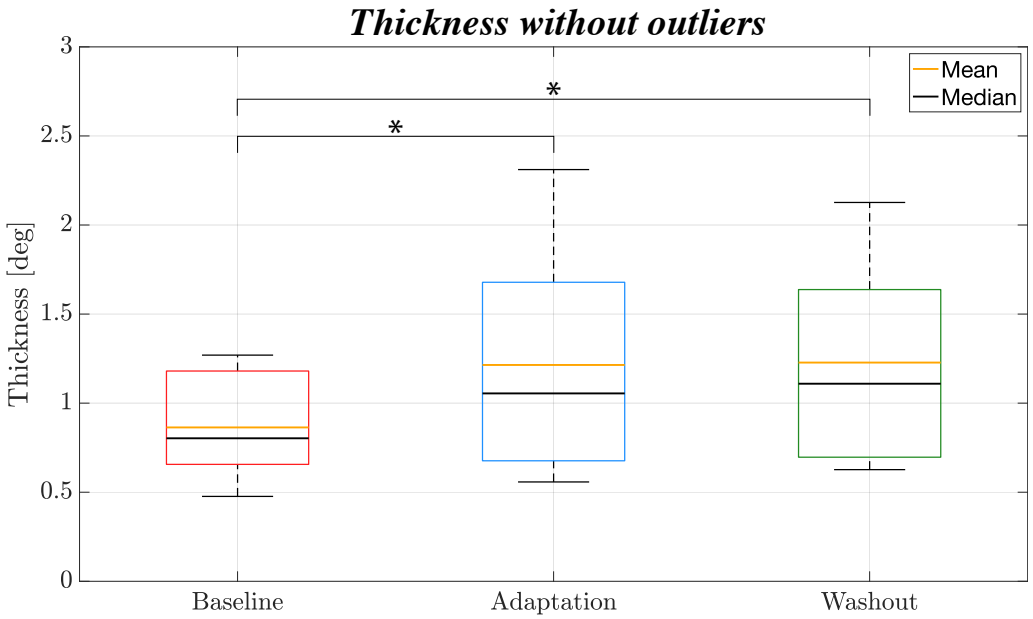

Figure 3.14: Boxplot of *Thickness* over sessions. Outliers are not included.

such that the error (A_{sum}) becomes equal to the one committed during the baseline (if possible), also the *Thickness* should settle to the baseline values. However, this is just a speculation and future works will be devoted to experimentally investigate this aspect.

On the other hand, *Shape Index* was not found to be different over sessions (see Fig. 3.16), similarly to preliminary findings reported in [11]. This result can be interpreted so that the specific policy (*i.e.* the Donders' Law) used to combine wrist DOFs for solving the redundancy does not change when subjects have to adapt to a task-space visuomotor disturbance. This finding suggests that, even though the redundancy solutions are less constrained to lie on the Donders' surfaces obtained during baseline, the specific policy used to control the wrist in a kinematically redundant task is not disrupted. In other words, the Donders' surfaces remain similar themselves. In addition, we confirm previous results available in literature in which it is reported that Donders' Law, expressed as Donders' Surfaces, is subject specific (see Fig. 3.17) [112, 11]. Therefore, by recalling also that *Shape Index* does not change over days (see Section 3.3), it can ultimately defined as a subject-specific motor sign and eventually used as bio-marker for neurological pathologies that involve neuromuscular or muscle-skeletal disorders, such as Parkinson's Disease [53] or job-related disorders [126].

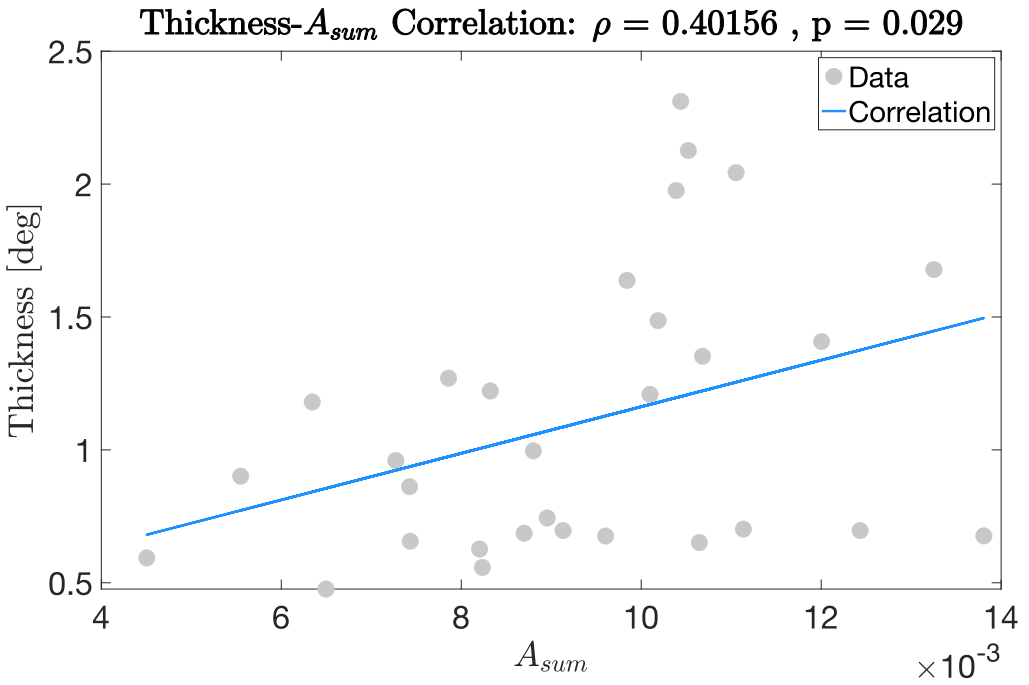

Figure 3.15: Correlation between *Thickness* and A_{sum}: p = 0.03, $\rho = 0.4$.

3.4 Conclusions

In this work we aimed at studying the problem of redundancy management of the wrist during pointing tasks. We studied two different aspects of this topic: i) whether the Donders' Law is stable over days for a single individual (see Section 3.2) and ii) whether it is influenced by a visuomotor disturbance provided in the task space (see Section 3.3). To this aim, we enrolled two group of subjects and we studied the two scientific questions separately. Concerning the first scientific question (Section 3.2), we found that *Shape Index* is stable over time (days). In other words, *Shape Index* that defines the peculiar shape of the Donders' Surface, which in turn represents the geometrical representation of the Donders' Law, does not significantly differs over days. This finding suggests that Donders' Law can be considered as a reliable model to describe redundancy control policy. On the other hand, in Section 3.3 we demonstrated two aspects related to wrist redundancy during pointing tasks. The first one is that motor redundancy persists even though subjects have to adapt to a visuomotor disturbance. The second aspect is that the control policy implemented, *i.e.* the *Shape Index*, does not change (significantly) between sessions characterized by the presence of a visuomo-

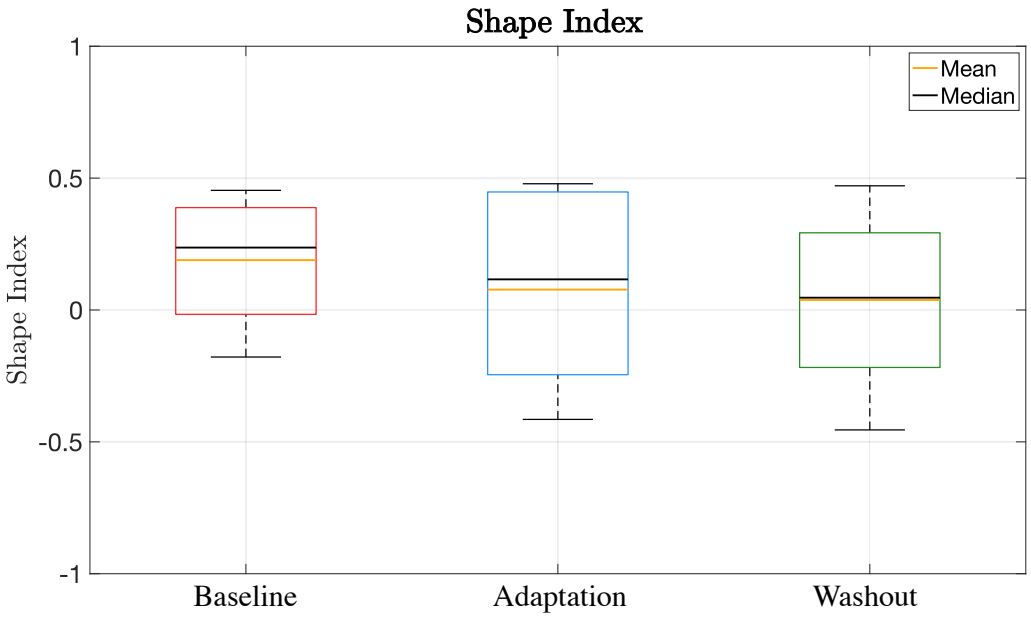

Figure 3.16: *Shape Index* over sessions.

tor disturbance. Moreover, in both studies we obtained that *Shape Index* is subject-specific.

The main conclusions that emerge from the two experiments are the following:

- there is a correlation between the accuracy in the task space (A_{sum}) and and the accuracy in implementing the Donders' Law (*Thickness*);
- the specific solutions that subjects use to manage redundancy, *i.e.* the shape of the Donders' surfaces, remain unaltered both over time (in terms of days) and in presence of a visuomotor disturbance provided in the task space.

Future works will aim at studying wrist redundancy management during pointing tasks in subjects affected by Parkinson's Disease, in order to define novel protocol for assessing the motor symptoms of the pathology and optimizing its treatment [62, 127]. In addition, we will test the pointing with the wrist during non-invasive stimulation techniques of the brain, *e.g.* transcranial Direct Current Stimulation (tDCS) [128], in order to investigate which are the brain areas mainly involved in managing the redundancy of the wrist.

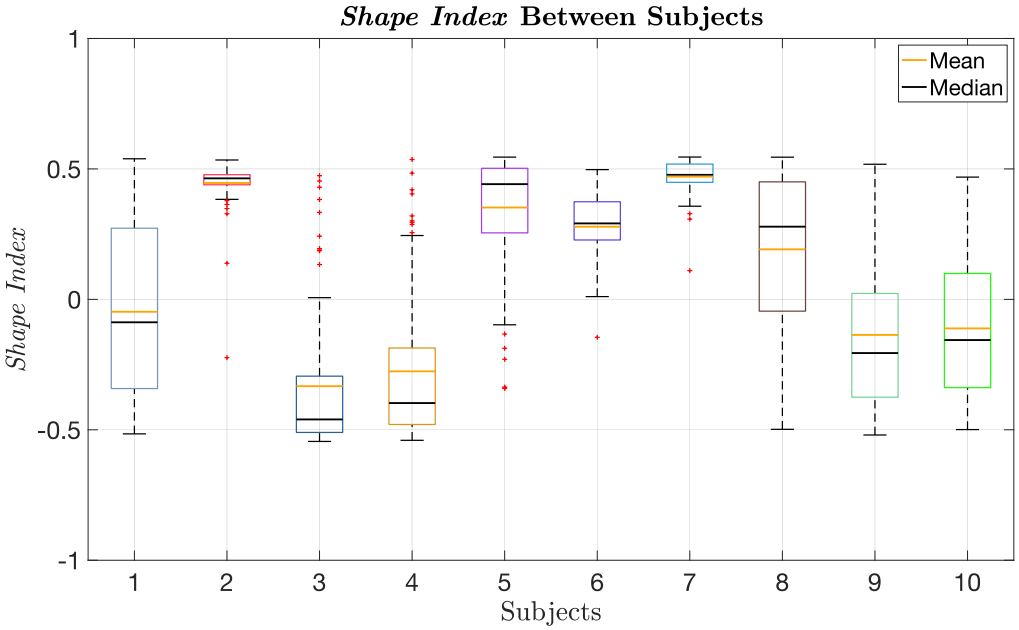

Figure 3.17: *Shape Index* over subjects, including all trials.

Chapter 4

PDMeter: a Wearable Robot to Study the Wrist Impedance

As reviewed in Chapter 2, the modulation of the impedance is the simplifying solution adopted by the *CNS* to implement a safe, graceful and efficient human-environment interaction. Moreover, this capability is significantly reduced when a movement disorder (*e.g.* the Parkinson's Disease) occurs.

Currently available devices are not suitable to perform an estimation of the wrist mechanical impedance, declined in the wrist rigidity in the Parkinson's Disease, within unstructured environments. Moreover, this aspect becomes crucial when considering the Parkinson's Disease, in which such devices would allow performing a continuous (at-home) and quantitative assessment of the wrist rigidity, leading to an overall optimization of the clinical therapy.

To this aim, the present chapter will present the design and the experimental validation of a portable wrist exoskeleton in estimating wrist impedance/stiffness both in healthy subjects and in PD patients.

4.1 Introduction

Human wrist plays a crucial role in performing interactive tasks, such as activities of daily living (ADLs) or occupational, recreational and sport activities. If we look such motor tasks under the point of view of the human motor control, what emerges is the astonishing capability of the Neuromuscular System to implement a stable, fast and safe interaction control of the joints enrolled in the movement. Such a capability may arise from the modulation of mechanical impedance, *i.e.* the general dynamical mapping between movement and force/torque, leading to an effective and energy-efficient stabilitazion of unstable dynamics [43, 67, 36, 4]. Although in the past few decades several researchers focussed in estimating upper limb passive impedance and in particular its statical component, *i.e.* the passive stiffness [34, 14, 129, 35], fewer studies investigated the impedance of the wrist. Recently, few works described the passive stiffness of the wrist [47, 48, 49, 51] and even less the passive wrist impedance [45, 46]. Nonetheless, all these studies rely on cumbersome robotic devices which are not suitable to investigate wrist impedance neither in unstructured environments, nor during performing ADLs. Therefore, due to their intrinsic limitations, such systems cannot be employed in estimating the active stiffness of the wrist, which differently to the passive one it takes into account also the voluntary component of the movement.s Indeed, measuring the *passive wrist impedance* means gently perturb the wrist and record the induced movement, *i.e.* position, velocity and acceleration. To this aim, researchers employed bulky and expensive robots, typically designed for rehabilitation purposes, which need to be used in well-structured environment. On the other hand, in the Authors' knowledge, no one has implemented so far an estimation of wrist impedance in unstructured environments using portable robotic devices, although it is crucial for studying the human motor control. Indeed, measuring the wrist impedance in unstructured environments, would enable to continuously record such a source of information, even during ADLs, leading to develop new experimental protocols, which would allow to further investigate the human motor control during active and interactive task.

Measuring joint impedance in unstructured environment may be of great interest also to study neurological disorders, such as Parkinson's Disease (PD), in order to assess the disease in clinical settings or even at home, being the PD related rigidity well described by the wrist impedance [65]. The PD is an neurological disorder with an overall prevalence of 0.3%, increasing up to more than 3% in the population above 80 years old, and an incidence estimated to range between 5 to 35 cases per 100'000 individuals each year [53]. Its three cardinal motor symptoms are *bradykinesia*, *resting tremor* and

rigidity, which is clinically defined as the increased resistance in response to the passive motion of joints. Despite the disease can be symptomatically treated using drugs acting on the dopamine pathway, such as *L-DOPA* [55], dopaminoagonists [56], continuous biochemical infusion of *L-DOPA* [57], or Deep Brain Stimulation [58], patients still suffer of wide fluctuations of the symptoms, reflecting the fluctuations of dopamine level into the brain. Therefore, a continuous daily motor monitoring may help in patients' management [59]. The clinical assessment of PD is performed on the basis of rating scales and the most used is the MDS-UPDRS, which mainly focuses on the wrist and the elbow joints for what concerns the clinical rigidity assessment of the upper limb [54]. Anyhow, these scales may suffer of objectiveness lacking, because they are dependent on the expertise of the clinicians, and their administration is time consuming [60].

Wrist rigidity is a clinically assessed parameter and one of the physical quantities that best fits with its definition is the *wrist stiffness*, i.e. the static part of the torque-angle relationship at the wrist joint. While Wearable motion sensors, such as Magneto-Inertial Measurements Units (M-IMU), have been successfully used to describe the most relevant PD motor symptoms [130] such as bradykinesia [61], [62], tremor [63], [64], and axial symptoms involving gait, balance and posture [131], [132], the estimation of joint stiffness requires the use of an actuated system which provides mechanical perturbation to the joint under analysis. For this reason, an assessment of rigidity in an unstructured environment has been poorly investigated since it is hard to achieve with instrumentation currently available [51].

To date, in order to quantitatively assess the rigidity, researchers have focused on different joints and considered either *automatic systems* [133], [134] [135], [136], or *manual systems*, i.e. unactuated [65], [137], [138], [139], [140], [141]. On the other hand, the wrist stiffness has been widely measured in healthy subjects by using bulky and general purpose *robotic systems* [49], [48], [46]. Commonly, automatic and robotic systems used to measure rigidity and wrist stiffness are not specifically designed for such a purpose; rather they are conceived mostly for rehabilitation applications, thus embedded with bulky high-torque actuators. This aspect strongly hinders their employment in unstructured environments. Conversely, manual systems are less complex, purposely designed to be portable. Nonetheless, such devices require the presence of a human operator who provide the mechanical perturbation, since they are not actuated.

In this scenario, we focussed on the design of a portable wrist exoskeleton, hereafter called PDMeter, to achieve the following objectives:

1. to estimate wrist stiffness/impedance in unstructured environments;

2. to define novel paradigms for estimating the wrist stiffness/impedance during the activities of daily living, in order to improve the knowledge on PD and its abnormalities in motor control [67].

3. to implement a continuous daily motor monitoring of PD patients for optimizing the treatment of the pathology [142, 59];

4. to perform the assessments mainly in non-clinical environments, in order to reduce the costs and personnel time;

4.2 PDMeter Design

After an accurate analysis of the state of the art, we defined the following design requirements:

- portable and long-term wrist wearable robotic device;
- two working modalities: The design goal was to conceive a compact and portable device, suitable to be worn continuously and comfortably for few hours at home. From a functional point of view, we identified two working modalities:
    1. *Transparent Mode* (TM): the device is supposed to be as transparent as possible to the user's action while she/he is performing tasks that involve both wrist Flexion-Extension (FE) and Radial-Ulnar Deviation (RUD).
    2. *Measuring Mode* (MM): the device has to measure the wrist FE stiffness by applying a low torque to the wrist around FE and measuring the induced angular displacement.

We adopted a mechatronic approach that will be presented in the rest of this section.

4.2.1 Mechanical design

The number of the Degrees of Freedom (DOFs) of the kinematic chain has been determined employing the Chebychev–Grubler–Kutzbach criterion [143]:

$$F = \lambda(l - j - 1) + \sum_{i=1}^{j} f_i. \tag{4.1}$$

Equation (4.1) allows evaluating the number of DOFs (F) of the whole closed mechanism (PDmeter and human chain) assuming as known the number of independent links (l), the number of joints (j) and the sum of the DOFs for each joint (f_i) that compose the closed kinematic chain. Concerning λ, it is a parameter whose value is equal to 6 when considering 3D movements. When the user wears the device, it has to comply with both the two working modalities above defined. This condition allowed us to to define that the number of DOFs needed is equal to 2 ($F = 2$), leading to $l = j$ and $\sum_{i=0}^{j} f_i = 8$. Thus, the kinematic structure of the PDMeter has been conceived to consist of 5 revolute joints (see Fig. 4.1):

- three joints have their axes parallel to human RUD axis, enabling movements along RUD (hereafter referred as the *RUD chain*);
- two joints have their axes parallel to human FE axis (hereafter referred as the *FE chain*);

The described kinematic solution is presented in Fig. 4.7 that shows also the whole structure of the PDMeter, including the actuator. Concerning the

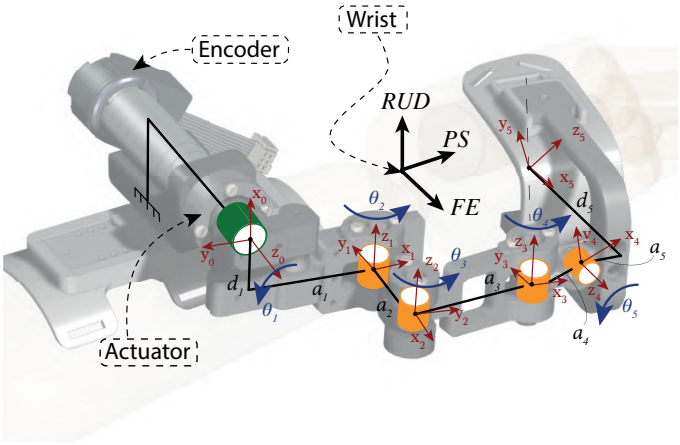

Figure 4.1: Overview of the PDMeter structure. The frame shows the rotation axes of the three joints of the wrist, i.e. RUD, FE and Prono-Supination (PS). Furthermore, the model of the kinematic structure is superimposed and all the reference frames are placed according the Denavit-Hartemberg criterion [144].

actuation system, it has been designed in order to find a trade-off between the two working modalities (TM and MM), aiming to optimize both the overall weight and size of the device. In this regard, we defined the requirements for the overall size, the overall weight and the range of motion (ROM) to guarantee the user movements along both FE and RUD (expressed in table

4.1). Moreover, we defined the 1-DOF planar model of the mechanism, i.e. its projection onto the plane of the FE movements. This planar model is presented in Fig. 4.2, in which:

- the revolute joint 1 corresponds to the actuator (green circle);
- the prismatic joint represents the model of the passive revolute joints of the RUD chain in the plane of FE movements (the orange rectangle);
- the pink revolute joint is the model of the wrist FE.

Table 4.1: Mechanical requirements for the PDMeter system. The mobile part of the structure is meant the links going from m_1 to m_5, whilst concerning the mass of the hand we referred to [145]. Regarding the wrist rotations, we referred to [146]: positive FE rotations mean wrist flexion, while negative FE rotations mean wrist extension; positive RUD rotations mean ulnar deviation, while negative RUD rotations mean radial deviation.

Parameter	***Maximal value***
Overall size of the mobile elements	150 mm
Overall mass of the mobile elements	300 g
Hand mass (m_6)	480 g
FE ROM	$-40\ deg \div +20\ deg$
RUD ROM	$-20\ deg \div +25\ deg$

During TM, as said above, the system has to follow the user movements, being as transparent as possible. Thus:

- the driver of the mechanism is the FE joint ($\varphi_{FE}(t)$);
- the actuation system can be thought as a passive joint.

In this regard, applying the *principle of virtual work*, and neglecting the contribute of the friction at the joints, the dynamics can be expressed by the following equation:

$$\tau_M \delta\varphi_1 + \sum_{i=1}^{5} \boldsymbol{P_i} \cdot \delta \boldsymbol{G_i} = \sum_{i=1}^{5} m_i \ddot{\boldsymbol{G}}_{\boldsymbol{i}} \cdot \delta \boldsymbol{G_i} + \sum_{i=1}^{5} I_i \ddot{\varphi}_i \delta\varphi_i, \tag{4.2}$$

in which:

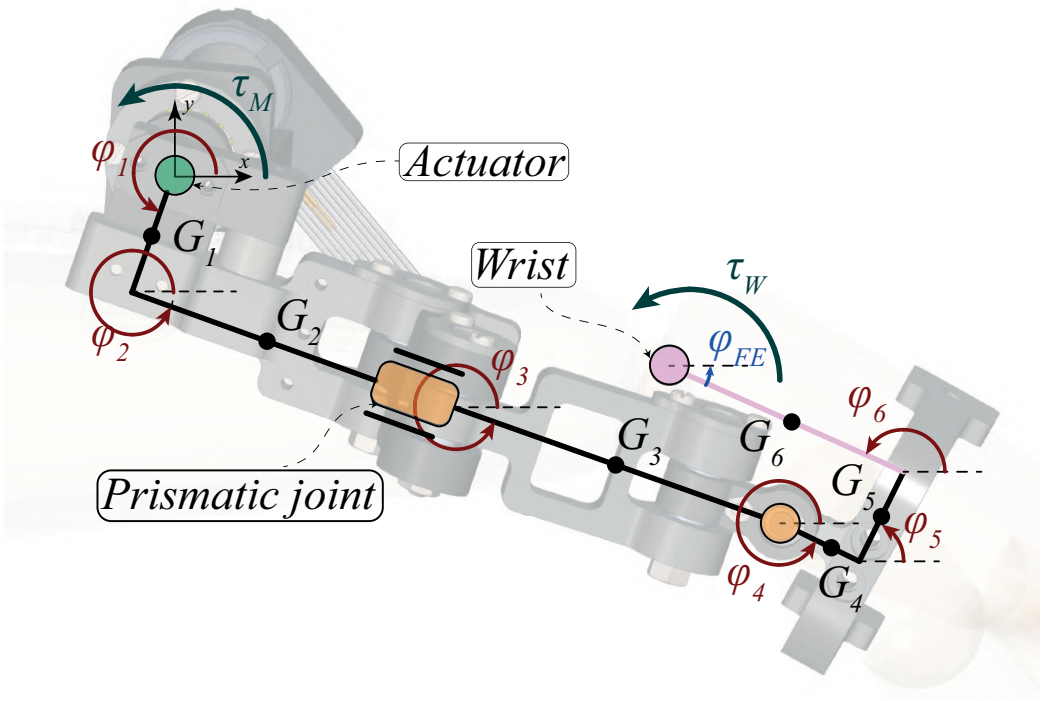

Figure 4.2: Kinematic model of the PDMeter projected onto a plane parallel to the *RUD-PS* plane.

- $\boldsymbol{P_i} = m_i\boldsymbol{g}$ is the weight force vector of the i-th link;
- $\boldsymbol{G_i}$ is the position of center of mass of the i-th link (black circle in Fig. 4.2), $\delta\boldsymbol{G_i}$ its infinitesimal variation and $\ddot{\boldsymbol{G}}_{\boldsymbol{i}}$ its acceleration.
- I_i is the moment of inertia of the i-th link;
- τ_M is the torque applied by the actuation system;
- φ_i is the i-th joint variable, $\delta\varphi_i$ its infinitesimal variation, while $\ddot{\varphi}_i$ is the i-th joint angular acceleration.

In order to define a value of τ_M that complies with the natural motion of the wrist during ADLs, we defined the wrist trajectory along FE as a fifth-degree polynomial [147] characterized by the following boundary conditions [146]:

$$\begin{cases} \varphi_{FE}(0) = -60\ deg, \varphi_{FE}(t_{end}) = 60\ deg \\ \dot{\varphi}_{FE}(0) = 0\ \frac{deg}{s}, \dot{\varphi}_{FE}(t_{end}) = 0\ \frac{deg}{s} \\ \ddot{\varphi}_{FE}(0) = 0\ \frac{deg}{s^2}, \ddot{\varphi}_{FE}(t_{end}) = 0\ \frac{deg}{s^2} \\ t_{end} = 0.3s \end{cases} \tag{4.3}$$

On the other hand, during MM the actuator must exert a load to the user's wrist along FE, i.e. the driver of the mechanism is the actuator, while the wrist is passively moved. Thus, in this condition the dynamics is expressed by the following equation:

$$\tau_M \delta\varphi_1 + \tau_W \delta\varphi_{FE} + \sum_{i=1}^{6} \boldsymbol{P_i} \cdot \delta \boldsymbol{G_i} = \sum_{i=1}^{6} m_i \ddot{\boldsymbol{G}}_{\boldsymbol{i}} \cdot \delta \boldsymbol{G_i} + \sum_{i=1}^{6} I_i \ddot{\varphi}_i \delta\varphi_i, \qquad (4.4)$$

in which all terms are the same of (4.2) except for:

- all inertial terms and the weights forces take into account also the hand (link 6 in the planar model presented in Fig. 4.2);
- the actuation system must be able to exert a known torque to the wrist, expressed as τ_W.

The value of τ_W depends on the specific algorithm implemented for measuring the wrist stiffness. Specifically, in this regard we took into account two different solutions. The first one (MM 1) basis on an exertion of a known *quasi-static* τ_W and the measurement of the induced angular displacement. According to Powell et al. [135], τ_W has a ramp-and-hold behaviour, producing a wrist angular displacement along FE of $(-20 \div +20) deg$ with a velocity of 50 $\frac{deg}{s}$. Since τ_W andΔ φ_{FE} are known, the value of the stiffness can be evaluated employing the following linear regression:

$$K_{FE} = \frac{\tau_W}{\Delta\varphi_{FE}} \qquad (4.5)$$

The second solution (MM 2) consists in an adaption to the wrist of the method proposed by Palazzolo et al. [148] similarly to [149]. They are based on the exertion of *pseudo-random perturbations* to the wrist along FE, with a frequency ranging from 5 Hz to 20 Hz, and an amplitude ranging from 0.1 to 0.4 Nm. The numerical solution both of (4.2) and (4.4) led us to define the requirements of an actuation system to comply with each condition, as reported in table 4.2. Such requirements, led us to select a commercial actuation system, manufactured by *Maxon Motors Inc.*, and composed of the following elements:

- a DC Brushed Motor: model DCX 22L @ 12V, nominal torque equal of 29.5 mNm;
- a 2-stage Planetary Gear-Head: model GPX 22 with reduction ratio (i_{GH}) equal to 28 and an efficiency (η_{GH}) equal to 0.81;

Table 4.2: Mechanical requirements for both MM and TM. The condition MM 2 has been evaluated considering the maximal torque applicable (0.4 Nm). All values reported take into account of a Safety Factor.

Mode	***Torque [Nm]***	***Speed [rpm]***	***Power [W]***
TM	∼0.43	∼38	∼1.7
MM 1	∼1	∼2.9	∼0.32
MM 2	∼0.75	∼0.67	∼0.05

- an incremental encoder: model HEDL 5540 with a count per turn (CPT) equal to 500, that considering the characteristics of the actuator and gear-head, it provides a resolution evaluated as $\frac{2\pi}{CPT \cdot 4 \cdot i_{GH}}$, and equal to about six milli-degrees.

Finally, we focussed on the design of the force sensor aiming to sense the actual torque applied to the user's wrist. In this regard, referring to Fig. 4.3, the relationship between the force sensed by the sensor (F_s) and the torque applied by the actuator is the following:

$$F_s = \frac{\tau_M}{d}. \tag{4.6}$$

Furthermore, in order to relieve the force sensor from non-axial loads we

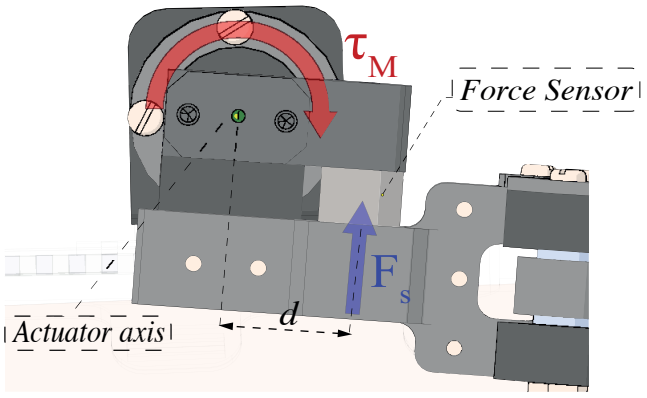

Figure 4.3: Loads chart used to design the force sensor. The amplitude of F_s has been evaluated considering the maximal torque that actuator can exert. While, the distance d is fixed and equal to 19 mm.

adopted the solution presented in Fig. 4.4. In particular, it consists in connecting the mobile chain to the actuator case employing a ball bearing,

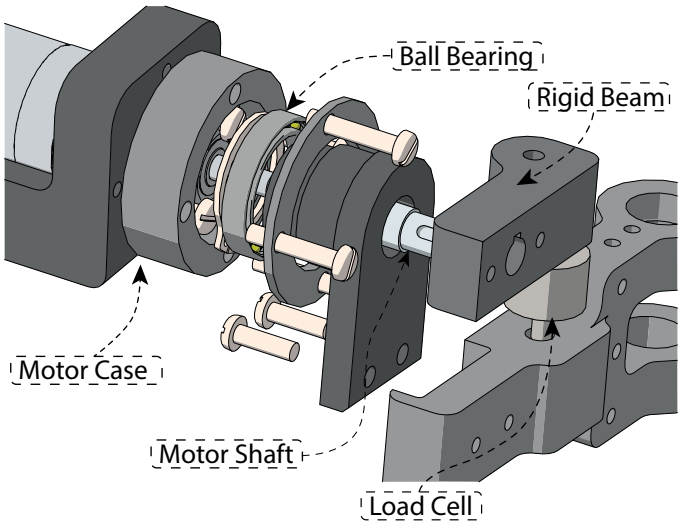

Figure 4.4: Connection between mobile chain and actuator case for relieving the force sensor from non-axial loads.

in order to avoid errors in force measurements. As conclusion, considering in (4.6) the maximal applicable actuator torque to the sensor, we chose the commercially available force sensor described in table 4.3: model *Elaf T1 Amplified Load Cell* by TE connectivity Inc. In conclusion, the relationship between F_s and τ_W, can be evaluated combining (4.4) and (4.6).

Table 4.3: Main measurements features of the force sensor embedded into the structure: Elaf T1 Amplified Load Cell by TE connectivity Inc.

Parameter	***Typical Value***
FSO	±50 N
Supply Voltage	5 V
Output Span	[4 (3% FSO)] V

After having designed the actuator system and the force sensor to embed, we optimized the length of the links a_2, a_3, a_4 and a_5 in order to:

- allow the user to move freely along RUD during ADLs;
- minimize the sum of the length of the 4 links ($\sum_{i=2}^{5} a_i$).

Furthermore, we optimized the overall weight of the device employing a Finite Element Method (FEM) analysis. In particular, we employed the FEM to

both lighten the structure and verify it. In this regard, in order to evaluate the structure robustness we employed the structural security factor (SSF) of the structure, defined as:

$$SSF = \frac{\sigma_{SN}}{\sigma_{VM}},$$

where σ_{SN} and σ_{VM} are respectively the yield stress and the Von Mises stress of each link. As presented in Fig. 4.5 for the most critical parts, SSF is is always greater than 4 (minimal value among all parts assessed) when the torque exerted to the structure is equal to 2 Nm, an higher value than the maximal load that the actuator can exert.

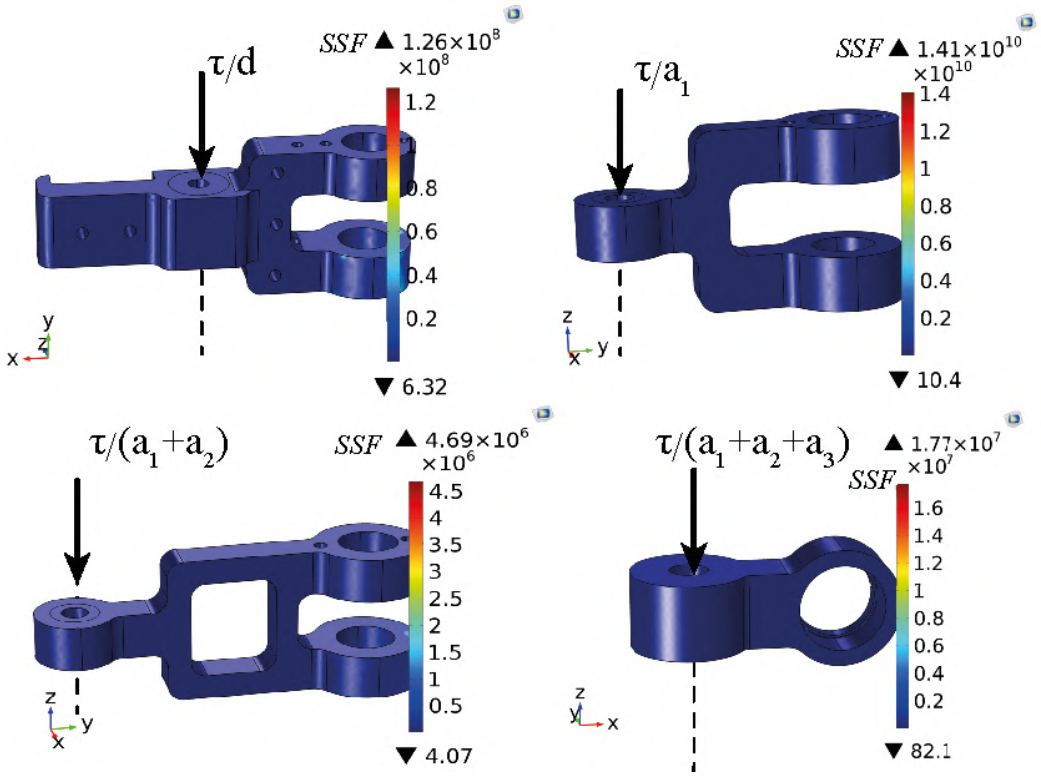

Figure 4.5: FEM analysis carried out on the most critical parts of the structure. The numerical value of d has been defined in Fig. 4.3, while concerning the other lengths, they are expressed in table **??**.

4.2.2 Electronics and Sensory System Design

We designed a single and compact Printed Circuit Board (PCB) (see Fig. 4.7 (A)) in order to meet the requirements on wearability and portability. It implements three core functions:

- Overall Management to manage the behaviour of the whole system and the communication with an external device.
- Actuation Control to control the actuation system by using a low-level driver (ESCON Module 24/2 by Maxon Motors Inc) which is also capable to measure the current adsorbed by the motor and the joint speed.
- Power Management to manage the energy flowing into the system and to recharge the 4-cell Lithium-Ion battery embedded.

By means of either a Bluetooth Low Energy module or a UART module, the device is capable to exchange data with an external laptop/smartphone/tablet, in charge of recording received data by employing a custom developed software.

The schematic of the designed electronic system is presented in Fig. 4.6 (A). It is based on two microcontrollers (MCUs, STM32F446, STMicroelectronics Inc.):

- the first MCU (MCU-1) is in charge of supervising the device and exchange data with an external computer/tablet/smartphone through an UART module (FT32, FTDI Chip Inc.) or a Bluetooth Low Energy module (SPBTLE-RF, STMicroelectronics Inc.);
- the second MCU (MCU-2) is in charge of implementing the control strategies presented in Section 4.4.1 and of sending to the low-level driver (Escon Module 24/2) the desired current/voltage to be set at the motor windings by means of a PWM signal (see Fig. 4.9). Moreover, MCU-2 is in charge of measuring the motor rotation sensed by the incremental encoder by means of the embedded Quadrature Encoder Interface (QEI).

The communication between the two microcontrollers is implemented through UART protocol.

The board embeds also the following modules:

- a 16-bit/4-channel ADC converter (MAX1167, Maxim Integrated Inc.), which is in charge of digitally converting the force sensed by the load-cell, the current absorbed by the actuator and the speed of the motor

(being the last two signals both acquired by the Escon Module); the ADC communicates with the MCU-2 through SPI protocol;

- a battery charger module (MAX187, Maxim Integrated Inc.), which is able to charge the 4-cell Lithium-Ion battery pack embedded; the module is supplied at 15 V.

- a fuel gauge chip (LTC2944, Linear Technology Inc.), which measures the left charge of the battery; this module communicates with the MCU-1 through I^2C protocol;

The PCB manufactured is presented in Fig. 4.6 (B). Its mass is reported in Table 4.4 and it has the following dimensions: $130.0 \times 81.5 \times 1.64$ mm^3.

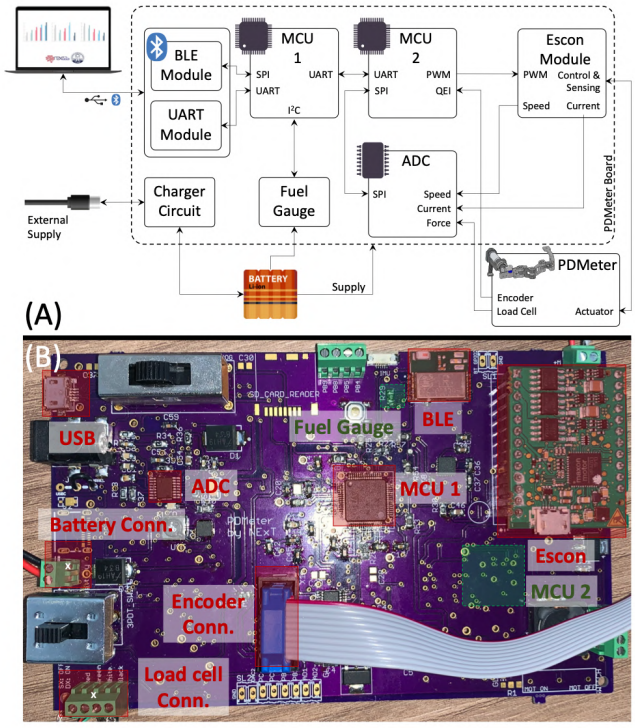

Figure 4.6: (A) Schematic chart of the electronic system. (B) Overview of the manufactured PCB with the main components highlighted. Specifically, the components highlighted in red are placed on the top layer, while the ones highlighted in green are placed on the bottom layer, thus not visible in the picture.

4.3 PDMeter Overview

4.3.1 Mechanical structure and actuation

The presented design led to the structure presented in in Fig. 4.7 (A), composed of five DOFs, of which four are passive and one is actuated (Fig. 4.7 (B)).

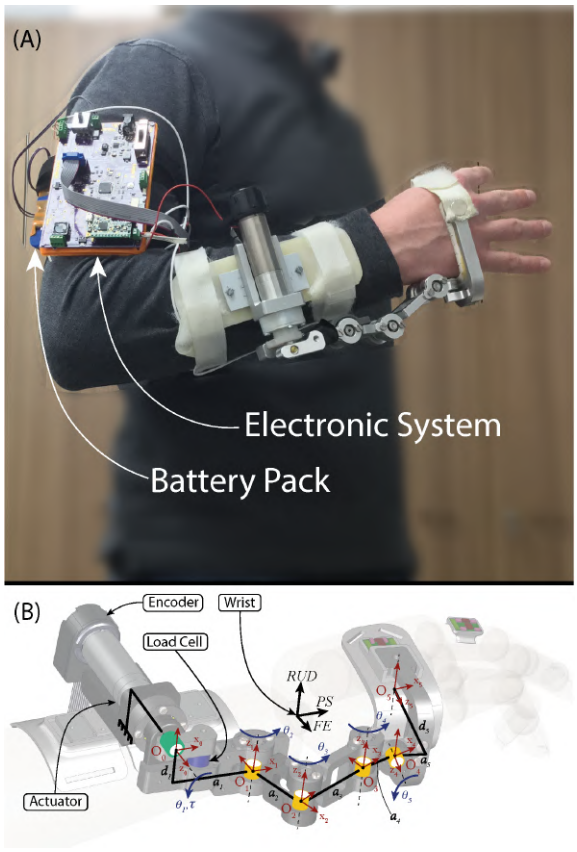

Figure 4.7: A) Overview of the PDMeter. B) Kinematic structure superimposed to arm-hand system. Yellow joints are passive while the green joint is actuated. The reference frames (O_i, $i = \{0, 1, 2, 3, 4, 5\}$) of the mechanical structure have been placed according to the Denavit-Hartemberg convention [150]. Denavit-Hartemberg parameters are reported in Appendix 4.3.2.

The selected actuation system is manufactured by Maxon Motor Inc. It includes a DC brushed motor (rated power: 15.4 W), a 2-stage planetary gear-head (reduction ratio: 28:1) and an optical incremental encoder (resolution: 500 counts per turn, resulting in a maximum resolution of $6{\cdot}10^{-3}$ deg).

In order to measure the torque applied by the actuator to the wrist, the system embeds a load cell within the kinematic chain, as reported in Fig. 4.7

(B). Moreover, the torque applied by the actuator can be measured also by using the current sensor embedded in the low level motor controller adopted (see section 4.2.2 for further information).

The total mass of the system presented in Fig. 4.7 (A), including the actuator, the battery pack, the electronic board and its case, and the hand/forearm supports, is 911 g. The mass of the single sub-parts are reported in Table 4.4.

Table 4.4: Mass values of the PDMeter sub-parts.

Component	***Mass*** **[kg]**	***Material***
Complete device	0.580	Al 6082
Mobile parts	0.250	Al 6082
Battery Pack	0.200	–
PCB	0.065	–
PCB Case	0.066	PLA

For the sake of the completeness, Table 4.5 includes the electromechanical properties of the actuation system. The main dimensions of the device are

Table 4.5: Characteristics of the actuation system, manufactured by Maxon Motor Inc.

Parameter	***Value***
Motor	
Rated Power	$15.4\ W$
Nominal Torque	$29.5 \cdot 10^{-3}$ N m
Mass	$96.1 \cdot 10^{-3}$ kg
Tensor of inertia	$\begin{bmatrix} 0 & 0 & 0 \\ 0 & 0 & 0 \\ 0 & 0 & 9.8 \cdot 10^{-7} \end{bmatrix}$ kg $\cdot$ m^2
Gear-head	
Reduction ratio	28
Efficiency	0.81
Number of stages	2
Mass	$60 \cdot 10^{-3}$ kg

reported in Fig. 4.8.

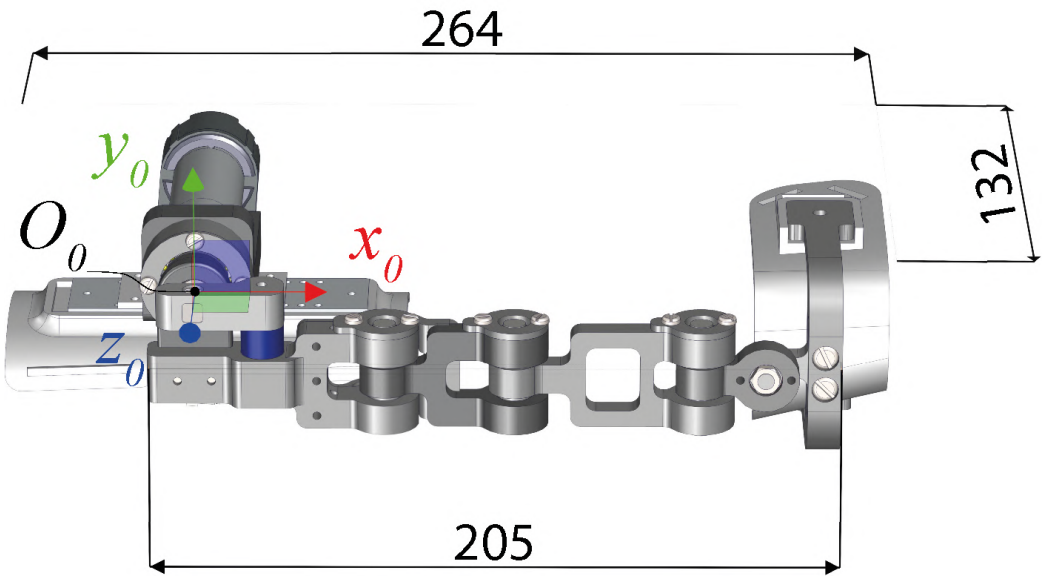

Figure 4.8: Main dimensions of the PDMeter expressed in millimeter. The frame O_0 is used to compute the inertia matrix in the showed configuration (worst case scenario).

To estimate the inertia perceived by the user, we considered the worst case scenario: the configuration shown in Fig. 4.8 is the one with the highest perceived inertia at the user's hand when moving around FE axis. In such a configuration, the inertia tensor of the mobile part (referred to the frame O_0), including the inertia of the actuator calculated at the gear-head output shaft, is:

$$\begin{bmatrix} 2.2 \cdot 10^{-4} & -4.9 \cdot 10^{-4} & -2.3 \cdot 10^{-4} \\ -4.9 \cdot 10^{-4} & 3.5 \cdot 10^{-3} & 1.0 \cdot 10^{-5} \\ -2.3 \cdot 10^{-4} & 1.0 \cdot 10^{-5} & 4.3 \cdot 10^{-3} \end{bmatrix} \text{ kg} \cdot \text{m}^2 \tag{4.7}$$

4.3.2 Kinematic and Dynamic Models

The kinematic model of the device is reported in Fig. 4.7 (B). Denavit-Hartemberg (DH) parameters are presented in Table 4.7.

According to the Lagrange Formulation [151], and neglecting friction, the dynamics of the device in the joint space can be expressed as:

$$\boldsymbol{B}(\boldsymbol{q})\ddot{\boldsymbol{q}} + \dot{\boldsymbol{B}}(\boldsymbol{q})\dot{\boldsymbol{q}} - \frac{1}{2}\left\{\frac{\partial}{\partial \boldsymbol{q}}\left[\dot{\boldsymbol{q}}^T \boldsymbol{B}(\boldsymbol{q})\dot{\boldsymbol{q}}\right]\right\}^T + \boldsymbol{g}(\boldsymbol{q}) = \boldsymbol{\tau} + \boldsymbol{J}(\boldsymbol{q})^T \boldsymbol{F_h} \ . \tag{4.8}$$

Table 4.6: Mechanical parameters of the device. Both the centers of mass and the inertia tensors are expressed in the link frame, *i.e.* the parameters of the i-th link are expressed in the frame O_i, to which it is connected.

Link	*Mass* [kg]	*Inertia tensor* [kg·m^2]	*Center of mass* [m]
1	$3.9 \cdot 10^{-2}$	$\begin{bmatrix} 3.3 \cdot 10^{-6} & -3.0 \cdot 10^{-7} & 1.0 \cdot 10^{-7} \\ -3.0 \cdot 10^{-7} & 4.8 \cdot 10^{-5} & 0 \\ 1.0 \cdot 10^{-7} & 0 & 4.6 \cdot 10^{-5} \end{bmatrix}$	$[-2.6 \cdot 10^{-2} \quad 1.3 \cdot 10^{-4} \quad 5.6 \cdot 10^{-5}]$
2	$2.3 \cdot 10^{-2}$	$\begin{bmatrix} 2.4 \cdot 10^{-6} & 0 & 0 \\ 0 & 1.1 \cdot 10^{-5} & 0 \\ 0 & 0 & 9.9 \cdot 10^{-6} \end{bmatrix}$	$[-2.0 \cdot 10^{-2} \quad 0 \quad 5.9 \cdot 10^{-5}]$
3	$2.6 \cdot 10^{-2}$	$\begin{bmatrix} 2.8 \cdot 10^{-6} & 0 & 0 \\ 0 & 1.4 \cdot 10^{-5} & 0 \\ 0 & 0 & 1.2 \cdot 10^{-5} \end{bmatrix}$	$[2.0 \cdot 10^{-2} \quad 0 \quad 5.9 \cdot 10^{-5}]$
4	$8.8 \cdot 10^{-3}$	$\begin{bmatrix} 4.0 \cdot 10^{-7} & 0 & -4.0 \cdot 10^{-7} \\ 0 & 2.0 \cdot 10^{-6} & 0 \\ -4.0 \cdot 10^{-7} & 0 & 1.9 \cdot 10^{-6} \end{bmatrix}$	$[-9.5 \cdot 10^{-3} \quad 0 \quad 4.5 \cdot 10^{-3}]$
5	$3.6 \cdot 10^{-2}$	$\begin{bmatrix} 6.1 \cdot 10^{-5} & 0 & 0 \\ 0 & 4.1 \cdot 10^{-5} & 0 \\ 0 & 0 & 2.0 \cdot 10^{-5} \end{bmatrix}$	$[0 \quad 0 \quad 2.7 \cdot 10^{-2}]$

Table 4.7: Denavit-Hartemberg parameters of the PDMeter [150] [151].

Link	θ	α [rad]	$\boldsymbol{d}$ [mm]	$\boldsymbol{a}$ [mm]
1	θ_1	$-\frac{\pi}{2}$	22.5	56
2	θ_2	0	0	35
3	θ_3	0	0	55
4	θ_4	$\frac{\pi}{2}$	0	18
5	θ_5	0	65	17

In (4.8), vector $\boldsymbol{q} = [\theta_1, \theta_2, \theta_3, \theta_4, \theta_5]^T$ indicates the five joint angles while vector $\boldsymbol{\tau} = [\tau_1, 0, 0, 0, 0]^T$ denotes the joint torques (being τ_1 the only torque actively delivered by the actuator placed on the first joint). Vector $\boldsymbol{g}(\boldsymbol{q})$ indicates the gravitational torques. Vector $\boldsymbol{F_h}$ denotes the interaction forces/torques measured at the hand, while $\boldsymbol{J}(\boldsymbol{q})$ is the Jacobian matrix of the device. Finally, assuming that the motor frame is located on O_0, the matrix $\boldsymbol{B}(\boldsymbol{q})$ denotes the inertia tensor of the device, which can be calculated as:

$$\boldsymbol{B}(\boldsymbol{q}) = \sum_{i=1}^{5} \left(m_{l_i} \boldsymbol{J}_{p,l_i}^T \boldsymbol{J}_{p,l_i} + \boldsymbol{J}_{o,l_i}^T \boldsymbol{R}_i \, {}^i\boldsymbol{I}_{l_i} \boldsymbol{R}_i^T \boldsymbol{J}_{o,l_i} \right) + \boldsymbol{J}_{o,a}^T \boldsymbol{I}_a \boldsymbol{J}_{o,a} \ . \tag{4.9}$$

In (4.9), the following symbols were used:

- m_{l_i}: mass of the i-th link (l_i);

- ${}^{i}\boldsymbol{I}_{l_i}$: inertia tensor of the i-th link, referred to the frame placed at the i-th joint (O_i) to which it is connected;
- $\boldsymbol{I}_a$: inertia tensor of the motor, referred to the frame O_0;
- $\boldsymbol{R}_i$: rotation matrix expressing the rotation of the i-th frame (O_i) with respect the frame O_0. This matrix can be computed employing the DH criterion [150];
- $\boldsymbol{J}_{p,l_i}$ and $\boldsymbol{J}_{o,l_i}$: Jacobian matrices of the i-th link contributing to translations (subscript p) and rotations (subscript o), respectively;
- $\boldsymbol{J}_{o,a}$: Jacobian matrix contributing to rotation of the actuator embedded.

Jacobian and rotation matrices can be numerically computed according to the geometrical criterion, based on DH convention [150] and presented in [151], and using the numerical parameters reported in Tables 4.5, 4.6 and 4.7.

4.4 Device Characterization

We tested the device in terms of Range Of Motion (ROM), transparency perceived by the user in TM and performance of the actuator torque tracking in MM, with a pilot study in a single healthy volunteer.

4.4.1 Control strategy

The working modalities described in Section 4.2 have been implemented considering two control strategies, as described below.

TM control

We implemented the TM control in order to assure the transparency of the device to the users' motion, when it is not measuring the stiffness. This is a key aspect of the PDMeter. To this aim a direct force control approach was pursued, similarly to what proposed in [152]. To regulate human-robot interaction force, we implemented a closed-loop control, by using the load cell signal as feedback for a proportional regulator. Such a signal was filtered using a real-time 1^{st} order Butterworth low-pass filter (cut-off frequency: 3 Hz). When the actuator is controlled with a null reference force, it continuously moves to minimize the interaction force, with the resulting effect of accommodating an external imposed motion. Fig. 4.9 (A) presents the scheme of the proposed controller.

MM control

In order to estimate joint stiffness, the device delivers a torque profile, accurately measured, while recording at the same time wrist rotation around FE. On the basis of the desired torque τ_d, the microcontroller (MCU) defines the input for the motor driver. It includes an internal PI current regulator and sets the proper current value into the motor windings (Fig. 4.9 (B)).

4.4.2 ROM characterization

We measured the maximum angular excursion around FE, RUD and PS by using an optoelectronic motion capture system (Polaris Vicra®, NDI Inc.), by placing a marker on the dorsal surface of the hand. The wrist was externally moved to reach the extremal values of the ROM while recording the joint. Such measurements were performed twice: during free motion and while wearing the PDMeter. All angles are relative to the initial position of the hand, which was oriented to be parallel to the anatomical frontal plane.

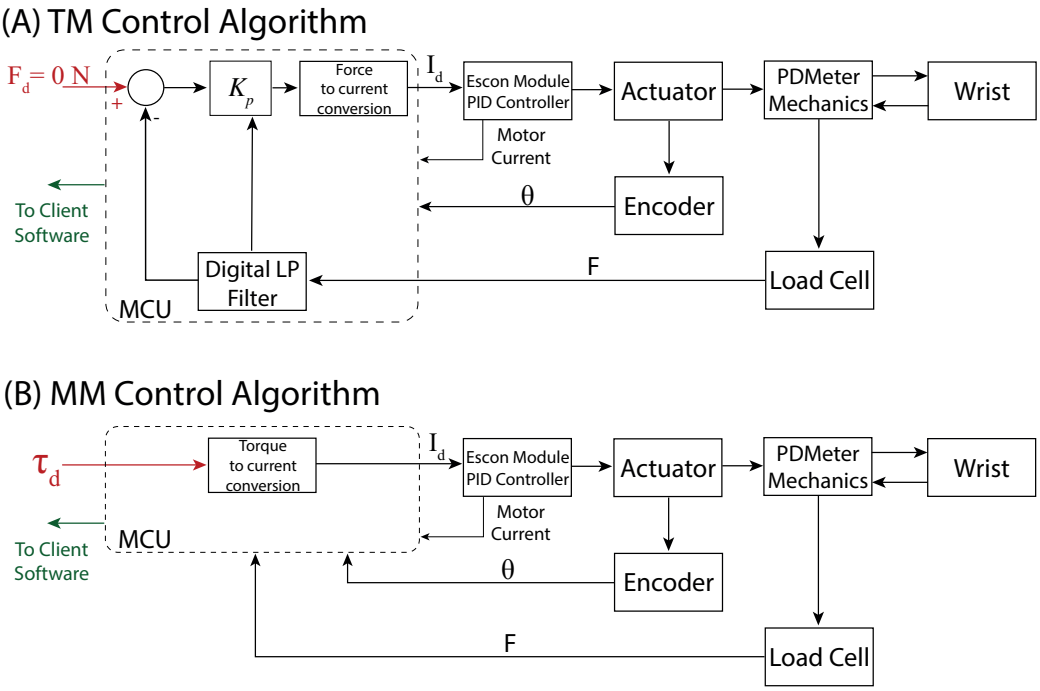

Figure 4.9: Implemented control algorithms for TM (A) and MM (B). The Escon Module implements a current controller and, in both cases, the control signal provided by the MCU is a desired current (I_d). F refers to the force read by the load cell while θ to the angle measured by the optical encoder. The MCU sends to the client software the reference signal provided to the low-lever actuator controller, the force measured by the load cell, the current measured by the current sensors and the angular displacement measured by the optical encoder.

Despite a minor reduction to the ROM with respect to the free physiological motion, results presented in Table 4.8 suggest that the kinematic hindrance due to the system may be considered negligible. Indeed, the motion recorded when the device was worn was found to be consistent with data reported in [146].

4.4.3 TM characterization

In order to measure the interaction force perceived by the user, we placed two force sensors, one on each side of the handle of the device, as shown in Fig. 4.10 (A). To this aim, we used two FSR® by Interlink Technology™, each of them connected to a separate Wheatstone Bridge [153]. According to this setup, we asked to the healthy volunteer to replicate a typical ADL with his arm wearing the PDMeter (Fig. 4.10 (B)). In particular, two sub-tasks were accomplished: *i)* taking and opening a bottle of water; *ii)* putting the water into a cup and drinking from it.

Table 4.8: Comparison of maximum wrist rotations in free motion condition and wearing the PDMeter device.

DOF	**Direction**	**ROM [deg]**	
		With PDMeter	Free motion
FE	Flexion	61	64
	Extension	57	57
RUD	Ulnar Deviation	33	38
	Radial Deviation	33	39
PS	Pronation	54	64
	Supination	41	74

The tasks were performed both in TM and with the actuator unpowered (Unpowered Mode, UM), with the final aim of comparing control-based active transparency with the intrinsic mechanical backdriveability of the device.

We evaluated the *Root Mean Square* (RMS) of the FSR® signals and then we calculated the average of the top and bottom sensors in both conditions. We repeated the same test three times for each condition. In TM the RMS of the measured force was found to be 4.3±0.3 N, while in UM it was 5.4±0.2 N.

4.4.4 MM characterization

We asked to the user to comfortably place his relaxed arm, wearing the PDMeter, on a forearm support of the chair. The FE axis was kept parallel to the gravity direction, as shown in Fig. 4.10 (B).

According to Fig. 4.11, we commanded the actuator with a triangular and a trapezoidal reference torque signal, in order to assess torque tracking capability. Both reference signals were repeated five times in all experimental sessions. The RMS error between the reference torque and the measured one (estimated by means of the motor current sensor) was evaluated as indicator of the controller performance (see Fig. 4.9 (B)). We varied the reference torque signal from the range of $[-500, 500]$ mN m to the range of of $[-900, 900]$ mN m (step: 100 mN m). Both reference signals had a fixed ramp duration (from 0 mN m to the peak value) of 5 s. Specifically, we selected this value since the measurement of wrist stiffness requires slow movements to neglect damping and inertia effects [48]. In addition, the trapezoidal reference signal had a holding torque with a duration of 0.5 s.

Results are reported in Table 4.9. The maximum RMS error was found to

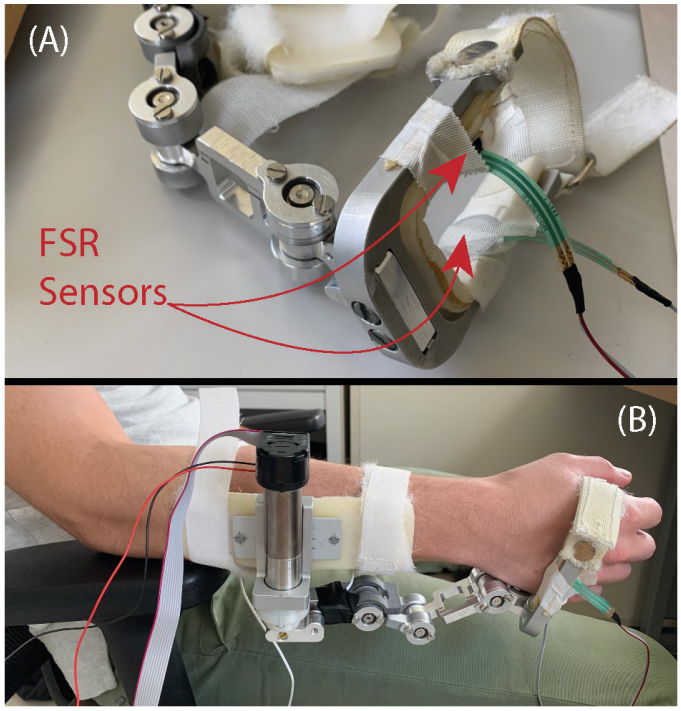

Figure 4.10: Overview of the system (B) and Focus on FSR sensors used (A): FSR® model 402 [154]. We placed the sensors on the top and on the bottom sides of the end-effector in order to measure the interaction force during both extension and flexion since the sensors can measure only compression.

Table 4.9: Results of the MM characterization in terms of torque tracking performance.

Peak reference torque [mN m]	**RMS torque error [mN m]**	
	Trapezoidal	Triangular
500	18.22	13.45
600	15.09	14.00
700	18.38	20.32
800	21.94	22.06
900	23.35	20.50

be lower than 2.54% when using a trapezoidal reference torque, in the range of $[-900, 900]$ mN m, and lower than 2.29% for the triangular reference torque.

Because of the negligible difference between the results obtained with the two reference torque signals, we decided to use the trapezoidal pattern for further experimental validation of stiffness measurement (section 4.5), in accordance with most of similar literature studies [48], [135].

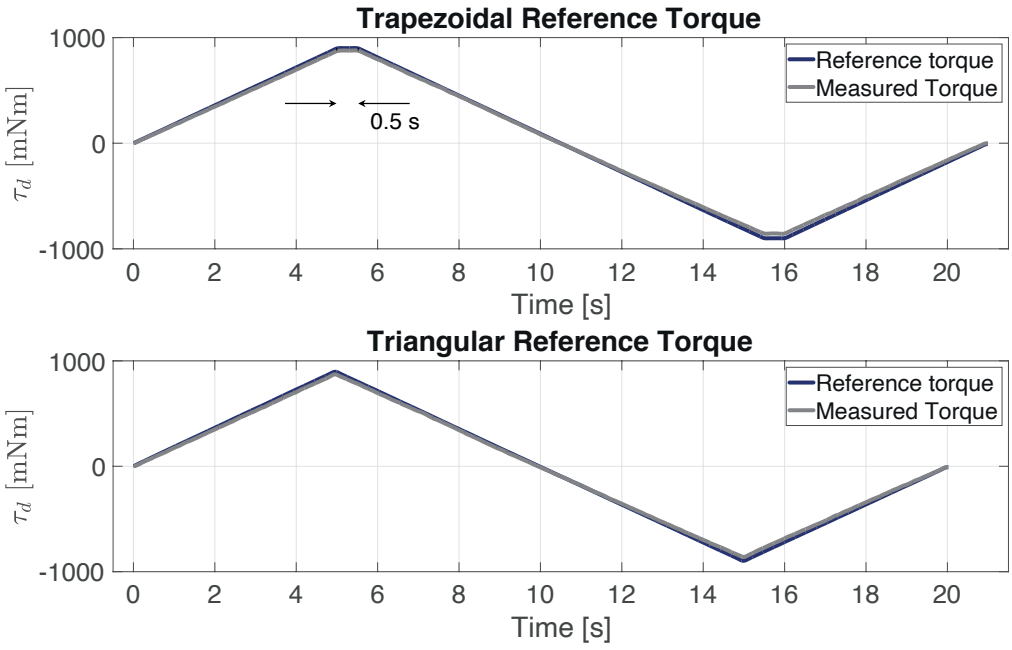

Figure 4.11: Reference torque and measured torque (measured by the motor current sensor) for the MM. The presented triangular reference torque has a 180 mNm/s slope as well as the trapezoidal one, which has in addition a holding torque with a duration of 0.5 s. In each experimental sessions such perturbation cycles are repeated 5 times.

4.4.5 Discussion

The main goal of this section was to present the experimental characterization of the PDMeter, a wearable mechatronic device conceived to estimate wrist stiffness/impedance and assess wrist rigidity in PD patients.

We demonstrated that the kinematic structure, the reduced weight and size of the mechanical components, and the implemented force control, allow to preserve the wrist motions during the accomplishment of relevant daily motor tasks, which is a key aspect to comfortably move the wrist and the forearm [146].

We implemented two alternative controllers, one to achieve high transparency during (TM) and the other one for high-fidelity torque tracking (MM), and we analyzed their performance during a test with a healthy volunteer. In TM the interaction force recorded between the hand and the end-effector of the device (RMS $\sim$ 4 N) does not worse the manipulation skills, accordingly to similar previous works [152]. Thanks to the reduced friction in the passive rotary joints, to the efficient gear-head in the actuated joint and to the lightweight mechanical design, the system showed to be highly intrinsi-

cally backdriveable in UM. It means that a satisfactory level of transparency is assured by the mechanical structure itself, even not relying on any peculiar smart active control of the actuator. This guarantees a high level of safety, an aspect that is crucial in the employment of the device when dealing with fragile users in an unstructured environment. However, the active control in TM was able to further minimize the mechanical impedance perceived by the user when compared with the exoskeleton used in UM (RMS decrease ~ 1 N). The choice of employing the active TM mode or not, may thus depend on the trade-off between the transparency needs and the consumption requirements for the specific application. Indeed, the intrinsic transparency requires only the recording electronics to be powered, with a consequent reduction of the needed battery and an even more lightweight possible design. In MM, i.e. when the device is used to measure the wrist stiffness, we obtained errors in torque tracking lower than 2.54%. This result is consistent with much more complex, general purpose and not portable robots [155]. This aspect may lead to employ our device also in contexts in which a finely applied torque to the wrist is crucial, such as in paediatric rehabilitation applications [156, 157], which could be even implemented in unstructured environments thanks to PDMeter characteristics, or when it comes to provide a haptic feedback in tele-operated tasks [158, 159].

4.5 Device Validation: Wrist Stiffness Estimation on Healthy Subjects and PD Patients

4.5.1 Materials and Methods

We validated the device in measuring the passive wrist stiffness around FE in 7 PD subjects (5 males and 2 females; age: 67 ± 11 years) and 14 healthy subjects (5 males and 9 females, age: 25 ± 2 years). The research was carried out in accordance with the Declaration of Helsinki and following amendments. All subjects gave written informed consent and the study was approved by relevant Ethics Committee (project: GR-2011-02352674).

Subjects were sitting on a chair wearing the PDMeter on their right wrist with the FE axis parallel to the gravity direction, as shown in Fig. 4.12. The neutral position of the wrist was defined according to [111]. The device was used in MM, with the trapezoidal torque pattern reference presented in Sec. 4.4.4, ranging from $[-0.9, 0.9]$ $N\,m$. Angle/torque data were recorded for the actuated joint. The torque perturbation was applied five times, thus

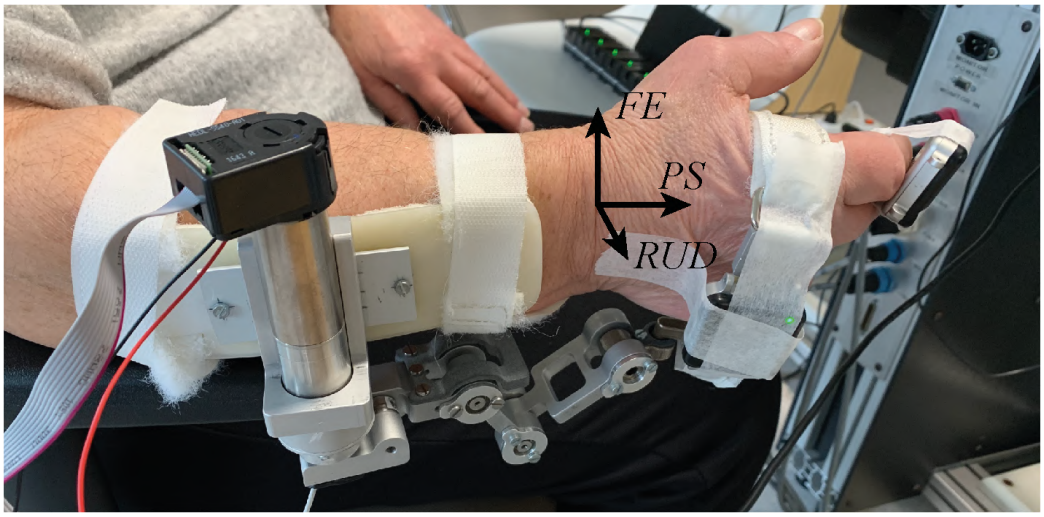

Figure 4.12: Overview of the setup of the experimental session. The reference frame of the wrist is superimposed.

leading to an overall duration of the session equal to 105 s.

During the measurement sessions all subjects were instructed to relax as much as possible for reducing the effect of the voluntary contraction on the stiffness. PD subjects were assessed twice: before (OFF condition) and after (ON condition) the L-DOPA medication, delivered at the peak of clinical efficacy. Moreover, the severity of the motor condition of all PD subjects was clinically assessed by using the MDS-UPDRS part III and the clinical scores are reported in Table 4.10.

Table 4.10: Clinical scores evaluated for PD subjects.

Groups	**MDS-UPDRS Right Arm Rigidity Score**	**MDS-UPDRS Total Score**
PD OFF	2.00 ± 0.58	36.43 ± 8.99
PD ON	1.43 ± 0.79	24.00 ± 10.26

We estimated the passive wrist stiffness by regressing the linear portion of the torque-angle curves recorded by the device [48]. We separated the five applied perturbations and we averaged the angle and torque signals across the three internal repetitions. To remove hysteresis from the analysis, we divided

the average torque-angle curve into four parts: from/toward the neutral position toward/from the extended wrist and from/toward the neutral position toward/from the flexed wrist. Among these conditions, we only considered data related to the movements starting from the neutral configuration and going toward the peripheral positions. We ran a linear fitting of these data and calculated the stiffness K as the slope of the best-fitting line (see Fig. 4.13).

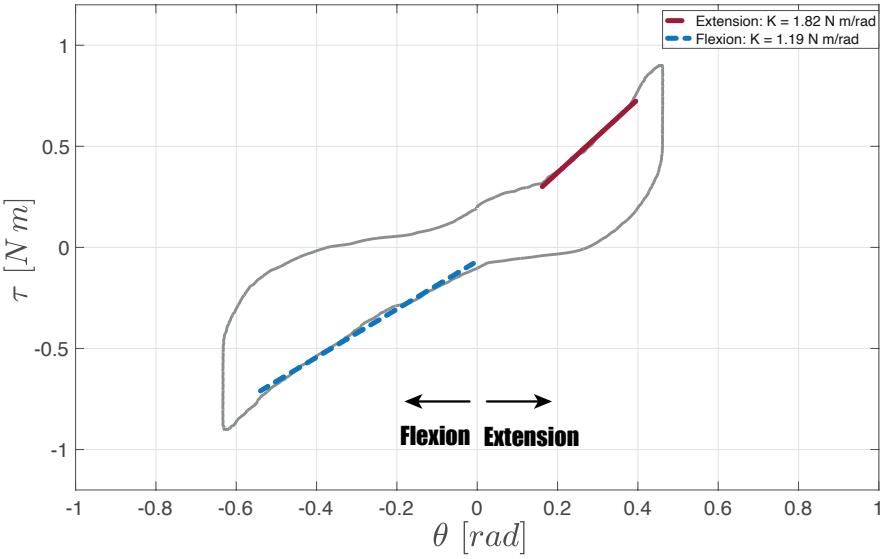

Figure 4.13: Torque-angle relationship for a representative healthy subject. Data are averaged over the three internal perturbations provided to the subject. Dashed lines indicate the fitting lines used to estimate both extension and flexion stiffness.

From a statistical point of view, we checked for the normality of the data by means of the Shapiro-Wilk test [115]. Since, not all dataset presented a normal distribution we opted to use in all cases non-parametric tests. In particular, we used Wilcoxon tests for comparing within subject differences, while we used a Mann-Whitney test for comparing between groups differences. JASP software [160] was used to perform all the statistical tests and a significance threshold of 0.05 was selected in all cases.

4.5.2 Results

We evaluated the wrist stiffness around Flexion (K_F) and Extension (K_E) for both healthy and PD subjects. Results are presented in Table 4.11, in

which the goodness of fitting is expressed in terms of R^2 coefficient, and in Fig. 4.14.

Table 4.11: Mean and Standard Deviation (SD) for all the stiffness values estimated by using the linear fitting.

Groups	**Stiffness**			
	Toward Extension		Toward Flexion	
	$K_E[\frac{\mathrm{N\,m}}{\mathrm{rad}}]$	R^2	$K_F[\frac{\mathrm{N\,m}}{\mathrm{rad}}]$	R^2
Healthy	1.77 ± 0.54	0.98 ± 0.02	1.43 ± 0.6	0.99 ± 0.01
PD OFF	2.86 ± 0.89	0.99 ± 0.01	2.26 ± 0.44	0.98 ± 0.01
PD ON	2.54 ± 0.69	0.99 ± 0.01	2.29 ± 0.49	0.98 ± 0.02

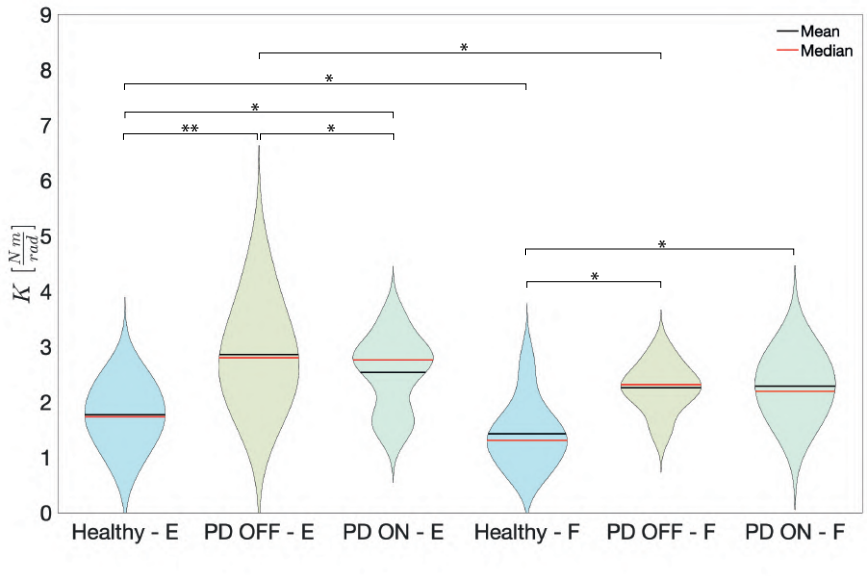

Figure 4.14: Violin plot of the stiffness values estimated. The label 'E' denotes the extension dataset, while the label 'F' denotes the flexion one.

Within Subject Comparisons

K_E is significantly higher than K_F in Healthy ($p = 0.020$, $W = 89$) and PD OFF ($p = 0.031$, $W = 27$) groups, while in PD ON the difference is not significant ($p = 0.219$, $W = 27$).

Furthermore, we analyzed differences between OFF and ON within PD subjects. Specifically, K_E is higher in PD OFF than in PD ON ($p = 0.016$, $W = 28$), while K_F remains fairly unaltered ($p = 0.813$, $W = 12$). Similarly, the total MDS-UPDRS Part III score is significantly higher in OFF condition than in ON condition ($p = 0.031$, $W = 27$), while the single rigidity score does not differ between OFF and ON ($p = 0.72$, $W = 10$).

Between Subject Comparisons

Both K_E and K_F are significantly smaller in Healthy Subjects than in both PD OFF group (K_E: $p = 0.006$, $U = 13$; K_F: $p = 0.016$, $U = 17$) and PD ON group (K_E: $p = 0.016$, $U = 17$; K_F: $p = 0.016$, $U = 17$).

4.5.3 Discussion

The main goal of this section was to present the experimental validation of the PDMeter in estimating the wrist stiffness both in PD and in Healthy subjects. We presented an experimental session carried out on PD and healthy subjects, aiming at validating the device in measuring the wrist stiffness. The PDMeter allowed to estimate the stiffness as different depending on the movement direction. Indeed, extension stiffness was higher than the flexion one both in Healthy and in PD subjects, congruently with the literature [48, 46]. Moreover, the device allowed to discriminate Healthy subjects from PD subjects, both in ON and OFF conditions, and PD subjects before and after getting the L-DOPA medication, in line with the MDS-UPDRS score. It is noteworthy that the p value, obtained in assessing differences between PD OFF and PD ON using the PDMeter ($p = 0.016$), is slower than the one obtained using the MDS-UPDRS Part III score ($p = 0.031$), at least for the extension stiffness. This may lead to hypothesize a higher sensitivity of the PDMeter with respect to clinical score.

Possible limitations in the PDMeter assessment capability may be caused by three different factors. Firstly, since all the different DOFs of wrist movements are strictly interdependent, it is expected that a single-DOF measure could not catch the whole complexity of the symptoms, and the employment of a multi-DOF assessment system would be potentially required. In this regards, we are planning to design a new and more complex version of the PDMeter including additional actuated DOFs. This system is expected to have increased size and weight thus becoming less suitable for at-home assessment and more indicated for use in a structured environment. Secondly, it is well known that the the whole information about the wrist rigidity can be found only using the more general *wrist impedance* instead of using only

its statical component, i.e. the wrist stiffness (e.g. [135], [46]). For this reason, future works will be devoted to derive an experimental protocol for estimating the whole wrist impedance, to further increase the relevance for the pathology assessment. Finally, the reason of the fault in discriminating extension stiffness from the flexion one in PD ON group and flexion stiffness between PD OFF and PD ON conditions may underlie in the anisotropic effect of the L-DOPA based medication. Indeed, it is known that L-DOPA affects more the flexor muscles which are the cause of the resistance during passive extension movements [134].

In addition, it is worth underlying that the values used for the wrist stiffness estimation refer to the actuator joint. This implies that when (4.5) is applied, the estimated stiffness does not coincide with the one of the wrist (in this case, around FE). Indeed, by using the signals recorded by the actuator, what (4.5) allows obtaining is actually the stiffness at the actuator joint and thus a wrist mechanical model should be taken into account [44, 51]. However, according to the results presented in this Section, the PDMeter is characterized by low friction and, as will be presented in 4.5 and 5.3.7, the movements applied by the robot to the subjects' wrist were low speed, which allows neglecting the contribution of the inertia of the entire device to the torque measured at the actuator joint. Therefore, we can assume that what we measure with the PDMeter is close to the FE joint stiffness/impedance, even though our estimation of wrist stiffness/impedance is probably higher to the real one. Another important aspect to point out is the fact that in the PDMEter the actuator is not aligned with the FE joint. The rational behind this choice was to locate the actuator on the subjects forearm more conveniently, because of the very low space available on the wrist. However, this choice has introduce the critical aspects:

- the need of a mechanical structure composed of passive joints to let the PDMeter move the wrist;
- the torque measured at the actuator joint is higher to the one that occurs at the FE joint, due to the presence of that kinematic chain;
- to evaluate the actual FE joint, it is needed to use a mechanical model that considers a closed loop kinematic chain composed of the one of the PDMeter and the one of the wrist, both connected at the hand; moreover, for a more accurate estimation, the model should take into account the compliance of the hand (due to soft tissues) [51, 161].

Implementing a 3D closed-loop dynamics is a hard task and therefore, in order to get an easier and more reliable solution, to obtain values at the FE

joint it could be beneficial to equip the PDMeter with supplementary sensors for recording directly the rotations of the wrist, *e.g.* using flexible sensors similarly to [162], and the interaction force at the hand, *e.g.* by locating the load cell at the end-effector of the PDMeter.

In general, the use of wearable devices as measurement tools could improve the assessment of the PD, thus leading to an optimization of the treatment of the pathology. The PDMeter could be provided to patients that need to be followed up for monitoring at home all motor symptoms continuously during the day. The portability feature could also allow to perform assessments (stiffness and, more generally, impedance) during the ADLs, thus usefully improving knowledge on human motor control and its abnormalities in neurological disorders.

4.6 Device Validation: Wrist Impedance Estimation on Healthy Subjects

4.6.1 Materials and Methods

Participants

We tested the device in 9 subjects (3 females and 6 males, age: 26 ± 4). The research was carried out in accordance with the Declaration of Helsinki and following amendments. All subjects gave written informed consent and the study was approved by the Institutional Ethics Committee (project no. GR-2011-02352674).

Control Strategy

We implemented a Position-Tracking controller using a Proportional-Derivative-Integrative (PID) algorithm (see Fig. 4.15). The MCU delegated to implement the Actuation Control, receives the endpoint angle from the client software and plans the desired trajectory ($\theta_d(t)$). Using the angle recorded by the optical encoder embedded (HEDL 5540 by Maxon Motor Inc., resolution: 500 counts per turn, resulting in a maximum resolution of $6 \cdot 10^{-3} deg$), we computed the error angle ($\tilde{\theta}$) and its derivatives to obtain the signal to be provided to the low level actuator controller, which set the proper value of current flowing into the motor windings. Planning and control were implemented with a refresh rate equal to 1.6 kHz, while the data were sent to the client software with a sampling rate equal to 250 Hz.

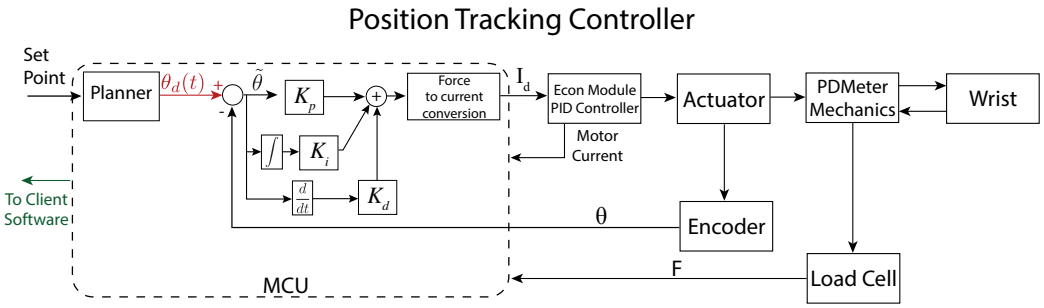

Figure 4.15: Position-Tracking controller implemented. The Escon Module implements a current controller and, in both cases, the control signal provided by the MCU is a current (I_d). F refers to the force read by the load cell, while θ refers to the angle measured by the optical encoder. The MCU sends the reference signal to the client software provided by the low-lever actuator controller, the force measured by the load cell, the current measured by the current sensors and the angular displacement measured by the optical encoder.

Protocol

Subjects were sitting on a chair wearing the PDMeter on their right wrist with the FE axis parallel to the gravity direction, as shown in Fig. 4.16. Moreover, in order to reduce the effect of voluntary contraction on the impedance estimated, we asked the subjects to relax as much as possible during the measurement sessions.

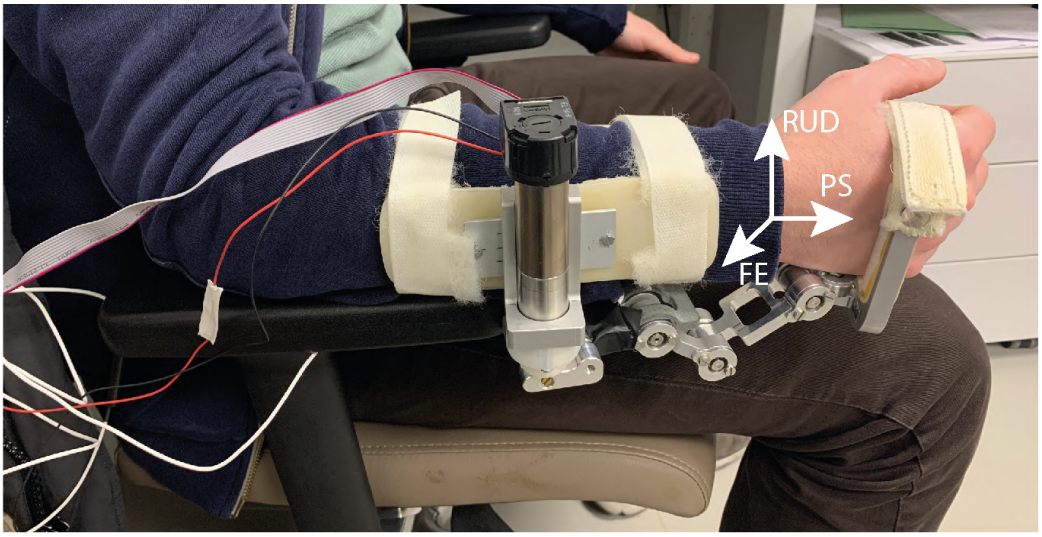

Figure 4.16: Overview of the setup for the experimental session. During the measurement sessions, the gravity acting on the wrist was not compensated.

Subjects underwent four recording sessions, in which the device moved the

wrist around FE on the basis of the reference signal presented in Fig. 4.17. Although the device behaved according to a PID algorithm, the performance of the position controller was limited by the low power characteristics of the actuator (15.4 W). Indeed, according to Fig 4.17, the error between θ_d and θ increased with the increase of the rotation applied to the wrist, due to an higher and higher wrist resistance torque. However, this aspect did not worsen the impedance estimated, since it was estimated using the measured values by the current sensor and the optical encoder. Moreover, each measurement session started with the wrist disposed in the neutral position, defined according to [111]. Movements from the neutral position to the extended/flexed configuration of the wrist were labelled as *Outward Movements*, while the opposite ones were labelled as *Backward Movements*. All measurement sessions started with an extension outward movement.

In each session, the ramps of the reference signal had a constant duration, thus ideally implying a constant velocity. Conversely, each session differed to each other for the duration of the ramps, which ranged from 5 s to 2 s. Lastly, in all cases the reference signal varied in the range of $[-20, 20]$ deg, leading the velocity to range between $\pm 4\ \frac{deg}{s}$ and $\pm 10\ \frac{deg}{s}$. Moreover, a holding time equal to 0.5 s was set in all sessions.

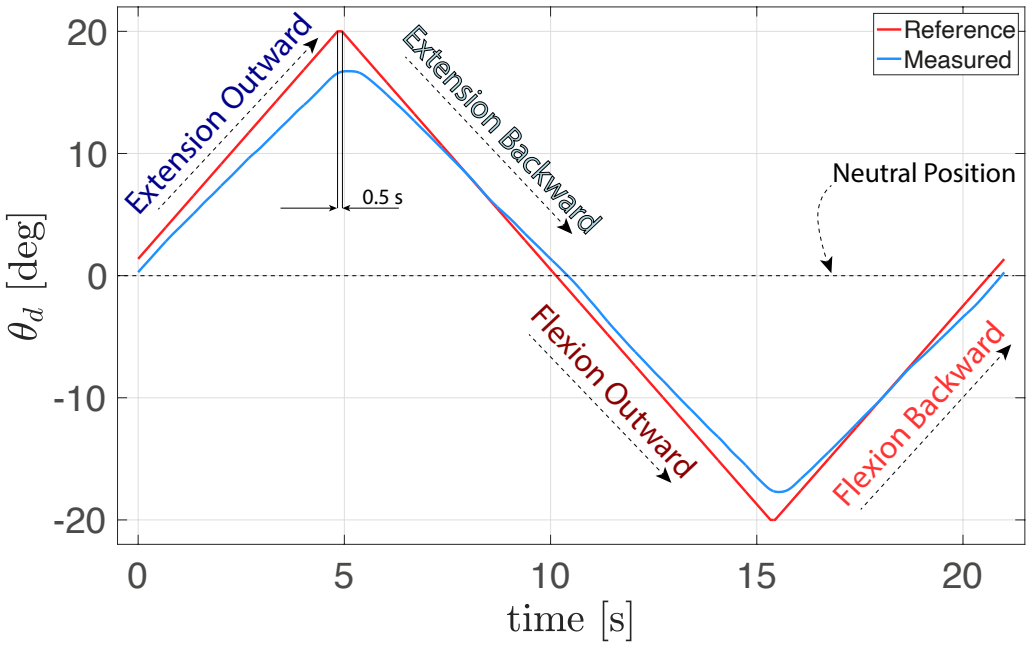

Figure 4.17: Reference signal θ_d (red line) used to control the PDMeter during one experimental sessions, characterized by a duration of the ramps of 5 s and an holding time equal to 0.5 s. The angle measured θ (blue line) is overimposed.

Wrist Impedance Model

The mechanical impedance of the wrist is the dynamical relationship between torque and movement at the wrist joint and, without loss of generality, it can be expressed as follows:

$$\boldsymbol{Z} = \boldsymbol{f}(\boldsymbol{\tau}, \boldsymbol{\theta}, \boldsymbol{\omega}, \boldsymbol{\alpha}), \tag{4.10}$$

with $\boldsymbol{Z}$ denoting the general 3D impedance, which takes into account all three DoFs of the wrist (Flexion-Extension, Radial-Ulnar Deviation and Prono-Supination); $\boldsymbol{\theta}$, $\boldsymbol{\omega}$ and $\boldsymbol{\alpha}$ denote the position, the velocity and the acceleration of the wrist; $\boldsymbol{\tau}$ denotes the interaction torque applied to the wrist [43]. Since the PDMeter has only one DoF actuated, it allows to measure only the impedance around FE, leading (4.10) to become scalar. Moreover, if we consider the mechanical system as characterized by linear time-invariant model, it is possible to describe the passive dynamics of the wrist as a standard second-order linear mechanical model:

$$\tau = K\theta + b\omega + J\alpha, \tag{4.11}$$

in which estimating the mechanical impedance means estimating the stiffness (K), the damping (b) and the inertia (J) coefficients.

During the four experimental sessions, the exoskeleton passively moved the wrist with four different low speeds. The first session was characterized by a constant velocity equal to $\pm 4\ \frac{deg}{s}$, the second one had a constant velocity equal to $\pm 5\ \frac{deg}{s}$, the third one equal to $\pm 6.7\ \frac{deg}{s}$ and the fourth one equal to $\pm 10\ \frac{deg}{s}$. Previous studies focussed on estimating the dynamics of the wrist, demonstrated that the factors which play the major contribution in wrist impedance are the stiffness and damping [33]. Therefore, we opted to neglect the FE wrist inertia and, in order to estimate the wrist impedance around FE, we considered the following linear mechanical model:

$$\tau(\theta,\omega) = K\theta + b\omega. \tag{4.12}$$

in which the stiffness and damping coefficients can be evaluated according to the following equations:

$$\begin{cases} K = \frac{\partial \tau}{\partial \theta} \\ b = \frac{\partial \tau}{\partial \omega} \end{cases} \tag{4.13}$$

Data Analysis

During the experimental sessions we recorded the torque applied by the actuator and the angle read by the optical encoder. In order to evaluate the

velocity, firstly we low-pass filtered the angle signal (cut-off: 3 Hz) and then we numerically differentiated it (by using the MATLAB's function *diff*).

For each session, the exoskeleton passively moved the wrist five times, of which we considered the three internal waves for averaging purposes (see Fig. 4.17). To remove non-linearity due to the hysteresis effect of the soft tissues within the wrist [**?**], we firstly separated the data into four constant-speed movements: toward wrist extension (extension outward), toward neutral position (extension backward), toward wrist flexion (flexion outward), and toward neutral position again (flexion backward). We also excluded the first and the last 0.4 s of each movement (see Fig. 4.18). Finally, we removed the offset from the torque, angle and velocity signals, by subtracting their first value in order to shift the torque-angle-velocity curve into the origin of the reference frame [48], leading to compute Δ values presented in Fig. 4.19. In the end, we run the following linear regression (using the MATLAB's function *regress*):

$$\Delta\tau_i = regress(\Delta\theta_i,\ \Delta\omega_i), \tag{4.14}$$

with i denoting the single movement among: i) extension outward, ii) extension backward, iii) flexion outward and iv) flexion backward. We then averaged the values of the coefficients along outward and backward movements both for extension (K_E and b_E) and flexion (K_F and b_F).

We considered as goodness of fit the R^2 returned by the *regress* function, and we discarded from the analysis any subjects with a R^2 lower than 0.6. Furthermore, we also opted to neglect from the statistical analysis negative stiffness and/or damping values.

From a statistical point of view, firstly we checked for the normality of the data by using the Shapiro-Wilk test [115], whose p-values are reported in Table 4.12. In order to check differences between flexion and extension both for stiffness and damping we used a two-tail paired sample analysis. Although all data analysed were normally distributed (see Table 4.12), we opted to use a non-parametric test (Wilcoxon test), in order to better deal with possible missing values. JASP software [160] was used to perform the statistical analysis and a significance threshold of 0.05 was selected in all cases.

4.6.2 Results

According to (4.12), the relationship between torque, angular displacement and angular velocity is represented by a plane, where the stiffness and the damping define its orientation in the space. An example of the mechanical impedance estimated of a representative subject is reported in Fig. 4.19, in

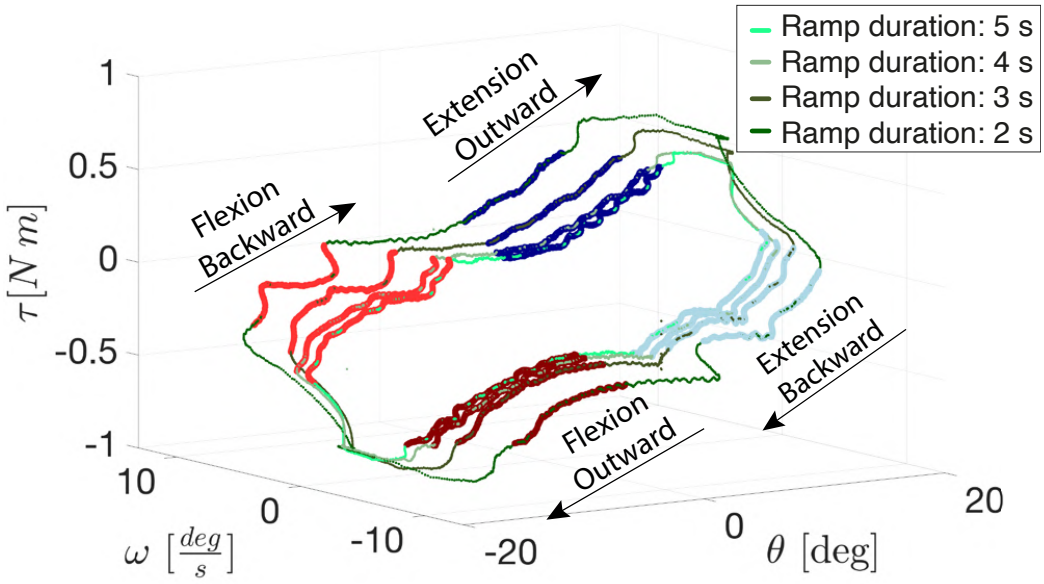

Figure 4.18: Torque-Angle-Velocity relationship for a representative subject. All four sessions are reported, each one plotted with a different shade of green. The highlighted portions represent the ones used to run the regressions (4.14). Specifically, the blue points are related to the extension, while the red ones are related to the flexion. Darker points refer to outward movements, while lighter ones refer to backward movements.

which two planes are drawn, one for extension movements and the other one for flexion ones.

All results are presented in Fig. 4.20 and summarized in Table 4.12.

According to the R^2 obtained, none of the regressions performed were discarded (all R^2 were higher than 0.6). Conversely, we discarded in the statistical analysis three negative damping values, all of them related to the flexion movement. No negative stiffness values were obtained.

The stiffness estimated ranged from 1.064 $\frac{N\,m}{rad}$ to 2.646 $\frac{N\,m}{rad}$ for the extension, and from 0.947 $\frac{N\,m}{rad}$ to 2.261 $\frac{N\,m}{rad}$ for the flexion. On the other hand, the damping estimated ranged from 0.211 $\frac{N\,ms}{rad}$ to 3.794 $\frac{N\,ms}{rad}$ for the extension, and from 0.022 $\frac{N\,ms}{rad}$ to 3.282 $\frac{N\,ms}{rad}$ for the flexion.

As expected, extension stiffness is significantly higher than flexion stiffness ($p = 0.027$, $W = 41$). Conversely, extension damping does not differ from the flexion one ($p = 0.164$, $W = 35$). Moreover, since R^2 values are always higher than 0.85 (see Table 4.12), it is possible to affirm that the hypothesis of linear relationship between torque, angle and velocity can be considered as reliable. Therefore, the linear model expressed in (4.12), is consistent in estimating the passive impedance of the wrist in our experimental conditions.

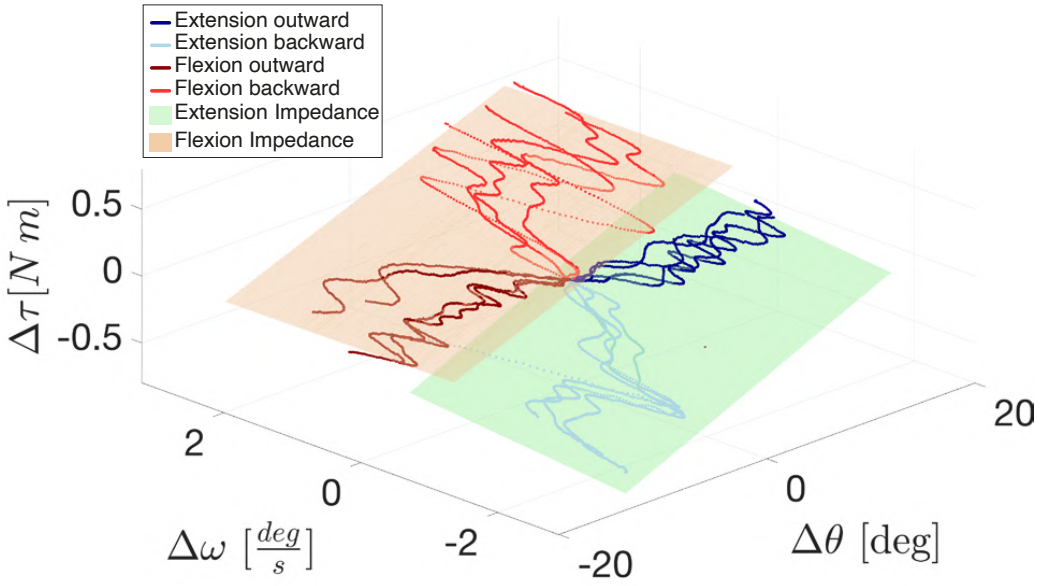

Figure 4.19: Impedance estimated for a representative subject. The measured Δ values are the ones used to run the regression. Regression planes are overimposed both for flexion and extension.

4.6.3 Discussion

To date, wrist impedance has been poorly described by researchers and within the few pieces of research in which such a topic was studied, researchers employed bulky, expensive and non-portable systems which need to be used in structured environments [45, 46]. In order to overcome such issues a portable exoskeleton is required to investigate wrist impedance in unstructured environment. Moreover, such a kind of system may enable in the future to study the wrist impedance during interactive tasks. Our research group recently developed a wrist exoskeleton with such characteristics, and in this work we aimed at demonstrating the reliability of our device in estimating the passive wrist impedance around FE. The final goal is to employ the PDMeter as a tool to investigate wrist impedance in unstructured environments, enabling the possibility to measure the active impedance during activities of daily living, denoting with active impedance the one which takes into account also the voluntary contribution of the subjects' movement.

To this aim we carried out a set of experiments in order to estimate the passive impedance of the wrist in nine healthy subjects. They underwent four experimental sessions, where the robot passively moved the wrist around the FE on the basis of a position controller presented in Fig. 4.15. Since the wrist

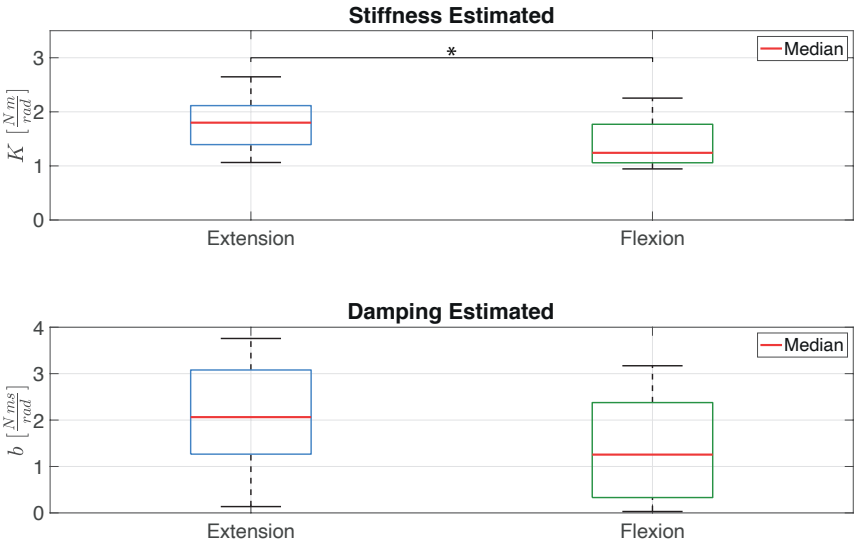

Figure 4.20: Box Plots of the stiffness and damping values estimated. The vertical axes are truncated to zero because negative values are not admissible.

was passively moved within the range of $[-20, 20]$ deg, it is noteworthy that the passive impedance estimated is mostly due to muscle stretch. Indeed, movements applied by the exoskeleton were small enough to avoid the wrist FE to reach its range of motion limits [163].

We considered the wrist as a linear and static second order mechanical system according to previous studies [46], and we neglected the contribution of the inertia due to the slow movements applied by the robot during the experimental sessions. Therefore, we evaluated the impedance by estimating the stiffness and the damping coefficients according to (4.12) and (4.14).

Passive FE stiffness reported in previous studies ranged from 0.5 $\frac{N\,m}{rad}$ [45] to 3 $\frac{N\,m}{rad}$ [39]. In this work we found a passive extension stiffness equal to 1.794 ± 0.514 $\frac{N\,m}{rad}$ for extension movements and a passive flexion stiffness equal to 1.418 ± 0.445 $\frac{N\,m}{rad}$, thus within the range of the values presented in literature. Moreover, we also confirm that passive extension stiffness is higher then the flexion one ($p = 0.027$), [48, 164], due to the higher summed physiological cross-sectional area (SPCA) of the flexors (muscles stretched during passive extension) than extensors (muscles stretched during passive flexion) [165].

To the best of our knowledge, this work is the first to test for potential differences in damping during flexion and extension. Specifically, we report

Table 4.12: Mean ± Standard-Deviation for all stiffness, damping and goodness of regression values (R^2) computed according to (4.14). The p-value of the Normality Test (Shapiro-Wilk) (p_{SW}) is also reported: $p_{SW} > 0.05$ indicates that the data are normally distributed.

Variable	**Toward Extension** (p_{SW})	**Toward Flexion** (p_{SW})
Stiffness $[\frac{N\,m}{rad}]$	1.794 ± 0.514 (0.744)	1.418 ± 0.445 (0.354)
Damping $[\frac{N\,ms}{rad}]$	2.054 ± 1.202 (0.876)	1.403 ± 1.196 (0.688)
R^2	0.904 ± 0.06	0.849 ± 0.07

values equal to $2.054 \pm 1.202 \frac{N\,ms}{rad}$ for the extension and $1.403 \pm 1.196 \frac{N\,ms}{rad}$ for the flexion, which did not significantly differ between flexion and extension, contrarily to what we found for the stiffness. In literature, very few studies systematically measured the damping, as already reported in [8], and the only results available report values in the range 0.02 - 0.03 $\frac{N\,ms}{rad}$ [45, 46]. The coefficients that we report are generally higher, ranging from 0.211 $\frac{N\,ms}{rad}$ to 3.794 $\frac{N\,ms}{rad}$ for the extension, and from 0.022 $\frac{N\,ms}{rad}$ to 3.282 $\frac{N\,ms}{rad}$ for the flexion. Such differences may be explained by the different devices used to carry out the experimental measurements. Indeed, in both cases the authors used end effector devices, which let them infer about rotational stiffness measuring linear forces and movements by using mathematical models. Conversely, we estimated the passive rotational damping using the data directly measured by the exoskeleton. Moreover, another possible reason of such a difference may underlie in the different movement imposed by the robots. Indeed, while prior studies imposed small range of motion with higher velocities, we opted to move the wrist slowly but with a range of motion comparable to the one typically spanned during the ADLs [146]. Such differences, may have led to a different contribution of the damping during the measurements, thus justifying the differences in the estimations. Finally, also the numerical differentiation of the joint rotation may have affected the estimation of the damping. Nonetheless, similarly to the stiffness estimation, the use of different devices changes the values recorded. Therefore, we are confident that our results are reliable and we will enrol a higher sample size in the future. Moreover, in order to improve the measurement characteristics of the device, we will embed a speed sensor to remove the noise introduced by numerical differentiation.

4.7 Conclusions

We presented a novel wrist exoskeleton, conceived to measure wrist stiffness/impedance in unstructured environments. Firstly we presented the design, then we presented the device characterization in terms of ROM allowed to the user, transparency achieved by the implemented transparent controller and torque tracking capabilities when the device is controlled to measure wrist stiffness. Specifically, we demonstrated that the when wearing the PDMete, wrist movements allowed are compatible with the ones required to perform ADLs [146].

Subsequently, we demonstrated that the device successfully allows measuring wrist stiffness in healthy subjects and PD patients to estimate wrist rigidity, one of the three cardinal motor symptoms in PD. Specifically, on the basis of the estimated wrist stiffness, the device allowed to successfully discriminate Healthy subjects from PD patients. Moreover, despite only for extension stiffness, the PDMeter significantly distinguished PD subjects in OFF condition from PD subjects in ON condition.

Lastly, we demonstrated the reliability of the presented exoskeleton in estimating the wrist impedance, in healthy subjects. Specifically, we confirmed previous results related to the significant difference between flexion stiffness and extension stiffness, while we did not find significant difference concerning the damping.

Future work will be devoted on the employment of the PDMeter for the assessment of the wrist rigidity and wrist impedance within unstructured environment, even considering a higher sample size of the PD population. Moreover, we will focus also on defining novel protocols to estimate wrist impedance during interactive tasks, *e.g.* ADLs of during human-human interactions [166, 167].

Chapter 5

Providing Feedback of a Supernumerary Robotic Limb through a Vibrotactile-Based Wearable Device

According to the background presented in Chapter 2, motor redundancy is the quintessential characteristic of the *Sensory Motor System*. To further improve able-bodied capabilities, redundancy can be considered again as the key-aspect, declined in supernumerary robotic limbs. Despite the huge amount of potentialities that they may enable, (*e.g.* rom dangerous conditions to health care applications or even to improve multi-tasking capabilities), their use is still confined in few applications. A poor embodiment of such devices, *i.e.* the representation within the brain of either the one's own body part or an external tool, may underlie to this aspect.

In order to fill this gap, within this chapter there will be presented a wearable device to provide proprioceptive feedback of an anthropomorphic supernumerary robotic limb to able-bodies subjects through vibrotactile stimulation.

5.1 Introduction

Since the discovery of fire, humans have always tried to exploit tools to overcome environmental challenges and to improve the effectiveness of their interaction with the external world. This millennial strife for improvement led to an unprecedented use of technologically advanced artificial devices to augment both physical and cognitive human capabilities [15, 68]. In this

scenario, supernumerary robotic limbs (SRLs) have gained momentum since they offer the chance of greatly enhancing the skills of able-bodied individuals [69, 18, 70]. However, to really benefit from an SRL, the user needs to be able to send command and receive feedbacks from the SRL seamlessly, as it happens with his own body [15, 73, 74]. This aspect is conceptualized in Fig. 5.1. Concerning the afferent component, when trying to close the sensorimotor loop between human and robot, research has often focused on one of the main sources of information regarding body posture and configuration, *i.e.* proprioception [168, 169]. Indeed, several types of proprioceptive feedback have been delivered through vibrotactile stimulation, such as device end-point position, the joint velocity, the interaction force and the error, meant as the distance from the target position, just to name a few [78, 170, 16].

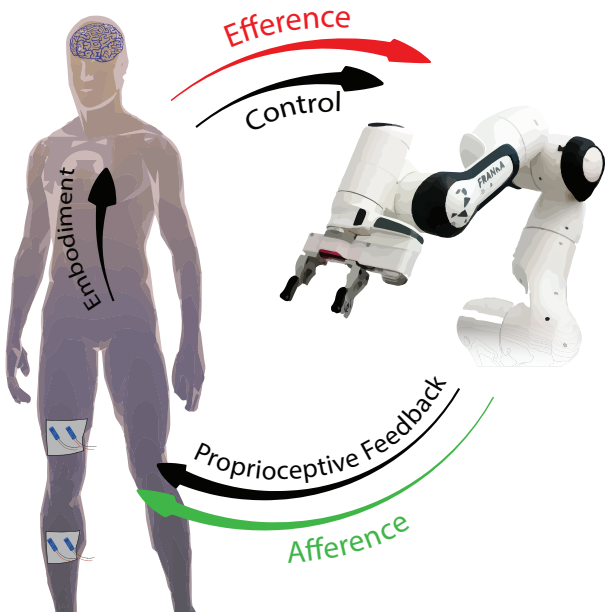

Figure 5.1: SRL loop scheme: the robot control represents the efferent part (red); the proprioceptive feedback represents the afferent part (green) required to close the loop. Vibrotactile stimulation can be used to provide the feedback through vibrators placed on the human skin. The sensory feedback also improves the SRL embodiment in the body schema.

However, just one attempt has been made to provide an active feedback of a SRL. Specifically, the Authors demonstrated that providing the grasping force of a artificial hand connected to a SRL increased the embodiment of the system [101, 102]. Nonetheless, no information about the kinematics or dynamics of the SRL is provided to the user.

In addition, another aspect to take into account is the following: during our daily routine, we can constantly integrate proprioceptive information to obtain an optimal motor control of our body [171] without waiting for a

specific movement to end, *i.e.* in real time. However, despite being studied in relation to prosthesis control or in a virtual environment, real-time delivery and decoding of proprioceptive feedback has never been tested for a proper SRL, as far as we know.

In this regard, in this chapter two studies will be presented, in which subjects received the feedback of a SRL while performing reaching tasks, through vibrotactile stimulation. The first one aims at studying which kind information is more informative to let subjects understand the posture of the SRL, between a kinematic feedback, *i.e.* related to the SRL movements in the task space, and a dynamic feedback, *i.e.* related to the SRL dynamics in terms joint torques. On the other hand, in the second study we investigated the feasibility for the subjects to understand in real-time the posture of the robot, relying on a kinematic feedback. In both cases we employed vibrotactile stimulation to convey proprioceptive feedback, being non-invasive, highly informative and easy to implement in a variety of experimental setups [103]. In Section 5.2 a description of the wearable system used to convey SRL feedback to the subjects is provided, while in

5.2 ViPro: a Wearable Device to Convey Feedback of a Supernumerary Robotic Limb through Vibrotactile Stimulation

In order to provide feedback of a SRL, we designed a wearable system based on a printed circuit board (PCB), hereafter called ViPro, based on a microcontroller (MCU, STM32F446 by STMicroelectronics Inc.). An overview of the whole system is presented in Fig. 5.2. It allows controlling eight pairs of eccentric vibrator motors (Model: 307-103 by Precision Microdrives Inc. [92]), driving the stimulation on the basis of the sensory data received from the robot. Each pair refers to a DOF, in which one vibrator is used to represent positive encoded values and the other one for negative encoded values. However, in both studies we carried out the experiments only testing two DOFs of the robot, thus involving only two pairs of vibration motors, aiming at reducing the complexity of the problem. Moreover, in both studies the vibrator motors were controlled such that their vibration amplitude were proportional to the encoded value of the robot. Specifically, the vibration amplitude refers to the the absolute value of the encoded value. Concerning the frequency of the vibration, it is related to vibration amplitude according to the specific vibrators used [92], since in vibration motors with an eccentric rotating mass such parameters depend to each other [93].

According to the specific information to convey to the subjects, the sensory data of the robot are sent to the embedded MCU (sampling rate equal to 200 Hz) via serial communication. In turn, the MCU defines a pulse width modulation (PWM) signal to the motor drivers (L293DD by STMicroelectronics Inc.), proportional to the encoded value to convey, in order to modulate the supply voltage of the motors:

$$V_{ij}(t) = \delta_i(t) V_{cc}. \tag{5.1}$$

In (5.1), $V_{ij}(t)$ denotes the actual supply voltage of the j-th motor ($j = \{1,2\}$) within the i-th pair, $\delta_i(t)$ denotes the duty cycle of the PWM control signal and V_{cc} the maximal supply voltage of the vibrators (equal to 3.6 V). Finally, the j-th motor is selected on the basis of the sign of the encoded value.

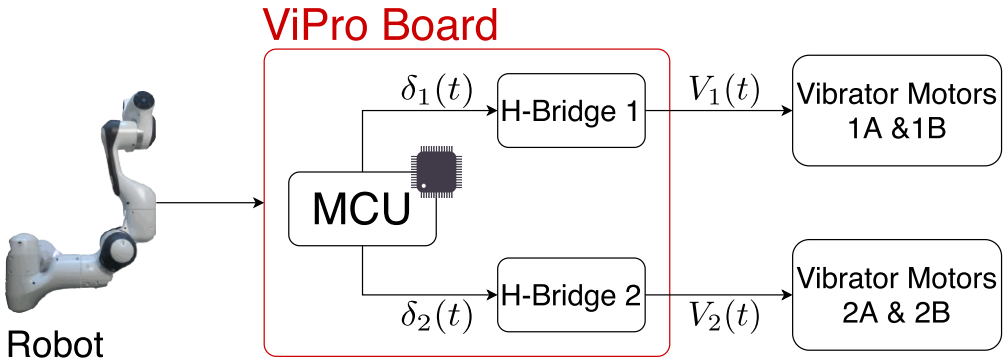

Figure 5.2: Logical Schematic of the ViPro system for two pair of motors. The instantaneous supply voltage of the vibrators, thus their vibration, is modulated by the MCU through two independent motor drivers (L293DD by STMicroelectronics Inc.). Each motor driver refers to a DOF and controls a couple of vibrators. Then, according to the sign of the information to be provided, the MCU selects which one of the two vibrators has to be turned on, *i.e.* A for positive values and B for negative ones.

5.3 Kinematic vs Dynamic Feedback of a Supernumerary Robotic Limb in Reaching Tasks

5.3.1 Population

We enrolled three subjects (two right-handed and one left-handed, aged from 23 to 25 years old) naive to the aim of the study.

5.3.2 Materials

In three-handed manipulation tasks, a SRL represents an additional arm to be employed [17]. Therefore, in order to minimize the subjects' proprioceptive feedback arising from their own arms, we opted to to place the feedback device on the their right leg which is not involved in the task (see Section 5.3.4). We selected the body-location of the vibration motors in order to keep them distant enough from the bones and from each other, such that the user could easily identify which motors are vibrating and clearly perceive the vibration amplitude [172]: one pair on the *rectus femoris* (1A) and the *biceps femoris* (1B), and the other one on the *peroneus longus* (2A) and *gastrocnemius* (2B) (see Fig. 5.3 (a)). In both cases, motors labeled with A refer to positive values of the feedback, while the ones labeled with B refer to negative values.

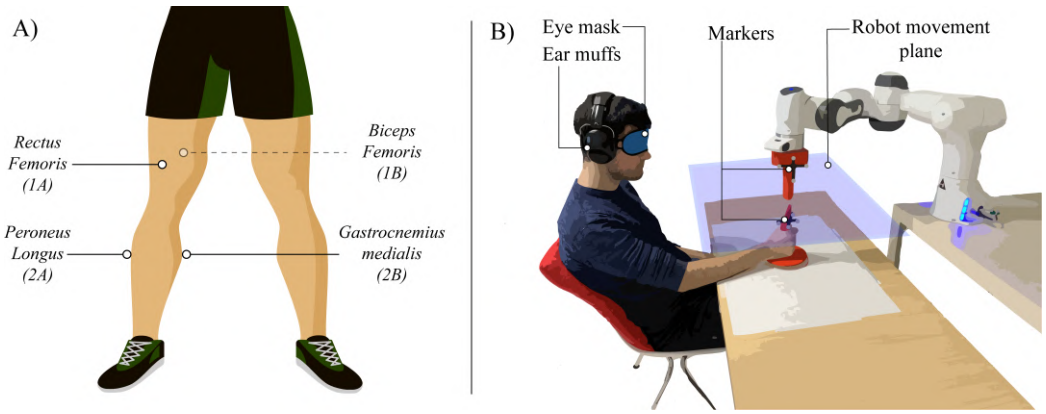

Figure 5.3: A) Body-location of the vibration motors to convey robot posture. B) Experimental setup with a subject sitting in front of the robot. The subject holds with his right hand a plastic handle. Another plastic tool is attached to the robot end-effector. Passive markers are attached on both the handles to track them using an infrared camera. The subject moves the handle on the table; the robot tool is moved on a parallel plane. The subject wears ear muffs and eye mask to suppress auditory and visual feedback.

5.3.3 Feedback Approaches

To perform a preliminary validation of the system, we selected two different approaches to represent the robot state: a kinematic approach and a dynamic one. The first method represents the state of the robot in terms of position of the robot end-effector in the workspace, expressed in the cartesian space (i.e. (x_{EE}, y_{EE}) in Fig. 5.4); whereas the latter conveys the torques which are applied to the active joints of the robot (i.e. J_2 and J_4 in Fig. 5.4).

We expected the kinematic approach to be the easiest to understand, since it directly provides information regarding the robot end-effector posi-

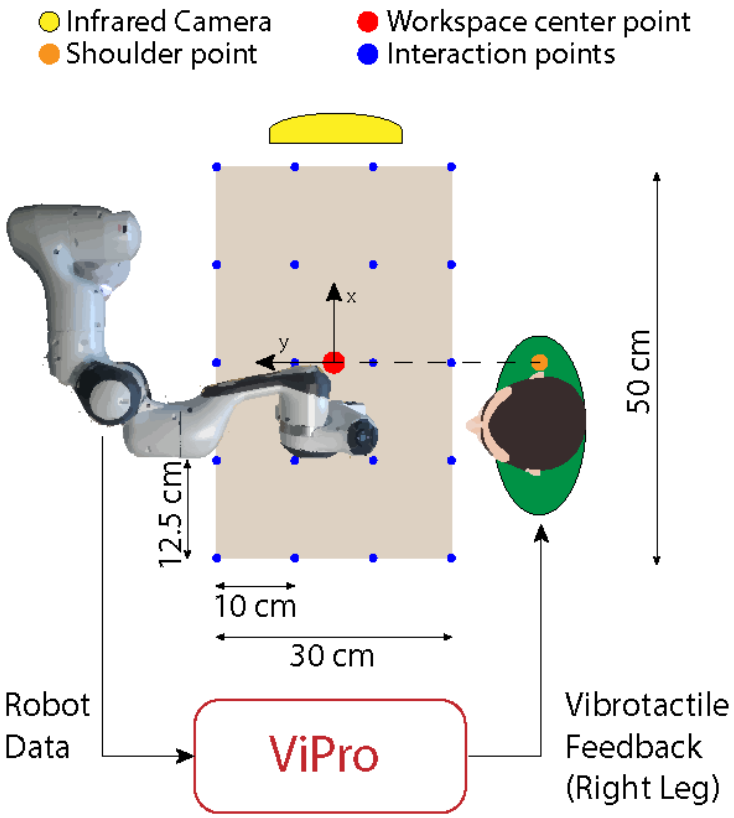

Figure 5.4: Experimental setup scheme: a 7-DOF anthropomorphic manipulator is employed as SRL; the subject is sitting in front of the robot, with the right shoulder (orange dot) aligned with the center of the workspace (red dot); the workspace is a 30x50 cm rectangle subdivided into 20 equally spaced target points (blue dots). Robot state is represented using the end-effector position in the cartesian space (x_{EE}, y_{EE}) or the torques applied to the two active joints J_2 and J_4.

tion to the subject. Conversely, the dynamic approach requires the subjects to learn the robot dynamical model (a strongly non non-linear mapping) to understand x_{EE} and y_{EE}. However, the latter approach may allow the subjects to better estimate x_{EE} and y_{EE} in case of external disturbances, such as obstacles or force fields.

In addition, concerning the kinematic approach, motors 1A and 1B refer to x_{EE}, while motors 2A and 2B refer to y_{EE}. Concerning the dynamic approach, motors 1A and 1B refer to J_2, while motors 2A and 2B refer to J_4.

5.3.4 Experimental Setup

A 7-DOF manipulator (Panda robot by Franka Emika GmbH) is used as SRL, of which only two joints were enabled during movements, *i.e.* J_2 and J_4. The robot is controlled through an GUI developed in c++, using the Qt

libraries, running on a computer with Ubuntu 16.04 O.S.

The robot moves the end-effector on a plane, within a 30 cm × 50 cm rectangle. The robot is controlled to perform straight movements from center to target with minimum-jerk trajectories. The duration of each movements is constant and equal to 4 s.

The workspace for the subjects consists of a 30 cm × 50 cm rectangle upon a table (30 cm below the robot workspace), clearly highlighted with adhesive tape. As shown in Fig. 5.4 and Fig. 5.3, the subject was sitting on a chair in front of the robot, close enough to the table to comfortably reach with the hand every point of the workspace. Subject's right shoulder is aligned with the center of the workspace. Twenty equally-spaced points within the workspace represent the target positions (blue dots in Fig. 5.4).

The subject moves his arm onto the table's plane, holding a plastic handle with spherical wheels, whereas the robot moves onto an upper plane (Fig. 5.3). To ensure planar movements, the subject is asked to keep the handle touching the table during the whole experiment.

A Polaris Vicra Camera (by Northern Digital Incorporated) is used to detect the position of the end-effector and the subject's hand, using passive reflective markers attached to the robot and the plastic handle. The infrared camera is placed sideways such that it has both markers within its field of view (see Fig. 5.4).

The vibrators are manually placed on the subjects' right leg, as show in Fig. 5.3, adjusting their position so that the subject can clearly perceive the full frequency range of the stimulation and easily discriminate which vibrator is delivering the stimulation [172].

5.3.5 Experimental Protocol

The robot performs planar movements starting from the center of the workspace (highlighted with the red dot in Fig. 5.4). While the robot is moving the subject receives the vibrotactile stimulation and, after the robot movement, subject is asked to move the handle on the table, reaching the same in-plane position of the robot end-effector.

The experimental protocol is composed of three phases (see Fig. 5.5): i) Familiarization; ii) Learning; iii) Test. Each subject performed the two conditions (type of feedback), in a randomized order in two different days.

Familiarization

The familiarization phase allows the subject to understand the task. During this phase the subject has a visual feedback (not wearing eye mask), but no

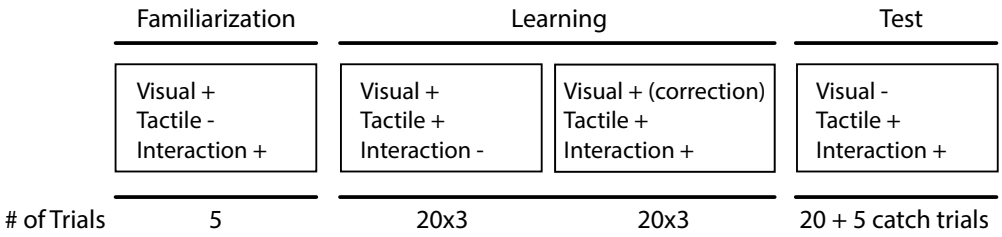

Figure 5.5: Overview of the experimental protocol phases.

vibrotactile feedback is given. The robot reaches five random points in the workspace. At the end of each robot movement, the subject is asked to move the handle on the table, reach the in-plane position of the end-effector and then return to the starting position.

Learning

The learning phase is further divided into two steps:

a. During the first one the subject has only to observe and associate the vibrotactile stimulus on the leg with the spatial motion of the robot without performing any movement. Auditory feedback is suppressed by ear muffs, as in all the other phases. The robot performs three series of 20 movements, randomly selected among the points highlighted on the workspace (see Fig. 5.4). The aim of this phase is to allow the subject to correlate the vibrotactile feedback to the position reached by the robot end-effector.

b. In the second learning step the robot performs again three series of 20 random movements. The subject perceives the proprioceptive feedback but is blindfolded. At the end of each robot movement (when the motors stop vibrating) the subject has to reach the point of the workspace corresponding to the position of the robot. Once the subject completed the reaching movement, the subject is allowed to see robot to understand if he reached the right position or to estimate the error magnitude. At the end of the movement, both robot and subject return to the starting position.

Test

In the test phase the robot executes 25 random movements. Twenty of them are associated with an informative vibrotactile feedback, whereas five movements are "catch trials" (or "control points") and provide a non-informative

feedback with a sinusoidal vibration pattern (with random phase shift), in order to confirm that an eventual improvement in the performance are due to the information provided through the motors and not to the vibration itself. Subjects are blindfolded for the whole phase and they are asked to reach the correct position, depending on the received feedback.

5.3.6 Data Analysis

The robot end-effector and the handle position were tracked using the infrared camera and processed in MATLAB^{TM} 2017. Since the handles could also rotate during the task, two constant homogeneous transformation matrices were considered in the data analysis to compute the actual position of the handle centers according to the equation:

$$^{b}T_{h} = ^{b}T_{m}\, ^{m}T_{h} \tag{5.2}$$

denoting $^{b}T_{h}$ the 4x4 homogeneous transformation matrix that represents the handle pose (h) in the base reference frame (b), $^{b}T_{m}$ the tracked marker pose and $^{m}T_{h}$ is the constant transformation between the handle center and the attached marker. Equation 5.3 was applied to both the hand and robot handles, using the corresponding constant matrix $^{m}T_{h}$.

In order to assess the subjects performance, we considered two indices:

- Position error, normalized with respect to the distance between the starting and target points;
- Time needed to execute the task;

The position error was computed as the cartesian norm between the handle and end-effector position on the plane, at the end of the task. The error was then normalized by the distance between the starting and target points, in order to take into account the trial difficulty. Indeed, far target required higher duration to be reached, and/or higher velocity which results in less accuracy. We did not consider the accuracy to be strictly related to the proprioception, which is known not to be homogeneous in space (the accuracy in locating the hand is higher if the hand is closer to the body) [173], because the task did not rely on proprioception only, even though the subject was blind-folded. Indeed, active movements and somatosensory information derived from the interaction between hand, handle and table were always present. The task started when the robot and the vibrotactile feedback stopped and it ended when the subject reached the target. In addition, also the task duration was then divided by the distance between the starting and target points, used as index of the trial difficulty.

Considering the low size of the population enrolled, to test within subjects the two provided feedback, we evaluated the effect size by computing the Cohen's d [174, 175]. Moreover, only the test phase was considered for the data analysis

5.3.7 Results

The average errors along the three subjects, during the test trials, are $89.5 \pm 37.2mm$ considering the position feedback and $194.8 \pm 88.5mm$ considering the torque feedback respectively, as depicted in Fig. 5.6.

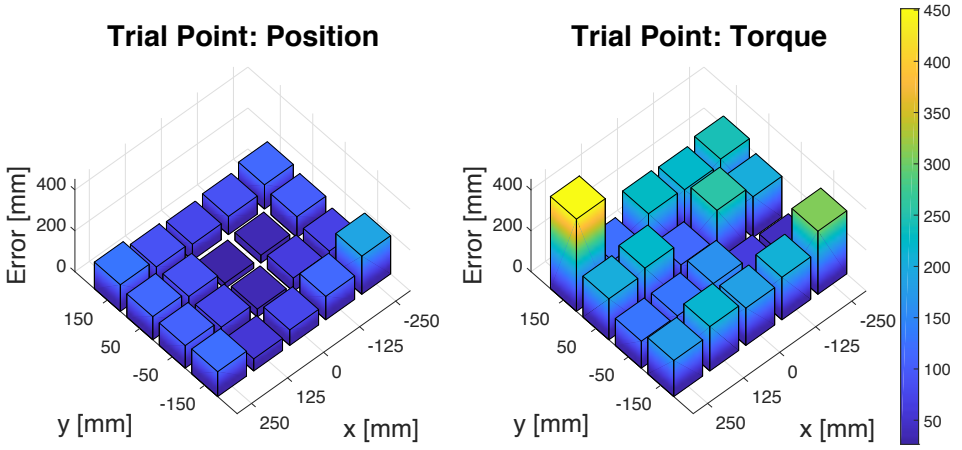

Figure 5.6: Spatial distribution of the average error over the workspace using the position and torque feedback encoding. Each bar represents a target point. The bar height is the error averaged along all subjects.

Taking into account the trial difficulty (represented by the distance between the starting and target points) the average error value resulted to be $48\% \pm 12\%$ considering the kinematic approach and $118\% \pm 72\%$ considering the dynamic one. Especially in the latter method, the worst errors are the targets close to the center, i.e. the easiest ones (as visible in Fig. 5.7); whereas the error values employing the position feedback are approximately equally distributed in the workspace.

Fig. 5.8 shows scatter-plot of the error and the trial duration, both divided by the target distance, for the two feedback types (computed among the 20 test trials) and for the control trials for the three subjects.

The normalized position errors, using the cartesian position feedback, resulted to be smaller than the ones obtained with the dynamic encoding.

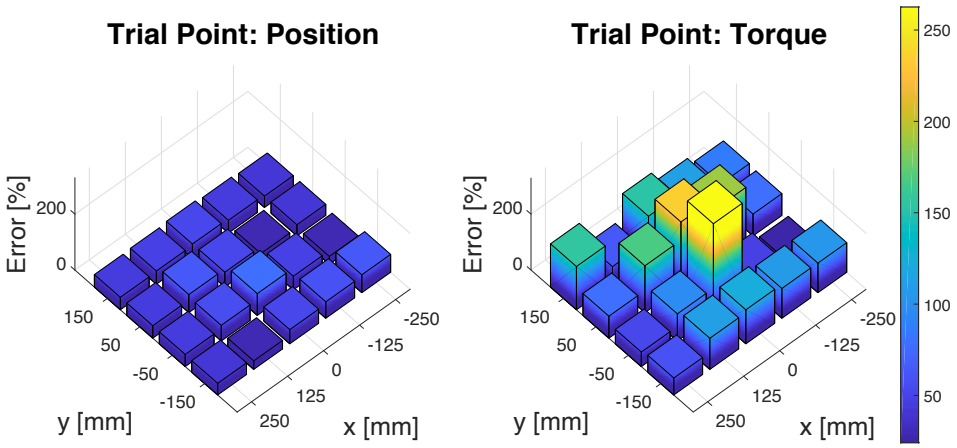

Figure 5.7: Spatial distribution of the average normalized error over the workspace using the position and torque feedback encoding. Each bar represents a target point. The bar height is the error (divided by the starting-target points distance) averaged along all subjects.

A huge difference between the approaches was found ($d = 4.278$) [174]. On the other hand, regarding the control points, a small difference was found between the errors obtained with the non-informative feedback and the ones achieved with the dynamic feedback approach ($d = 0.313$). Conversely, the kinematic encoding approach allowed subjects to achieve better performance ($d = 2.826$) than the control trials, in terms of errors.

Large differences occurred among the two feedback approaches in terms of task duration ($d = 1.682$); the mean duration of each trial (corresponding to one target point) is $9.10s \pm 1.68s$ and $7.26s \pm 1.46s$ for the torque and position feedback respectively (see Fig. 5.8). The same trend was found also considering the trial difficulty, *i.e.* by diving the value by the center-target distance ($d = 2.239$).

5.3.8 Discussion

The results related to the comparison with the catch trials suggest that when subjects are asked to replicate the posture of a SRL, the position based feedback is better than using joint torque based feedback (see Figures 5.7 and 5.8). Indeed, learning the dynamic model might be hard to achieve and a longer training would be needed. Conversely, the proposed kinematic feedback results to be more intuitive and therefore, in the presented task (reaching task without and interaction with the environment) could be considered more convenient for the subjects in terms of cognitive effort. Moreover, such

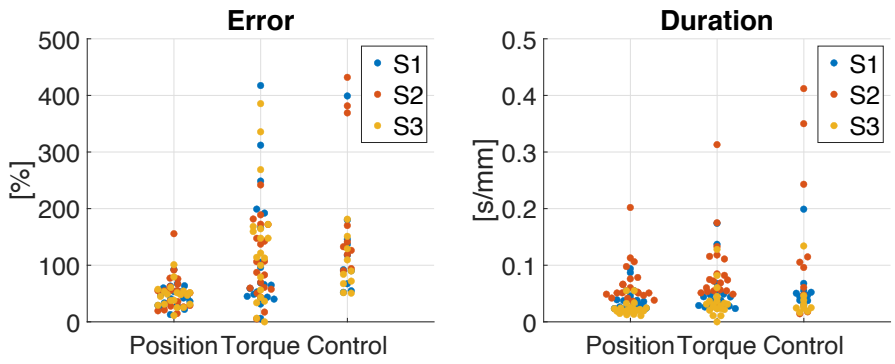

Figure 5.8: Left: Normalized position error during the test phase (twenty trials per subject) for all subjects. Right: Trial duration divided by the distance from the target during the test phase (twenty trials per subject), for all subjects.

results could have been affected by the trajectory implemented to control the robot. Indeed, the duration of robot movements was always the same, i.e. four seconds, even for small distances, thus leading the subjects to memorize the distance on the basis of the duration of the stimuli received.

Another aspect that is worth noting is the following: the torques required to slowly move the two active joints were low (robot configuration that has been adapted to the planar task) oscillating around zero (due to noise), leading the subject to be confused. In any case, the δ variability range, according to (5.1), was always adjusted according to the minimum and maximum values achievable with the employed feedback. In order to better understand the effectiveness of that feedback an additional, more complex, task should be tested and an interaction of the SRL with the environment might allow the dynamic approach to be more informative and effective.

The results prove the feasibility of the proposed system which seems effective in converting the state of a supernumerary robotic arm, coded using position feedback, into vibrotactile stimulation, easily understandable by subjects. The huge difference between the performance achieved employing the position feedback and the ones obtained in the catch trials is an evidence of that validation.

Moreover, the duration of the learning phase is not a negligible aspect. The choice of sixty trials for the two learning phases allowed to complete the whole experiment in a short span, i.e. less than one hour and half. Such a short duration could have been enough to learn how to benefit from the simpler feedback (cartesian position), but too short for the more complex dynamic feedback.

Furthermore, It is worth noting that the error magnitude is partially due to the inaccuracies of human beings in identifying the position of their own

arm when blind-folded. A weakness of this protocol might underlie in the use of the right arm and right leg instead of the dominant ones for each subject. Nevertheless, since each subject was tested with the same hand (and leg) on both the conditions, this choice may have affected the error magnitude, but not the overall comparison results.

5.4 Cartesian Space Feedback for Real-Time Tracking of a Supernumerary Robotic Limb

The aim of this study was to test the feasibility of a cartesian space feedback, *i.e.* kinematic feedback, for real-rime tracking of a SLR using the ViPro system.

5.4.1 Sensory Feedback

We deliver the state of the robot as the end-effector position with respect to the workspace center. The body location of the vibration motors is reported in Fig. 5.9 (A). Specifically, motors 1A and 1B are placed in correspondence of *tibialis anterior* and *gastrocnemius* respectively. Whereas, motors 2A and 2B are placed in correspondence of *gracilis* and *vastus lateralis* respectively. Motors 1A-1B refer to x_{EE}, while 2A-2B refer to y_{EE} (see Fig. 5.10 (b).

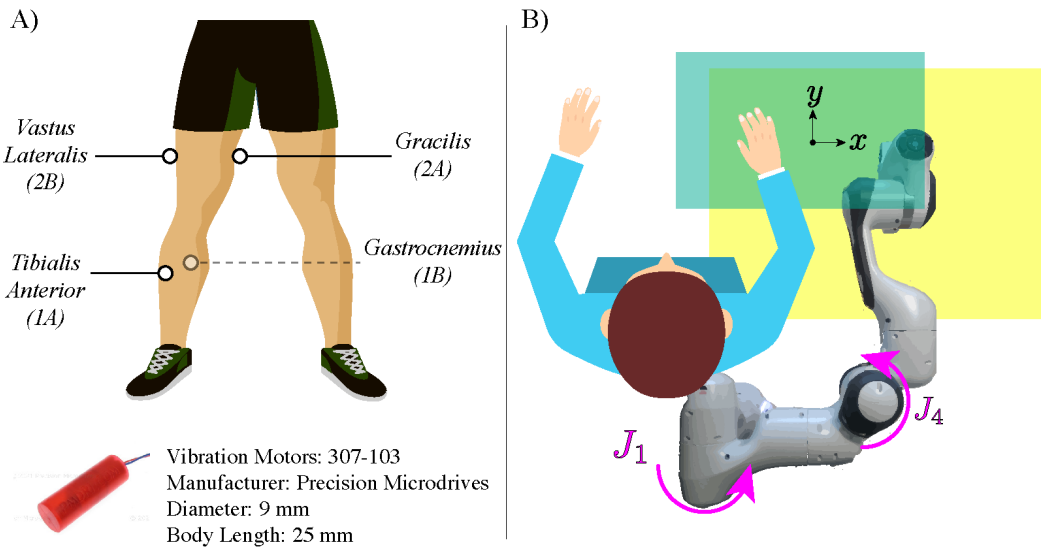

Figure 5.9: (A) Body location of motor vibrators. (B) Schematic overview of the relative position of the robot with respect the subject. The workspace is the overlapping area (in green) between the subject workspace (light blue) and the robot workspace (yellow).

It is important to note that the sensory feedback subjects were receiving, despite being the result of a sensory substitution, still behaved similarly to a proper proprioceptive signal: subjects received a continuous vibratory stimulation for as long as the robot end effector was not in the workspace center, and the vibration was modulated on the basis of the distance between end-effector and center. Vibration ceased only between one trial and another, to avoid sensory adaptation.

5.4.2 Experimental Setup

The setup used shares some similarities with the study reported in Section 5.3. However the main difference consists in the position of the robot with respect the subjects. Indeed, in this case the subjected is sitting with the robot emerging from his right side instead of being frontally (see Fig. 5.9 (B)).

As shown in Fig. 5.10, subjects were sitting in front of a transparent table with their right shoulder aligned with the second joint of the robot (J_2 in Fig. 5.9 (B)).

The robot is displaced in order to move on a lower plane (2 cm below the table) compared to subjects, so that they can see the robotic arm moving below the transparent table. A number of points equal to the total number of trials (248 points) is randomly generated within the workspace, representing the target positions the robot had to reach. Subjects are asked to move their arm onto the table plane, holding a plastic handle that can slide on the table with minimal friction (Fig. 5.10). A 7-DOF robotic manipulator, the Panda robot by Franka Emika GmbH, is used as SRL. Only two DOFs (second and fourth joint) have been enabled (see Fig. 5.9). The robot is controlled through an interface developed in C++ language, using the Qt libraries, running on a computer with Ubuntu 16.04 O.S.

Robot motions are planned to be human-like, i.e. implementing minimum jerk trajectories. Each movement has a duration ranging from 1.5 to 3.5 seconds, randomly selected in each trial. Movements are organized in groups of four trajectories, going from the center of the workspace to three consecutive points, and then going back to the center again. This should diminish the error propagation when subjects replicated the movement of the robot relying only on proprioceptive feedback. The workspace consists of a 45 cm $\times$ 50 cm rectangle upon the transparent table.

To ensure planar movements, the subject is asked to keep his back close to the chair and the handle touching the table during the whole experiment.

We used two infrared cameras (Prime x22 by Optitrack) to track the position of the end-effector and the subject's handle, using passive reflective

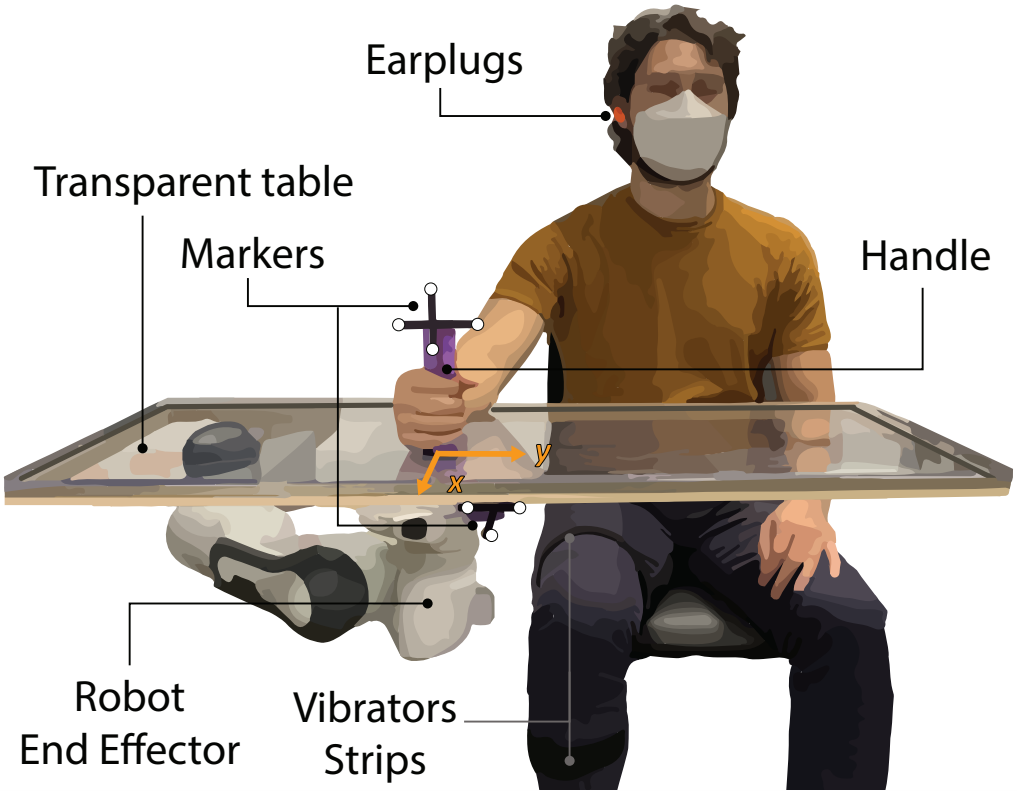

Figure 5.10: Experimental setup with a subject sitting laterally to the robot. The subject holds with his right hand a custom plastic handle. Another custom plastic support is attached to the robot end-effector to hold the marker. Passive markers are attached to both handle and support to track them using infrared cameras. The subject moves the handle on the transparent table while the robot end-effector moves below the table. The subject wears disposable earplugs and kept his eyes closed to suppress auditory and visual feedback respectively.

markers. We manually placed the vibrators on the subject's right leg, as show in Fig. 5.9, with the use of adjustable cloth strips to fine-tune the vibrators position.

5.4.3 Experimental Protocol

We enrolled four subjects (all right-handed, three female, aged 27±3) naive to the aim of the study, to run a pilot experiment. While the robot was moving, subject received the vibrotactile stimulation and were asked to follow the robot as closely as possible, by moving the handle on the table, for the whole duration of the robot motions. The trial started when the robot started moving and ended when the subject stopped his motion.

An overview of the experimental protocol is depicted in Fig. 5.11. It is composed of three phases: i) Familiarization; ii) Learning; iii) Test.

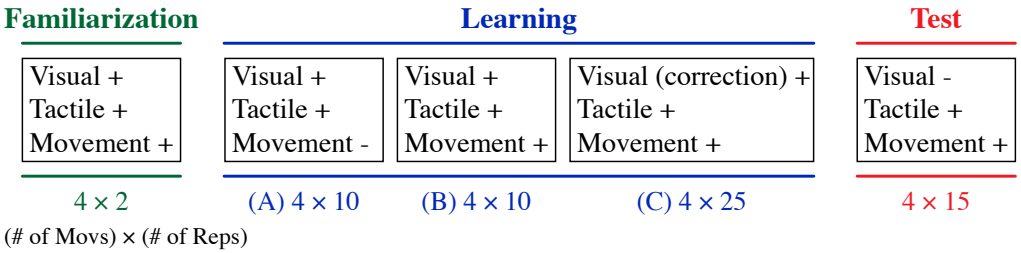

Figure 5.11: Experimental protocol implemented to the test the feasibility to track in real-time a SRL using vibrotactile feedback. The labels below the boxes represent the number of movements (before coming back to the center of the workspace) times the number of repetitions.

Familiarization

The familiarization phase allowed subjects to experience the task firsthand, while receiving both visual and vibrotactile feedback. The robot reached eight different random points in the workspace. Subjects were asked to follow the robot end-effector by moving the handle on the table. Auditory feedback was suppressed by wearing earplugs, as in all the other successive phases.

Learning

The learning phase was subdivided into three steps.

a. During Learning A, subjects had to observe the robot moving and pay attention to the vibratory feedback, and they were instructed to associate the vibrotactile stimulus on the leg with the spatial motion of the robot without performing any movement. The robot performed 10 series of 4 movements each (from center to point P1, P2, P3 and back to center), with each point randomly generated within the workspace. The aim of this phase was to allow the subject to understand the meaning of the vibratory pattern she/he received, by correlating the vibrotactile feedback to the position reached by the robot end-effector.

b. Learning B, repeated the same scenario of Learning A (10 series of 4 movements each, with new randomly generated points within the workspace), but this time subjects were instructed to follow the robot by moving the handle on the table. This phase had the goal to reinforce the association between vibrotactile feedback and robot movement, obtained during Learning A, as it was demonstrated that active movements facilitates associative learning [176].

c. Learning C, was similar to Learning B but subjects were instructed to keep their eyes closed while following the robot (no visual feedback) and

to open them only when they were satisfied with the reached position, at the end of the robot movement (when the vibratory feedback ceased). The robot performed 25 series of 4 movement each. By doing this, subjects were able to understand if they successfully reached the end-effector position, thus receiving a direct visual confirmation regarding their performance in the task and completing the learning process.

Test

Subjects executed the test without visual feedback (eyes closed) and were asked to follow the robot end-effector with the handle by relying exclusively on the vibratory feedback. The robot executed 15 series of 4 movements each, with each point randomly generated within the workspace. To avoid error's drift, when the robot came back to the center, the experimenter re-aligned the subject's handle to the center.

5.4.4 Data Analysis

The robot end-effector and the handle position were tracked using the infrared cameras and processed using MATLAB^{TM} 2020a. Since the handles could also rotate during the task, two constant homogeneous transformation matrices were taken into account in the data analysis to compute the actual position of the handle centers, according to the equation:

$$^{b}T_{h} = {}^{b}T_{m}\,{}^{m}T_{h} \tag{5.3}$$

denoting $^{b}T_{h}$ the 4x4 homogeneous transformation matrix that represents the handle pose (h) in the base reference frame (b), $^{b}T_{m}$ the tracked marker pose and $^{m}T_{h}$ the constant transformation between the handle center and the attached marker. Equation 5.3 was applied to both the hand and robot handles, using the corresponding constant matrix $^{m}T_{h}$.

Performance were evaluated only during the *test* session, measuring two indexes:

- *Position error*, computed as the Euclidean distance from the subject handle and the robot end-effector on the plane, for every time sample during each movement;
- *Delay* between the onset of the robot's and subject's movements;

5.4.5 Results

We computed the *Position Error* in two cases: i) in real time, *i.e.* considering the position error without any further processing, and ii) by applying a time shift to the recorded subject handle position equal to the subject's delay within the specific trial. Specifically, we considered the latter case in order to control for the effect of physiological reaction time. Subjects obtained an average *Position Error* equal to (0.084 ± 0.010) m and an average *Shifted Position Error* equal to (0.084 ± 0.003) m (see Fig. 4).

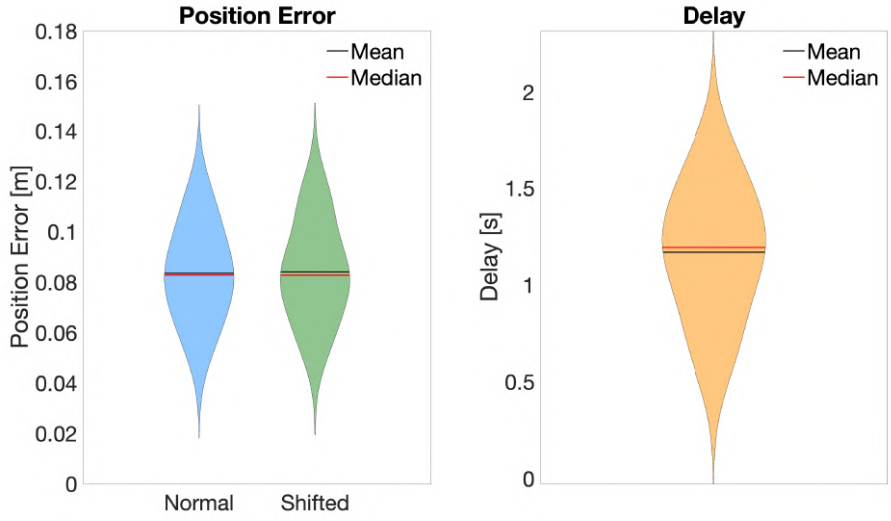

Figure 5.12: Average *Position Error* (normal and shifted) and average *Delay* computed along all trials.

Concerning the computed *Delays* (see Fig. 5.12), subjects started moving, on average, (1.169 ± 0.408) s after the robot movement onset.

5.4.6 Discussion

In this preliminary work we presented a system which employs vibrotactile stimulation to provide in real time the proprioceptive feedback of a supernumerary robotic limb. The system has been validated on four subjects using a kinematic approach, conveying the end-effector cartesian position with respect to the center of the workspace, through four eccentric-motor vibrators positioned on the subjects leg.

Results showed that Subject obtained, on average, a *Position Error* of approximately 8 cm. This might seem a non trivial error, but it is worth noting that the performance of subjects was analyzed during the *test* phase, when they were relying only on vibration-coded proprioceptive information

for judging the robot position. This, in addition to the relatively brief learning phase subjects underwent, and a probable parallax error related to the subjects' point of view, can easily justify a *Position Error* of such magnitude. Another interesting aspect which advocates for the reliability of the presented setup is the relatively low SD of the *Position Error* ($\leq$ 1 cm). Finally, the subjects' *Delay*, around 1 s, can account not only for the physiological reaction-time but also for the additional cognitive process required to translate the vibration pattern into information related to the trajectory on the plane. We reckon that implementing longer training sessions could improve subjects accuracy by reducing *Position Error* even further, and decrease the cognitive load by making the task more intuitive, which translates into smaller *Delays*. As a future work, we shall increase the number of subjects to confirm results obtained so far, and we shall implement a longer learning session in which visual feedback is gradually removed, to facilitate the passage from full visual feedback to exclusive proprioceptive reliance. Finally, analyzing subjects' performance during learning phase should give us a clear view of how the shift from vision to proprioception impacts the decoding of real time SRL kinematics feedback.

5.5 Conclusions

In this chapter we presented novel system to provide the proprioceptive feedback for a supernumerary robotic arm, using a vibrotactile stimulation The proposed platform aims at overcoming the lack of a proprioceptive feedback, meant as the state of the entire device, in the use of SRL. The proprioceptive feedback is conveyed through a vibrotactile stimulation on the subjects' leg skin, using four eccentric motors.

The system has been validated in two pilot studies. The first one (Section 5.3), involved three subjects using two different feedback encoding strategies: a kinematic approach, conveying the end-effector cartesian position and a dynamic method, using the torques recorded on the active joints. The results proved the effectiveness of the proprioceptive feedback system for a SRL using the position approach, showing hugely better performance ($d = 2.826$) compared to catch trials (providing non-informative feedback). On the other hand, the outcome related to the dynamic feedback approach seems to be significantly worse. Nevertheless, those results could be affected by the choice of a planar task and the absence of a robot-environment interaction. The second pilot study (Section 5.3), involved four subjects who were asked to replicate the robot movements in real time while receiving the vibrotactile feedback related to the robot end-effector. The results proved that subjects

could understand the robot movements with a delay around 1 s and position error around 8 cm.

Besides possible limitations of the protocols employed, the proposed system showed to be a valid test-bed to implement future more complex and refined tasks to investigate the encoding of supernumerary limbs proprioceptive feedback.

Future plans will consider tasks with external disturbances, such as obstacles to avoid, or additional force fields and tri-manual tasks. Furthermore, the system can be employed in studies focused on the SRL control strategies, assessing how the proprioceptive feedback affects the performance in controlling the robot.

Chapter 6

Conclusions and Outlook

Motor Redundancy is likely the main paradox of the Human Sensorymotor system. From one side, we interact with the environment during our everyday life safely, stably and gracefully [2, 3] and this is by far the distinctive signature that gave humans an evolutionary adavange [5, 177]. However, it requires the *CNS* to properly manage such an *abundance* [2, 5]. To this aim, various theories have postulated that the *CNS* il likely to implement a predictive planning and control (by employing *internal model*) and to adopt simplifying approaches to reduce the whole complexity [2, 5, 4, 178].

An example of simplifying approach used in unconstrained movements is the pointing task with the wrist. Indeed, even though the task requires two DOFs, the wrist has three DOFs and it has been demonstrated that the *CNS* does manage the redundancy by means the Donders' Law [112, 10, 11]. It poses that the DOF redundant is bonded to the other two DOFs according to a 2D surface, which is path dependent, subject specific and volatile (*i.e.* violations can occur [8]). In Chapter 3 we further investigated this topic by studying whether it is stable over time within subjects and whether the Donders' Law persists during motor adaptation. In both cases, we demonstrated that Donders' Law is a reliable model to describe motor redundancy of the wrist during pointing tasks. Indeed, it is stable over time (we studied the subjects involved in four different days) and it is conserved even during motor adaption. Future studies will aim at further investigating the management of motor redundancy during pointing tasks in terms of main cortical areas involved, *e.g.* by using neurophysiological techniques to modulate the brain activity to selectively study the outcome of the modulation.

Performing the everyday life tasks requires that we physically interact with the environment. To this aim, *CNS* is supposed to control the human-environment interaction through the modulation of the joint impedance [5, 4]. By adopting this approach, the *CNS* is capable to properly control the

torque exerted by joints leading to a proper interaction in the task space. In addition, controlling human-environment interactions by modulating the impedance allows the *CNS* to superimpose (linearly) the impedance for each aspect of the given task, despite the muscle-skeletal system is strongly non-linear [5, 4]. Another important aspect to point out is that, being of paramount importance in performing our activities of daily living, any disorder of the motor control that involves abnormalities in modulating the joint impedance may potentially hinder their execution, *e.g.* the Parkinson's Disease [53]. In this context, a continuous measurement of joint impedance is crucial, both to study how the *CNS* controls human-environment interactions [5] and to improve assessment (and thus the treatment) of neurological disorders, *e.g.* in case of Parkinson's Disease [59]. In order to enable a continuous measurement of the wrist impedance, we focussed on the development of a portable wrist exoskeleton, capable of estimating wrist stiffness/impedance around Flexion-Extension and allowing users to freely perform activities of daily living involving all wrist movements while wearing the device. In Chapter 4 we presented the design steps and the validation of the device in terms of stiffness/impedance estimation both in healthy subjects and in Parkinson's Disease Patients. Future works will aim at implementing novel protocol to estimate wrist stiffness during interactive tasks, by extending the current studies which use bulky and cumbersome devices which i) hinder the correct implementation of the tasks [179, 180] and ii) reduce the range of activity that it is possible to study, *e.g.* human-human interactive tasks. Moreover, in order to increase the accuracy in estimating the wrist impedance, both for studying human motor control and providing novel approaches to improve the assessment and the treatment of neurological disorders (focussing on Parkinson's Disease), we aim at further developing the presented wrist exoskeleton in order to enable 2D wrist impedance measurements, *i.e.* coupled joint impedance around Flexion-Extension and Radial-Ulnar Deviation.

In the last part of this thesis (Chapter 5) we studied motor redundancy from a different perspective, *i.e.* Supernumerary Robotic Limbs to augment physical capabilities of able-bodied individuals [69, 18, 70]. Indeed, the study of SRLs has gained momentum because of the appealing benefits they may provide in a wide range of application, *e.g.* from healthcare to multi-tasking capabilities [69, 18]. However, their use is still confined only in research applications and a possible explanation may underlie in the poor embodiment they induce in SRL users [72]. To this aim, implementing a bi-directional interface, by providing a supplementary sensory feedback related to the SRLs [15, 73, 74], may allow boosting embodiment leading to the increase of the users' satisfaction [71, 72]. This aspect may pave the way to brig such technology in our everyday life leading to a dramatic change (improvement) of

how we implement our daily activities [15, 72]. In this context, we developed a wearable system to provide supplementary feedback of a SRL through (non-invasive) vibrotactile stimulation. We tested the system in two scenarios, in which we studied whether the feedback provided was feasible to let subjects understand the posture and the movements of the robot considering 2D unconstrained reaching tasks. Specifically, in the fist study we tested two feedback approaches: i) a kinematic feedback, *i.e.* the cartesian position of the SRL end-effector and a dynamic feedback, *i.e.* the torque of the SRL actuator used during the movements (only 2 actuators were used). The results demonstrated that in planar center-to-target movements kinematic feedback allows subjects to reliably understand the movements of the SRL. In the second study, we aimed at investigating whether providing a kinematic feedback of the SRL, subjects could understand its movements in real-time. The Results obtained that, despite an average error between SRL and subjects' hand around 8 cm, they could track the SRL movements, demonstrating the feasibility of our approach. Future works will be implemented to use the presented platform in three-handed interactive tasks in order to i) further investigate the proper feedback to be provided during interactive tasks and ii) assess whether providing supplementary feedback allows the users to enhance their motor performance in controlling the *SRL*.

6.1 Major Contributions

Stability over time and robustness to a visuomotor disturbance of the Donders' law during pointing tasks

Despite the pointing task is kinematically redundant for the wrist, the motor redundancy is controlled through the Donders' Law [112, 10, 11]. Concerning this aspect, the main goal of this thesis was to study whether this simplifying approach is stable over time within subjects and whether a visuomotor disturbance influences this redundancy management policy. In Chapter 3, we experimentally demonstrated that Donders' Law does not vary i) neither over time (subjects tested in four different days) ii) nor when healthy individuals have to adapt to a visuomotor disturbance provided in the task space.

PDMeter: portable wrist exoskeleton to measure wrist impedance

A possible solution adopted by the *CNS* to properly implement the human-environment interaction may be the modulation of the joint impedance [5, 4]. Moreover, abnormalities in impedance modulation are typically due to neurological disorders, *e.g.* Parkinson's Disease [53]. In this context, a continuous

measurement of wrist impedance in unstructured environments, may lead to define novel protocols to study impedance modulation during interactive tasks, since currently used device are bulky and cumbersome, thus hindering a correct assessment of this parameter [179, 180, 51]. Moreover, regarding the Parkinson's Disease, a continuous assessment of the motor symptoms (the joint rigidity is one the three cardinal motor symptoms of this pathology [53]) is crucial in order to optimize the treatment, since currently available tools do not allow to trace the fluctuations in motor symptoms. Therefore, we developed a novel portable wrist exoskeleton and in Chapter 4 we presented its design and its validation in measuring the wrist stiffness/impedance both in healthy individuals and in Parkinson's Disease patients.

ViPro: a wearable device to provide vibrotactile feedback of a supernumerary robotic limb

The use of SRL to augment physical and cognitive capabilities of able-bodied individuals have gained momentum because of the appealing benefits this technology may provide in a wide range of applications [69, 18]. However, their use is still confined only in research applications and to overcome this aspect an improvement of their embodiment may be a possible and a possible explanation may underlie in the poor embodiment they induce in SRL users [72]. To this aim, a possible solution may be the implementation of a bi-directional interface, capable to both control and provide feedback of the SRL to the user. In this context, in Chapter 5 we presented wearable device capable of providing proprioceptive feedback of SRL through vibrotactile stimulation. Specifically, we demonstrated the feasibility of conveying supplementary feedback related to a SRL to let subjects understand the SRL movements during unconstrained motions, both offline and in real-time.

Bibliography

[1] R. Ajemian and N. Hogan, "Experimenting with theoretical motor neuroscience," *Journal of motor behavior*, vol. 42, no. 6, pp. 333–342, 2010.

[2] M. L. Latash and V. Zatsiorsky, *Biomechanics and motor control: defining central concepts*. Academic Press, 2015.

[3] M. L. Latash, "Human movements: Synergies, stability, and agility," in *Biomechanics of Anthropomorphic Systems*, pp. 135–154, Springer, 2019.

[4] N. Hogan and D. Sternad, "Dynamic primitives of motor behavior," *Biological cybernetics*, vol. 106, no. 11-12, pp. 727–739, 2012.

[5] N. Hogan, "Physical interaction via dynamic primitives," in *Geometric and Numerical Foundations of Movements*, pp. 269–299, Springer, 2017.

[6] A. J. Ijspeert, J. Nakanishi, H. Hoffmann, P. Pastor, and S. Schaal, "Dynamical movement primitives: learning attractor models for motor behaviors," *Neural computation*, vol. 25, no. 2, pp. 328–373, 2013.

[7] A. d'Avella, P. Saltiel, and E. Bizzi, "Combinations of muscle synergies in the construction of a natural motor behavior," *Nature neuroscience*, vol. 6, no. 3, pp. 300–308, 2003.

[8] D. Campolo, D. Accoto, D. Formica, and E. Guglielmelli, "Intrinsic constraints of neural origin: Assessment and application to rehabilitation robotics," *IEEE Transactions on Robotics*, vol. 25, no. 3, pp. 492–501, 2009.

[9] F. A. Mussa-Ivaldi, "Modular features of motor control and learning," *Current opinion in neurobiology*, vol. 9, no. 6, pp. 713–717, 1999.

[10] D. Campolo, F. Widjaja, M. Esmaeili, and E. Burdet, "Pointing with the wrist: a postural model for donders law," *Experimental brain research*, vol. 212, no. 3, pp. 417–427, 2011.

[11] D. Formica, D. Campolo, F. Taffoni, F. Keller, and E. Guglielmelli, "Motor adaptation during redundant tasks with the wrist," in *2011 Annual International Conference of the IEEE Engineering in Medicine and Biology Society*, pp. 4046–4049, IEEE, 2011.

[12] N. Hogan, "Impedance control: An approach to manipulation: Part itheory," 1985.

[13] T. Flash, "The control of hand equilibrium trajectories in multi-joint arm movements," *Biological cybernetics*, vol. 57, no. 4-5, pp. 257–274, 1987.

[14] H. Gomi and M. Kawato, "Equilibrium-point control hypothesis examined by measured arm stiffness during multijoint movement," *Science*, vol. 272, no. 5258, pp. 117–120, 1996.

[15] G. Di Pino, A. Maravita, L. Zollo, E. Guglielmelli, and V. Di Lazzaro, "Augmentation-related brain plasticity," *Frontiers in systems neuroscience*, vol. 8, p. 109, 2014.

[16] A. Sengül, G. Rognini, M. van Elk, J. E. Aspell, H. Bleuler, and O. Blanke, "Force feedback facilitates multisensory integration during robotic tool use," *Experimental brain research*, vol. 227, no. 4, pp. 497–507, 2013.

[17] E. Abdi, E. Burdet, M. Bouri, S. Himidan, and H. Bleuler, "In a demanding task, three-handed manipulation is preferred to two-handed manipulation," *Scientific reports*, vol. 6, p. 21758, 2016.

[18] F. Parietti and H. Asada, "Supernumerary robotic limbs for human body support," *IEEE Transactions on Robotics*, vol. 32, no. 2, pp. 301–311, 2016.

[19] L. L. Z. Bright, *Supernumerary robotic limbs for human augmentation in overhead assembly tasks*. PhD thesis, Massachusetts Institute of Technology, 2017.

[20] D. M. Wolpert, Z. Ghahramani, and M. I. Jordan, "An internal model for sensorimotor integration," *Science*, vol. 269, no. 5232, pp. 1880–1882, 1995.

[21] P. M. Bays and D. M. Wolpert, "Computational principles of sensorimotor control that minimize uncertainty and variability," *The Journal of physiology*, vol. 578, no. 2, pp. 387–396, 2007.

[22] P. Beckerle, C. Castellini, and B. Lenggenhager, "Robotic interfaces for cognitive psychology and embodiment research: a research roadmap," *Wiley Interdisciplinary Reviews: Cognitive Science*, vol. 10, no. 2, p. e1486, 2019.

[23] L. Raiano, G. Di Pino, A. Noccaro, D. Accoto, and D. Formica, "Design of a wearable mechatronic device to measure the wrist rigidity in parkinson's disease patients," in *2018 7th IEEE International Conference on Biomedical Robotics and Biomechatronics (Biorob)*, pp. 497–502, IEEE, 2018.

[24] L. Raiano, G. Di Pino, L. Di Biase, M. Tombini, N. L. Tagliamonte, and D. Formica, "Pdmeter: A wrist wearable device for an at-home assessment of the parkinsons disease rigidity," *IEEE Transactions on Neural Systems and Rehabilitation Engineering*, 2020.

[25] L. Raiano, G. Di Pino, and D. Formica, "Flexion-extension wrist impedance estimation using a novel portable wrist exoskeleton: a pilot study," in *2020 8th IEEE RAS/EMBS International Conference for Biomedical Robotics and Biomechatronics (BioRob)*, pp. 440–445, IEEE.

[26] A. Noccaro, L. Raiano, M. Pinardi, D. Formica, and G. Di Pino, "A novel proprioceptive feedback system for supernumerary robotic limb," in *2020 8th IEEE RAS/EMBS International Conference for Biomedical Robotics and Biomechatronics (BioRob)*, pp. 1024–1029, IEEE.

[27] N. Bernstein, "The co-ordination and regulation of movements: Conclusions towards the study of motor co-ordination," *Biodynamics of Locomotion*, pp. 104–113, 1967.

[28] F. Martini, M. J. Timmons, R. B. Tallitsch, W. C. Ober, C. W. Garrison, K. B. Welch, and R. T. Hutchings, *Human anatomy*. Pearson/Benjamin Cummings San Francisco, CA, 2006.

[29] P. Tommasino and D. Campolo, "Task-space separation principle: a force-field approach to motion planning for redundant manipulators," *Bioinspiration & biomimetics*, vol. 12, no. 2, p. 026003, 2017.

[30] M. A. Admiraal, M. J. Kusters, and S. C. Gielen, "Modeling kinematics and dynamics of human arm movements," *Motor control*, vol. 8, no. 3, pp. 312–338, 2004.

[31] A. Zonnino and F. Sergi, "Model-based analysis of the stiffness of the wrist joint in active and passive conditions," *Journal of Biomechanical Engineering*, vol. 141, no. 4, 2019.

[32] T. Flash and B. Hochner, "Motor primitives in vertebrates and invertebrates," *Current opinion in neurobiology*, vol. 15, no. 6, pp. 660–666, 2005.

[33] S. K. Charles and N. Hogan, "Dynamics of wrist rotations," *Journal of biomechanics*, vol. 44, no. 4, pp. 614–621, 2011.

[34] F. A. Mussa-Ivaldi, N. Hogan, and E. Bizzi, "Neural, mechanical, and geometric factors subserving arm posture in humans," *Journal of Neuroscience*, vol. 5, no. 10, pp. 2732–2743, 1985.

[35] P. K. Artemiadis, P. T. Katsiaris, M. V. Liarokapis, and K. J. Kyriakopoulos, "Human arm impedance: Characterization and modeling in 3d space," in *2010 IEEE/RSJ International Conference on Intelligent Robots and Systems*, pp. 3103–3108, IEEE, 2010.

[36] D. W. Franklin, G. Liaw, T. E. Milner, R. Osu, E. Burdet, and M. Kawato, "Endpoint stiffness of the arm is directionally tuned to instability in the environment," *Journal of Neuroscience*, vol. 27, no. 29, pp. 7705–7716, 2007.

[37] T. E. Milner, "Adaptation to destabilizing dynamics by means of muscle cocontraction," *Experimental brain research*, vol. 143, no. 4, pp. 406–416, 2002.

[38] D. W. Franklin, R. Osu, E. Burdet, M. Kawato, and T. E. Milner, "Adaptation to stable and unstable dynamics achieved by combined impedance control and inverse dynamics model," *Journal of neurophysiology*, vol. 90, no. 5, pp. 3270–3282, 2003.

[39] S. De Serres and T. Milner, "Wrist muscle activation patterns and stiffness associated with stable and unstable mechanical loads," *Experimental brain research*, vol. 86, no. 2, pp. 451–458, 1991.

[40] N. Hogan, "Adaptive control of mechanical impedance by coactivation of antagonist muscles," *IEEE Transactions on automatic control*, vol. 29, no. 8, pp. 681–690, 1984.

[41] E. R. Kandel, J. H. Schwartz, T. M. Jessell, D. of Biochemistry, M. B. T. Jessell, S. Siegelbaum, and A. Hudspeth, *Principles of neural science*, vol. 4. McGraw-hill New York, 2000.

[42] P. Tommasino, *Task-space Separation Principle: From Human Postural Synergies to Bio-inspired Motion Planning for Redundant Manipulators*. Springer, 2018.

[43] N. Hogan, "The mechanics of multi-joint posture and movement control," *Biological cybernetics*, vol. 52, no. 5, pp. 315–331, 1985.

[44] A. W. Peaden and S. K. Charles, "Dynamics of wrist and forearm rotations," *Journal of biomechanics*, vol. 47, no. 11, pp. 2779–2785, 2014.

[45] C. Gielen and J. C. Houk, "Nonlinear viscosity of human wrist," *Journal of Neurophysiology*, vol. 52, no. 3, pp. 553–569, 1984.

[46] K. Park, P.-H. Chang, and S. H. Kang, "In vivo estimation of human forearm and wrist dynamic properties," *IEEE Transactions on Neural Systems and Rehabilitation Engineering*, vol. 25, no. 5, pp. 436–446, 2016.

[47] A. B. Leger and T. E. Milner, "Passive and active wrist joint stiffness following eccentric exercise," *European journal of applied physiology*, vol. 82, no. 5-6, pp. 472–479, 2000.

[48] D. Formica, S. K. Charles, L. Zollo, E. Guglielmelli, N. Hogan, and H. I. Krebs, "The passive stiffness of the wrist and forearm," *Journal of neurophysiology*, vol. 108, no. 4, pp. 1158–1166, 2012.

[49] W. B. Drake and S. K. Charles, "Passive stiffness of coupled wrist and forearm rotations," *Annals of biomedical engineering*, vol. 42, no. 9, pp. 1853–1866, 2014.

[50] A. L. Pando, H. Lee, W. B. Drake, N. Hogan, and S. K. Charles, "Position-dependent characterization of passive wrist stiffness," *IEEE Transactions on Biomedical Engineering*, vol. 61, no. 8, pp. 2235–2244, 2014.

[51] D. Formica, M. Azhar, P. Tommasino, and D. Campolo, "A geometric framework for the estimation of joint stiffness of the human wrist," in *2019 IEEE 16th International Conference on Rehabilitation Robotics (ICORR)*, pp. 151–156, IEEE, 2019.

[52] H. I. Krebs, B. T. Volpe, D. Williams, J. Celestino, S. K. Charles, D. Lynch, and N. Hogan, "Robot-aided neurorehabilitation: a robot for wrist rehabilitation," *IEEE transactions on neural systems and rehabilitation engineering*, vol. 15, no. 3, pp. 327–335, 2007.

[53] W. Poewe, K. Seppi, C. M. Tanner, G. M. Halliday, P. Brundin, J. Volkmann, A.-E. Schrag, and A. E. Lang, "Parkinson disease," *Nature reviews Disease primers*, vol. 3, p. 17013, 2017.

[54] C. G. Goetz, B. C. Tilley, S. R. Shaftman, G. T. Stebbins, S. Fahn, P. Martinez-Martin, W. Poewe, C. Sampaio, M. B. Stern, R. Dodel, *et al.*, "Movement disorder society-sponsored revision of the unified parkinson's disease rating scale (mds-updrs): Scale presentation and clinimetric testing results," *Movement disorders*, vol. 23, no. 15, pp. 2129–2170, 2008.

[55] S. Fahn, "Parkinson disease, the effect of levodopa, and the elldopa trial," *Archives of neurology*, vol. 56, no. 5, pp. 529–535, 1999.

[56] A. J. Manson, K. Turner, and A. J. Lees, "Apomorphine monotherapy in the treatment of refractory motor complications of parkinson's disease: long-term follow-up study of 64 patients," *Movement disorders: official journal of the Movement Disorder Society*, vol. 17, no. 6, pp. 1235–1241, 2002.

[57] C. W. Olanow, K. Kieburtz, P. Odin, A. J. Espay, D. G. Standaert, H. H. Fernandez, A. Vanagunas, A. A. Othman, K. L. Widnell, W. Z. Robieson, *et al.*, "Continuous intrajejunal infusion of levodopa-carbidopa intestinal gel for patients with advanced parkinson's disease: a randomised, controlled, double-blind, double-dummy study," *The Lancet Neurology*, vol. 13, no. 2, pp. 141–149, 2014.

[58] L. di Biase and A. Fasano, "Low-frequency deep brain stimulation for parkinson's disease: Great expectation or false hope?," *Movement Disorders*, vol. 31, no. 7, pp. 962–967, 2016.

[59] S. Patel, K. Lorincz, R. Hughes, N. Huggins, J. Growdon, D. Standaert, M. Akay, J. Dy, M. Welsh, and P. Bonato, "Monitoring motor fluctuations in patients with parkinson's disease using wearable sensors," *IEEE transactions on information technology in biomedicine*, vol. 13, no. 6, pp. 864–873, 2009.

[60] G. Rizzo, M. Copetti, S. Arcuti, D. Martino, A. Fontana, and G. Logroscino, "Accuracy of clinical diagnosis of parkinson disease: a systematic review and meta-analysis," *Neurology*, vol. 86, no. 6, pp. 566–576, 2016.

[61] S. Summa, J. Tosi, F. Taffoni, L. Di Biase, M. Marano, A. C. Rizzo, M. Tombini, G. Di Pino, and D. Formica, "Assessing bradykinesia in parkinson's disease using gyroscope signals," in *Rehabilitation Robotics (ICORR), 2017 International Conference on*, pp. 1556–1561, IEEE, 2017.

[62] L. di Biase, S. Summa, J. Tosi, F. Taffoni, M. Marano, A. Cascio Rizzo, F. Vecchio, D. Formica, V. Di Lazzaro, G. Di Pino, *et al.*, "Quantitative analysis of bradykinesia and rigidity in parkinsons disease," *Frontiers in neurology*, vol. 9, p. 121, 2018.

[63] G. Di Pino, D. Formica, J.-M. Melgari, F. Taffoni, G. Salomone, L. di Biase, E. Caimo, F. Vernieri, and E. Guglielmelli, "Neurophysiological bases of tremors and accelerometric parameters analysis," in *2012 4th IEEE RAS & EMBS International Conference on Biomedical Robotics and Biomechatronics (BioRob)*, pp. 1820–1825, IEEE, 2012.

[64] L. di Biase, J.-S. Brittain, S. A. Shah, D. J. Pedrosa, H. Cagnan, A. Mathy, C. C. Chen, J. F. Martín-Rodríguez, P. Mir, L. Timmerman, *et al.*, "Tremor stability index: a new tool for differential diagnosis in tremor syndromes," *Brain*, vol. 140, no. 7, pp. 1977–1986, 2017.

[65] B. K. Park, Y. Kwon, J.-W. Kim, J.-H. Lee, G.-M. Eom, S.-B. Koh, J.-H. Jun, and J. Hong, "Analysis of viscoelastic properties of wrist joint for quantification of parkinsonian rigidity," *IEEE Transactions on Neural Systems and Rehabilitation Engineering*, vol. 19, no. 2, pp. 167–176, 2010.

[66] S. Chapuis, L. Ouchchane, O. Metz, L. Gerbaud, and F. Durif, "Impact of the motor complications of parkinson's disease on the quality of life," *Movement disorders: official journal of the Movement Disorder Society*, vol. 20, no. 2, pp. 224–230, 2005.

[67] E. Burdet, R. Osu, D. W. Franklin, T. E. Milner, and M. Kawato, "The central nervous system stabilizes unstable dynamics by learning optimal impedance," *Nature*, vol. 414, no. 6862, p. 446, 2001.

[68] S.-w. Leigh, H. Agrawal, and P. Maes, "Robotic symbionts: Interweaving human and machine actions," *IEEE Pervasive Computing*, vol. 17, no. 2, pp. 34–43, 2018.

[69] F. Y. Wu and H. Asada, "Bio-artificial synergies for grasp posture control of supernumerary robotic fingers," 2014.

[70] C. I. Penaloza and S. Nishio, "Bmi control of a third arm for multitasking," *Science Robotics*, vol. 3, no. 20, p. eaat1228, 2018.

[71] D. J. Tyler, "Neural interfaces for somatosensory feedback: bringing life to a prosthesis," *Current opinion in neurology*, vol. 28, no. 6, p. 574, 2015.

[72] T. R. Makin, F. de Vignemont, and A. A. Faisal, "Neurocognitive barriers to the embodiment of technology," *Nature Biomedical Engineering*, vol. 1, no. 1, pp. 1–3, 2017.

[73] A. W. Shehata, L. F. Engels, M. Controzzi, C. Cipriani, E. J. Scheme, and J. W. Sensinger, "Improving internal model strength and performance of prosthetic hands using augmented feedback," *Journal of neuroengineering and rehabilitation*, vol. 15, no. 1, p. 70, 2018.

[74] S. Manoharan and H. Park, "Supernumerary body schema extension to non-corporeal object by adding artificial tactile feedback using electrical stimulation," in *2019 9th International IEEE/EMBS Conference on Neural Engineering (NER)*, pp. 989–992, IEEE, 2019.

[75] M. O. Ernst and M. S. Banks, "Humans integrate visual and haptic information in a statistically optimal fashion," *Nature*, vol. 415, no. 6870, pp. 429–433, 2002.

[76] R. J. van Beers, D. M. Wolpert, and P. Haggard, "When feeling is more important than seeing in sensorimotor adaptation," *Current biology*, vol. 12, no. 10, pp. 834–837, 2002.

[77] A. V. Cuppone, V. Squeri, M. Semprini, L. Masia, and J. Konczak, "Robot-assisted proprioceptive training with added vibro-tactile feedback enhances somatosensory and motor performance," *PloS one*, vol. 11, no. 10, p. e0164511, 2016.

[78] A. R. Krueger, P. Giannoni, V. Shah, M. Casadio, and R. A. Scheidt, "Supplemental vibrotactile feedback control of stabilization and reaching actions of the arm using limb state and position error encodings," *Journal of neuroengineering and rehabilitation*, vol. 14, no. 1, p. 36, 2017.

[79] L. Popović-Maneski, S. Došen, and G. Bijelić, "Maxsens: A flexible matrix electrode for sensory substitution," in *Converging Clinical and Engineering Research on Neurorehabilitation*, pp. 481–485, Springer, 2013.

[80] M. Franceschi, L. Seminara, S. Dosen, M. Strbac, M. Valle, and D. Farina, "A system for electrotactile feedback using electronic skin and flexible matrix electrodes: Experimental evaluation," *IEEE transactions on haptics*, vol. 10, no. 2, pp. 162–172, 2016.

[81] K. Li, Y. Fang, Y. Zhou, and H. Liu, "Non-invasive stimulation-based tactile sensation for upper-extremity prosthesis: a review," *IEEE Sensors Journal*, vol. 17, no. 9, pp. 2625–2635, 2017.

[82] B. Stephens-Fripp, G. Alici, and R. Mutlu, "A review of non-invasive sensory feedback methods for transradial prosthetic hands," *IEEE Access*, vol. 6, pp. 6878–6899, 2018.

[83] F. Clemente, M. D'Alonzo, M. Controzzi, B. B. Edin, and C. Cipriani, "Non-invasive, temporally discrete feedback of object contact and release improves grasp control of closed-loop myoelectric transradial prostheses," *IEEE Transactions on Neural Systems and Rehabilitation Engineering*, vol. 24, no. 12, pp. 1314–1322, 2015.

[84] H. J. Witteveen, H. S. Rietman, and P. H. Veltink, "Vibrotactile grasping force and hand aperture feedback for myoelectric forearm prosthesis users," *Prosthetics and orthotics international*, vol. 39, no. 3, pp. 204–212, 2015.

[85] C. J. Hasson and J. Manczurowsky, "Effects of kinematic vibrotactile feedback on learning to control a virtual prosthetic arm," *Journal of neuroengineering and rehabilitation*, vol. 12, no. 1, p. 31, 2015.

[86] G. K. Patel, S. Dosen, C. Castellini, and D. Farina, "Multichannel electrotactile feedback for simultaneous and proportional myoelectric control," *Journal of neural engineering*, vol. 13, no. 5, p. 056015, 2016.

[87] M. Štrbac, M. Belić, M. Isaković, V. Kojić, G. Bijelić, I. Popović, M. Radotić, S. Došen, M. Marković, D. Farina, *et al.*, "Integrated and flexible multichannel interface for electrotactile stimulation," *Journal of neural engineering*, vol. 13, no. 4, p. 046014, 2016.

[88] S. Casini, M. Morvidoni, M. Bianchi, M. Catalano, G. Grioli, and A. Bicchi, "Design and realization of the cuff-clenching upper-limb force feedback wearable device for distributed mechano-tactile stimulation of normal and tangential skin forces," in *2015 IEEE/RSJ International Conference on Intelligent Robots and Systems (IROS)*, pp. 1186–1193, IEEE, 2015.

[89] D. Prattichizzo, F. Chinello, C. Pacchierotti, and M. Malvezzi, "Towards wearability in fingertip haptics: a 3-dof wearable device for cutaneous force feedback," *IEEE Transactions on Haptics*, vol. 6, no. 4, pp. 506–516, 2013.

[90] C. Pacchierotti, S. Sinclair, M. Solazzi, A. Frisoli, V. Hayward, and D. Prattichizzo, "Wearable haptic systems for the fingertip and the hand: taxonomy, review, and perspectives," *IEEE transactions on haptics*, vol. 10, no. 4, pp. 580–600, 2017.

[91] Y. Ueda and C. Ishii, "Development of a feedback device of temperature sensation for a myoelectric prosthetic hand by using peltier element," in *2016 International Conference on Advanced Mechatronic Systems (ICAMechS)*, pp. 488–493, IEEE, 2016.

[92] "Model no. 307-103.002 9mm vibration motor - 25mm type - precision microdrives inc.." `https://www.precisionmicrodrives.com/product/307-103-002-9mm-vibration-motor-25mm-type`. Online; accessed on 2020/11/04.

[93] "Eccentric Rotating Mass Vibration Motors - ERMs." `https://www.precisionmicrodrives.com/vibration-motors/eccentric-rotating-mass-vibration-motors-erms/`. Online; accessed on 2020/11/03.

[94] "Vibrotactile feedback - vibrotac." `https://www.sensodrive.de/products/vibrotactile-feedback.php`. Online; accessed on 2020/11/03.

[95] "MaxSens Stimlator by Tecnalia Inc.." `https://www.tecnalia.com/images/stories/Catalogos/MaxSens_ENG.pdf`. Online; accessed on 2020/11/03.

[96] C. Pacchierotti, G. Salvietti, I. Hussain, L. Meli, and D. Prattichizzo, "The hring: A wearable haptic device to avoid occlusions in hand tracking," in *2016 IEEE Haptics Symposium (HAPTICS)*, pp. 134–139, IEEE, 2016.

[97] D. Leonardis, M. Solazzi, I. Bortone, and A. Frisoli, "A wearable fingertip haptic device with 3 dof asymmetric 3-rsr kinematics," in *2015 IEEE World Haptics Conference (WHC)*, pp. 388–393, IEEE, 2015.

[98] L. Treers, R. Lo, M. Cheung, A. Guy, J. Guggenheim, F. Parietti, and H. Asada, "Design and control of lightweight supernumerary robotic limbs for sitting/standing assistance," in *International Symposium on Experimental Robotics*, pp. 299–308, Springer, 2016.

[99] R. Khodambashi, G. Weinberg, W. Singhose, S. Rishmawi, V. Murali, and E. Kim, "User oriented assessment of vibration suppression by command shaping in a supernumerary wearable robotic arm," in *2016 IEEE-RAS 16th International Conference on Humanoid Robots (Humanoids)*, pp. 1067–1072, IEEE, 2016.

[100] M. Hao, J. Zhang, K. Chen, H. Asada, and C. Fu, "Supernumerary robotic limbs to assist human walking with load carriage," *Journal of Mechanisms and Robotics*, vol. 12, no. 6, 2020.

[101] T. Sasaki, M. Y. Saraiji, C. L. Fernando, K. Minamizawa, and M. Inami, "Metalimbs: Metamorphosis for multiple arms interaction using artificial limbs," in *ACM SIGGRAPH 2017 Posters*, pp. 1–2, 2017.

[102] M. Y. Saraiji, T. Sasaki, K. Kunze, K. Minamizawa, and M. Inami, "Metaarms: Body remapping using feet-controlled artificial arms," in *Proceedings of the 31st Annual ACM Symposium on User Interface Software and Technology*, pp. 65–74, 2018.

[103] J. T. Dennerlein, P. A. Millman, and R. D. Howe, "Vibrotactile feedback for industrial telemanipulators," in *Sixth Annual Symposium on Haptic Interfaces for Virtual Environment and Teleoperator Systems, ASME International Mechanical Engineering Congress and Exposition*, vol. 61, pp. 189–195, 1997.

[104] D. M. Wolpert, "Computational approaches to motor control," *Trends in cognitive sciences*, vol. 1, no. 6, pp. 209–216, 1997.

[105] E. Todorov, W. Li, and X. Pan, "From task parameters to motor synergies: A hierarchical framework for approximately optimal control of redundant manipulators," *Journal of robotic systems*, vol. 22, no. 11, pp. 691–710, 2005.

[106] E. Guigon, P. Baraduc, and M. Desmurget, "Computational motor control: redundancy and invariance," *Journal of neurophysiology*, vol. 97, no. 1, pp. 331–347, 2007.

[107] M. Desmurget, H. Gréa, and C. Prablanc, "Final posture of the upper limb depends on the initial position of the hand during prehension movements," *Experimental brain research*, vol. 119, no. 4, pp. 511–516, 1998.

[108] C. Gielen, E. Vrijenhoek, T. Flash, and S. Neggers, "Arm position constraints during pointing and reaching in 3-d space," *Journal of neurophysiology*, vol. 78, no. 2, pp. 660–673, 1997.

[109] J. F. Soechting, C. A. Buneo, U. Herrmann, and M. Flanders, "Moving effortlessly in three dimensions: does donders' law apply to arm movement?," *Journal of Neuroscience*, vol. 15, no. 9, pp. 6271–6280, 1995.

[110] D. Tweed and T. Vilis, "Geometric relations of eye position and velocity vectors during saccades," *Vision research*, vol. 30, no. 1, pp. 111–127, 1990.

[111] G. Wu, F. C. Van der Helm, H. D. Veeger, M. Makhsous, P. Van Roy, C. Anglin, J. Nagels, A. R. Karduna, K. McQuade, X. Wang, *et al.*, "Isb recommendation on definitions of joint coordinate systems of various joints for the reporting of human joint motionpart ii: shoulder, elbow, wrist and hand," *Journal of biomechanics*, vol. 38, no. 5, pp. 981–992, 2005.

[112] D. Campolo, D. Formica, E. Guglielmelli, and F. Keller, "Kinematic analysis of the human wrist during pointing tasks," *Experimental brain research*, vol. 201, no. 3, pp. 561–573, 2010.

[113] S. K. Charles and N. Hogan, "The curvature and variability of wrist and arm movements," *Experimental brain research*, vol. 203, no. 1, pp. 63–73, 2010.

[114] J. J. Koenderink and A. J. Van Doorn, "Surface shape and curvature scales," *Image and vision computing*, vol. 10, no. 8, pp. 557–564, 1992.

[115] N. M. Razali, Y. B. Wah, *et al.*, "Power comparisons of shapiro-wilk, kolmogorov-smirnov, lilliefors and anderson-darling tests," *Journal of statistical modeling and analytics*, vol. 2, no. 1, pp. 21–33, 2011.

[116] JASP Team, "JASP (Version 0.14)[Computer software]," 2020.

[117] R. Shadmehr and J. W. Krakauer, "A computational neuroanatomy for motor control," *Experimental brain research*, vol. 185, no. 3, pp. 359–381, 2008.

[118] K. P. Tee, D. W. Franklin, M. Kawato, T. E. Milner, and E. Burdet, "Concurrent adaptation of force and impedance in the redundant muscle system," *Biological cybernetics*, vol. 102, no. 1, pp. 31–44, 2010.

[119] S.-H. Zhou, D. Oetomo, Y. Tan, E. Burdet, and I. Mareels, "Modeling individual human motor behavior through model reference iterative learning control," *IEEE Transactions on Biomedical Engineering*, vol. 59, no. 7, pp. 1892–1901, 2012.

[120] G. R. Dorman, K. C. Davis, A. W. Peaden, and S. K. Charles, "Control of redundant pointing movements involving the wrist and forearm," *Journal of neurophysiology*, vol. 120, no. 5, pp. 2138–2154, 2018.

[121] M. A. Smith, A. Ghazizadeh, and R. Shadmehr, "Interacting adaptive processes with different timescales underlie short-term motor learning," *PLoS biology*, vol. 4, no. 6, p. e179, 2006.

[122] R. Shadmehr and F. A. Mussa-Ivaldi, "Adaptive representation of dynamics during learning of a motor task," *Journal of Neuroscience*, vol. 14, no. 5, pp. 3208–3224, 1994.

[123] O. Donchin, J. T. Francis, and R. Shadmehr, "Quantifying generalization from trial-by-trial behavior of adaptive systems that learn with basis functions: theory and experiments in human motor control," *Journal of Neuroscience*, vol. 23, no. 27, pp. 9032–9045, 2003.

[124] J. Diedrichsen, O. White, D. Newman, and N. Lally, "Use-dependent and error-based learning of motor behaviors," *Journal of Neuroscience*, vol. 30, no. 15, pp. 5159–5166, 2010.

[125] O. Krigolson and C. Holroyd, "Evidence for hierarchical error processing in the human brain," *Neuroscience*, vol. 137, no. 1, pp. 13–17, 2006.

[126] V. Woods, "Musculoskeletal disorders and visual strain in intensive data processing workers," *Occupational medicine*, vol. 55, no. 2, pp. 121–127, 2005.

[127] J. Goyal, P. Khandnor, and T. C. Aseri, "Classification, prediction, and monitoring of parkinsons disease using computer assisted technologies: A comparative analysis," *Engineering Applications of Artificial Intelligence*, vol. 96, p. 103955, 2020.

[128] M. A. Nitsche, L. G. Cohen, E. M. Wassermann, A. Priori, N. Lang, A. Antal, W. Paulus, F. Hummel, P. S. Boggio, F. Fregni, and A. Pascual-Leone, "Transcranial direct current stimulation: State of the art 2008," *Brain Stimulation*, vol. 1, no. 3, pp. 206–223, 2008.

[129] T. E. Milner and D. W. Franklin, "Impedance control and internal model use during the initial stage of adaptation to novel dynamics in humans," *The Journal of physiology*, vol. 567, no. 2, pp. 651–664, 2005.

[130] Á. Sánchez-Ferro, M. Elshehabi, C. Godinho, D. Salkovic, M. A. Hobert, J. Domingos, J. M. Van Uem, J. J. Ferreira, and W. Maetzler, "New methods for the assessment of parkinson's disease (2005 to 2015): A systematic review," *Movement Disorders*, vol. 31, no. 9, pp. 1283–1292, 2016.

[131] J. C. Schlachetzki, J. Barth, F. Marxreiter, J. Gossler, Z. Kohl, S. Reinfelder, H. Gassner, K. Aminian, B. M. Eskofier, J. Winkler, *et al.*, "Wearable sensors objectively measure gait parameters in parkinsons disease," *PloS one*, vol. 12, no. 10, p. e0183989, 2017.

[132] J. Tosi, S. Summa, F. Taffoni, L. di Biase, M. Marano, A. C. Rizzo, M. Tombini, E. Schena, D. Formica, and G. Di Pino, "Feature extraction in sit-to-stand task using m-imu sensors and evaluatiton in parkinson's disease," in *2018 IEEE International Symposium on Medical Measurements and Applications (MeMeA)*, pp. 1–6, IEEE, 2018.

[133] M. Lakie, E. Walsh, and G. Wright, "Resonance at the wrist demonstrated by the use of a torque motor: an instrumental analysis of muscle tone in man.," *The Journal of physiology*, vol. 353, no. 1, pp. 265–285, 1984.

[134] R. Xia, K. Markopoulou, S. Puumala, and W. Z. Rymer, "A comparison of the effects of imposed extension and flexion movements on parkinsonian rigidity," *Clinical Neurophysiology*, vol. 117, no. 10, pp. 2302–2307, 2006.

[135] D. Powell, A. J. Threlkeld, X. Fang, A. Muthumani, and R. Xia, "Amplitude-and velocity-dependency of rigidity measured at the wrist in parkinsons disease," *Clinical Neurophysiology*, vol. 123, no. 4, pp. 764–773, 2012.

[136] T. Perera, W.-L. Lee, M. Jones, J. L. Tan, E. L. Proud, A. Begg, N. C. Sinclair, R. Peppard, and H. J. McDermott, "A palm-worn device to quantify rigidity in parkinsons disease," *Journal of neuroscience methods*, vol. 317, pp. 113–120, 2019.

[137] T. Endo, R. Okuno, M. Yokoe, K. Akazawa, and S. Sakoda, "A novel method for systematic analysis of rigidity in parkinson's disease," *Movement disorders: official journal of the Movement Disorder Society*, vol. 24, no. 15, pp. 2218–2224, 2009.

[138] M. P. Caligiuri, "Portable device for quantifying parkinsonian wrist rigidity," *Movement disorders*, vol. 9, no. 1, pp. 57–63, 1994.

[139] A. Prochazka, D. J. Bennett, M. J. Stephens, S. K. Patrick, R. Sears-Duru, T. Roberts, and J. H. Jhamandas, "Measurement of rigidity in parkinson's disease," *Movement disorders: official journal of the Movement Disorder Society*, vol. 12, no. 1, pp. 24–32, 1997.

[140] M. K. Mak, E. C. Wong, and C. W. Hui-Chan, "Quantitative measurement of trunk rigidity in parkinsonian patients," *Journal of neurology*, vol. 254, no. 2, pp. 202–209, 2007.

[141] B. Sepehri, A. Esteki, E. Ebrahimi-Takamjani, G.-A. Shahidi, F. Khamseh, and M. Moinodin, "Quantification of rigidity in parkinsons disease," *Annals of Biomedical engineering*, vol. 35, no. 12, pp. 2196–2203, 2007.

[142] G. Abbruzzese, "Optimising levodopa therapy," *Neurological Sciences*, vol. 29, no. 5, pp. 377–379, 2008.

[143] R. M. Murray, Z. Li, S. S. Sastry, and S. S. Sastry, *A mathematical introduction to robotic manipulation*. CRC press, 1994.

[144] R. S. Hartenberg and J. Denavit, *Kinematic synthesis of linkages*. McGraw-Hill, 1964.

[145] N. NASA, "ANTHROPOMETRY AND BIOMECHANICS," *Man systems integration standards*, vol. 1.

[146] A. K. Palmer, F. W. Werner, D. Murphy, and R. Glisson, "Functional wrist motion: a biomechanical study," *Journal of Hand Surgery*, vol. 10, no. 1, pp. 39–46, 1985.

[147] R. Stein, F. Cody, and C. Capaday, "The trajectory of human wrist movements," *Journal of neurophysiology*, vol. 59, no. 6, pp. 1814–1830, 1988.

[148] J. J. Palazzolo, *Robotic Technology to Aid and Assess Recovery and Learning in Stroke Patients*. PhD Thesis, Massachusetts Institute of Technology, Cambridge, MA, USA, 2005.

[149] V. Falzarano, G. Petrella, F. Marini, M. W. Holmes, L. Masia, P. Morasso, and J. Zenzeri, "Preliminary evaluation of a robotic measurement system for the assessment of wrist joint spasticity," in *2020 8th IEEE RAS/EMBS International Conference for Biomedical Robotics and Biomechatronics (BioRob)*, pp. 539–544, IEEE.

[150] R. S. Hartenberg and J. Denavit, "A kinematic notation for lower pair mechanisms based on matrices," *Journal of Applied Mechanics*, vol. 22, pp. 215–221, 1955.

[151] L. Sciavicco and B. Siciliano, "Modeling and control of robot manipulators, 1996," *New York: MacGraw-Hill*.

[152] N. L. Tagliamonte, M. Scorcia, D. Formica, D. Campolo, and E. Guglielmelli, "Effects of impedance reduction of a robot for wrist rehabilitation on human motor strategies in healthy subjects during pointing tasks," *Advanced Robotics*, vol. 25, no. 5, pp. 537–562, 2011.

[153] F. Cordella, F. Taffoni, L. Raiano, G. Carpino, M. Pantoni, L. Zollo, E. Schena, E. Guglielmelli, and D. Formica, "Design and development of a sensorized cylindrical object for grasping assessment," in *2016 38th Annual International Conference of the IEEE Engineering in Medicine and Biology Society (EMBC)*, pp. 3366–3369, IEEE, 2016.

[154] "FSR 402 by Interlink Electronics product page."

[155] A. Erwin, N. Moser, C. G. McDonald, and M. K. OMalley, "A bowden cable-based series elastic actuation module for assessing the human wrist," in *ASME 2018 Dynamic Systems and Control Conference*, pp. V001T07A001–V001T07A001, American Society of Mechanical Engineers, 2018.

[156] L. Z. Tong, H. T. Ong, J. X. Tan, J. Lin, E. Burdet, S. Ge, and C. L. Teo, "Pediatric rehabilitation with the reachman's modular handle," in *2015 37th Annual International Conference of the IEEE Engineering in Medicine and Biology Society (EMBC)*, pp. 3933–3936, IEEE, 2015.

[157] F. Marini, C. M. Hughes, V. Squeri, L. Doglio, P. Moretti, P. Morasso, and L. Masia, "Robotic wrist training after stroke: Adaptive modulation of assistance in pediatric rehabilitation," *Robotics and Autonomous Systems*, vol. 91, pp. 169–178, 2017.

[158] R. J. Stone, "Haptic feedback: A brief history from telepresence to virtual reality," in *International Workshop on Haptic Human-Computer Interaction*, pp. 1–16, Springer, 2000.

[159] A. Gupta and M. K. O'Malley, "Design of a haptic arm exoskeleton for training and rehabilitation," *IEEE/ASME Transactions on mechatronics*, vol. 11, no. 3, pp. 280–289, 2006.

[160] JASP Team, "JASP (Version 0.9.2)[Computer software]," 2019.

[161] D. Campolo, "Cartesian stiffness for wrist joints: analysis on the lie group of 3d rotations and geometric approximation for experimental evaluation," *Computer methods in biomechanics and biomedical engineering*, vol. 16, no. 9, pp. 975–986, 2013.

[162] A. Carnevale, C. Massaroni, D. L. Presti, J. Di Tocco, M. Zaltieri, D. Formica, U. G. Longo, E. Schena, and V. Denaro, "Conductive textile element embedded in a wearable device for joint motion monitoring," in *2020 IEEE International Symposium on Medical Measurements and Applications (MeMeA)*, pp. 1–6, IEEE, 2020.

[163] H. W. Axelson and K.-E. Hagbarth, "Human motor control consequences of thixotropic changes in muscular short-range stiffness," *The Journal of physiology*, vol. 535, no. 1, pp. 279–288, 2001.

[164] N. Rijnveld and H. I. Krebs, "Passive wrist joint impedance in flexion-extension and abduction-adduction," in *2007 IEEE 10th International Conference on Rehabilitation Robotics*, pp. 43–47, IEEE, 2007.

[165] R. V. Gonzalez, T. S. Buchanan, and S. L. Delp, "How muscle architecture and moment arms affect wrist flexion-extension moments," *Journal of biomechanics*, vol. 30, no. 7, pp. 705–712, 1997.

[166] G. Ganesh, A. Takagi, R. Osu, T. Yoshioka, M. Kawato, and E. Burdet, "Two is better than one: Physical interactions improve motor performance in humans," *Scientific reports*, vol. 4, p. 3824, 2014.

[167] A. Takagi, G. Ganesh, T. Yoshioka, M. Kawato, and E. Burdet, "Physically interacting individuals estimate the partners goal to enhance their movements," *Nature Human Behaviour*, vol. 1, no. 3, pp. 1–6, 2017.

[168] U. Proske and S. C. Gandevia, "The proprioceptive senses: their roles in signaling body shape, body position and movement, and muscle force," *Physiological reviews*, vol. 92, no. 4, pp. 1651–1697, 2012.

[169] M. Pinardi, F. Ferrari, M. DAlonzo, F. Clemente, L. Raiano, C. Cipriani, and G. Di Pino, "Doublecheck: a sensory confirmation is required to own a robotic hand, sending a command to feel in charge of it," *Cognitive Neuroscience*, pp. 1–13, 2020.

[170] E. J. Earley, K. J. Kaveny, R. E. Johnson, L. J. Hargrove, and J. W. Sensinger, "Joint-based velocity feedback to virtual limb dynamic perturbations," in *2017 International Conference on Rehabilitation Robotics (ICORR)*, pp. 1313–1318, IEEE, 2017.

[171] K. P. Körding and D. M. Wolpert, "Bayesian decision theory in sensorimotor control," *Trends in cognitive sciences*, vol. 10, no. 7, pp. 319–326, 2006.

[172] E. Wentink, A. Mulder, J. S. Rietman, and P. H. Veltink, "Vibrotactile stimulation of the upper leg: Effects of location, stimulation method and habituation," in *2011 Annual International Conference of the IEEE Engineering in Medicine and Biology Society*, pp. 1668–1671, IEEE, 2011.

[173] E. T. Wilson, J. Wong, and P. L. Gribble, "Mapping proprioception across a 2d horizontal workspace," *PloS one*, vol. 5, no. 7, 2010.

[174] S. S. Sawilowsky, "New effect size rules of thumb," *Journal of Modern Applied Statistical Methods*, vol. 8, no. 2, p. 26, 2009.

[175] C. O. Fritz, P. E. Morris, and J. J. Richler, "Effect size estimates: current use, calculations, and interpretation.," *Journal of experimental psychology: General*, vol. 141, no. 1, p. 2, 2012.

[176] K. M. Trewartha, S. Case, and J. R. Flanagan, "Integrating actions into object location memory: A benefit for active versus passive reaching movements," *Behavioural brain research*, vol. 279, pp. 234–239, 2015.

[177] S. H. Johnson-Frey, "The neural bases of complex tool use in humans," *Trends in cognitive sciences*, vol. 8, no. 2, pp. 71–78, 2004.

[178] E. Burdet, D. W. Franklin, and T. E. Milner, *Human robotics: neuromechanics and motor control*. MIT press, 2013.

[179] M. S. Erden and A. Billard, "Hand impedance measurements during interactive manual welding with a robot," *IEEE transactions on robotics*, vol. 31, no. 1, pp. 168–179, 2015.

[180] T. Tsuji, Y. Takeda, and Y. Tanaka, "Analysis of mechanical impedance in human arm movements using a virtual tennis system," *Biological cybernetics*, vol. 91, no. 5, pp. 295–305, 2004.